[American Journal of Science, Vol. 318, October, 2018, P. 799–860, DOI 10.2475/08.2018.01]

American Journal of Science

OCTOBER 2018

DOES LARGE IGNEOUS PROVINCE VOLCANISM ALWAYS PERTURB THE MERCURY CYCLE? COMPARING THE RECORDS OF OCEANIC ANOXIC EVENT 2 AND THE END-CRETACEOUS TO OTHER MESOZOIC EVENTS

LAWRENCE M.E. PERCIVAL*,§§§,†, HUGH C. JENKYNS*, TAMSIN A. MATHER*, ALEXANDER J. DICKSON*,‡, SIETSKE J. BATENBURG*, MICHA RUHL*,‡‡, STEPHEN P. HESSELBO**, RICHARD BARCLAY***, IAN JARVIS§, STUART A. ROBINSON*, and LINEKE WOELDERS§§,‡‡‡

ABSTRACT. Mercury (Hg) is increasingly being used as a sedimentary tracer of Large Igneous Province (LIP) volcanism, and supports hypotheses of a coincidence between the formation of several LIPs and episodes of mass extinction and major environmental perturbation. However, numerous important questions remain to be answered before Hg can be claimed as an unequivocal fingerprint of LIP volcanism, as well as an understanding of why some sedimentary records document clear Hg enrichment signals whilst others do not. Of particular importance is evaluating the impact of different volcanic styles on the global mercury cycle, as well as the role played by depositional processes in recording global Hg-cycle perturbations. Here, new mercury records of Cretaceous Oceanic Anoxic Event 2 (OAE 2: ~94 Ma) and the latest Cretaceous (~67–66.0 Ma) are presented. OAE 2 is associated with the emplacement of multiple, predominantly submarine, LIPs; the latest Cretaceous with subaerial volcanism of the Deccan Traps. Both of these connections are strongly supported by previously published trends towards unradiogenic osmium- (Os) isotope values in globally distributed sedimentary records. Hg data from both events show considerable variation between different locations, attributed to the effectiveness of different sediment types in registering the Hg signal, with lithologically homogeneous records documenting more clear Hg enrichments than sections with major changes in lithology such as limestones to claystones or organic-rich shales. Crucially, there is no geographically consistent signal of sedimentary Hg enrichment in stratigraphic records of either OAE 2 or the latest Cretaceous that matches Os-isotope evidence for LIP emplacement, indicating that volcanism did not cause a global Hg perturbation throughout the entire eruptive history of the LIPs formed at those times. It is suggested that the discrepancy between Os-isotope and Hg trends in records of OAE 2

* Department of Earth Sciences, University of Oxford, South Parks Road, Oxford, OX1 3AN, United Kingdom
** Camborne School of Mines and Environment and Sustainability Institute, University of Exeter, Penryn Campus, Penryn, Cornwall, TR10 9FE, United Kingdom
*** Smithsonian Institution, PO Box, 37012, MRC 121, Washington, D.C., 20013-7012, United States
§ Department of Geography and Geology, Kingston University London, Penrhyn Road, Kingston upon Thames, KT1 2EE, United Kingdom
§§ KU Leuven, Division of Geology, Department of Earth and Environmental Sciences, B-3001, Leuven, Belgium
§§§ Institute of Earth Sciences, Géopolis, University of Lausanne, CH-1015 Lausanne, Switzerland
‡ Department of Earth Sciences, Royal Holloway University of London, Egham, Surrey, TW20 0EX, United Kingdom
‡‡ Department of Geology, Trinity College Dublin, The University of Dublin, Dublin 2, Ireland
‡‡‡ Institute of Arctic and Alpine Research, University of Colorado Boulder, Boulder, Colorado, United States of America
† Corresponding author's email: lawrence.percival11@gmail.com

is caused by the limited dispersal range of Hg emitted from submarine volcanoes compared to the global-scale distribution of Os. A similar lack of correlation between these two proxies in uppermost Cretaceous strata indicates that, although subaerial volcanism can perturb the global Hg cycle, not all subaerial eruptions will do so. These results highlight the variable impact of different volcanogenic processes on the efficiency of Hg dispersal across the globe. Factors that could influence the impact of LIP eruptions on the global mercury cycle include submarine *versus* subaerial volcanism, volcanic intensity or explosivity, and the potential contribution of thermogenic mercury from reactions between ascending magma and surrounding organic-rich sediments.

Key words: mercury, Cenomanian–Turonian OAE, end-Cretaceous, Large Igneous Province, volcanic style, depositional environment

INTRODUCTION

Sedimentary mercury (Hg) concentrations have been utilized in a number of studies to investigate the link between major environmental perturbations and Large Igneous Province (LIP) eruptions (fig. 1: for example, Sanei and others, 2012; Percival and others, 2015; Thibodeau and others, 2016; Font and others, 2016; Charbonnier and Föllmi, 2017; Charbonnier and others, 2017; Jones and others, 2017; Racki and others, 2018), and have also been used to investigate volcanism during times not associated with global climate change (Rakociński and others, 2018; Charbonnier and others, 2018a). The use of Hg as a volcanic tracer is based on the known emission of the element from modern volcanoes to the atmosphere and oceans, and the relatively long atmospheric residence time of gaseous elemental mercury (0.5–2 years; Schroeder and Munthe, 1998; Blum and others, 2014), allowing it to be distributed globally before being deposited in sediments (fig. 2: Slemr and others, 1985; Pyle and Mather, 2003). However, the impact of specific volcanic and sedimentological processes on Hg emissions and their sedimentary record remains relatively poorly constrained. In this study, new Hg concentration data are presented from sedimentary records of two Mesozoic events associated with LIP eruptions: the Cenomanian–Turonian Oceanic Anoxic Event (OAE 2: ~94 Ma), and latest Cretaceous environmental change (~66 Ma) prior to the end-Cretaceous (K–Pg) extinction. The LIPs associated with these two events have a number of features that contrast with each other, as well as with other Mesozoic LIPs, whilst the sedimentary records of both events have also been well studied using other proposed proxies for LIP volcanism (see below). Thus, a comparison of these two events is ideally suited to determining which volcanic processes might be important in producing a global-scale perturbation of the Hg cycle, and improving understanding of sedimentary Hg as a signature of LIP volcanism.

The Link Between Large Igneous Provinces (LIPs) and Phanerozoic Events

The link between LIPs and environmental perturbations is founded chiefly on a well-established correlation between the ages of individual geological events and LIPs within the last 300 Myr, based on U-Pb and Ar-Ar geochronology of LIP basalts and sedimentary records (fig. 1: see also for example, Courtillot and Renne, 2003; Bond and Wignall, 2014). LIPs represent the geologically rapid emplacement of enormous quantities of magmatic material, with a main phase of emplacement thought to have typically lasted ~1 Myr (Coffin and Eldholm, 1994). The majority of continental LIP extrusives are believed to have comprised effusively erupted tholeiitic basalts, although evidence for more silicic fractions and/or explosive volcanism has been documented for numerous mafic LIPs (Ross and others, 2005; Bryan and others, 2010). Four LIPs have been dated to broadly the same age as OAE 2: the Caribbean–Columbian Plateau, the High Arctic LIP, the Ontong-Java Plateau, and the Madagascan Province (for example, Storey and others, 1995; Neal and others, 1997; Snow and others, 2005;

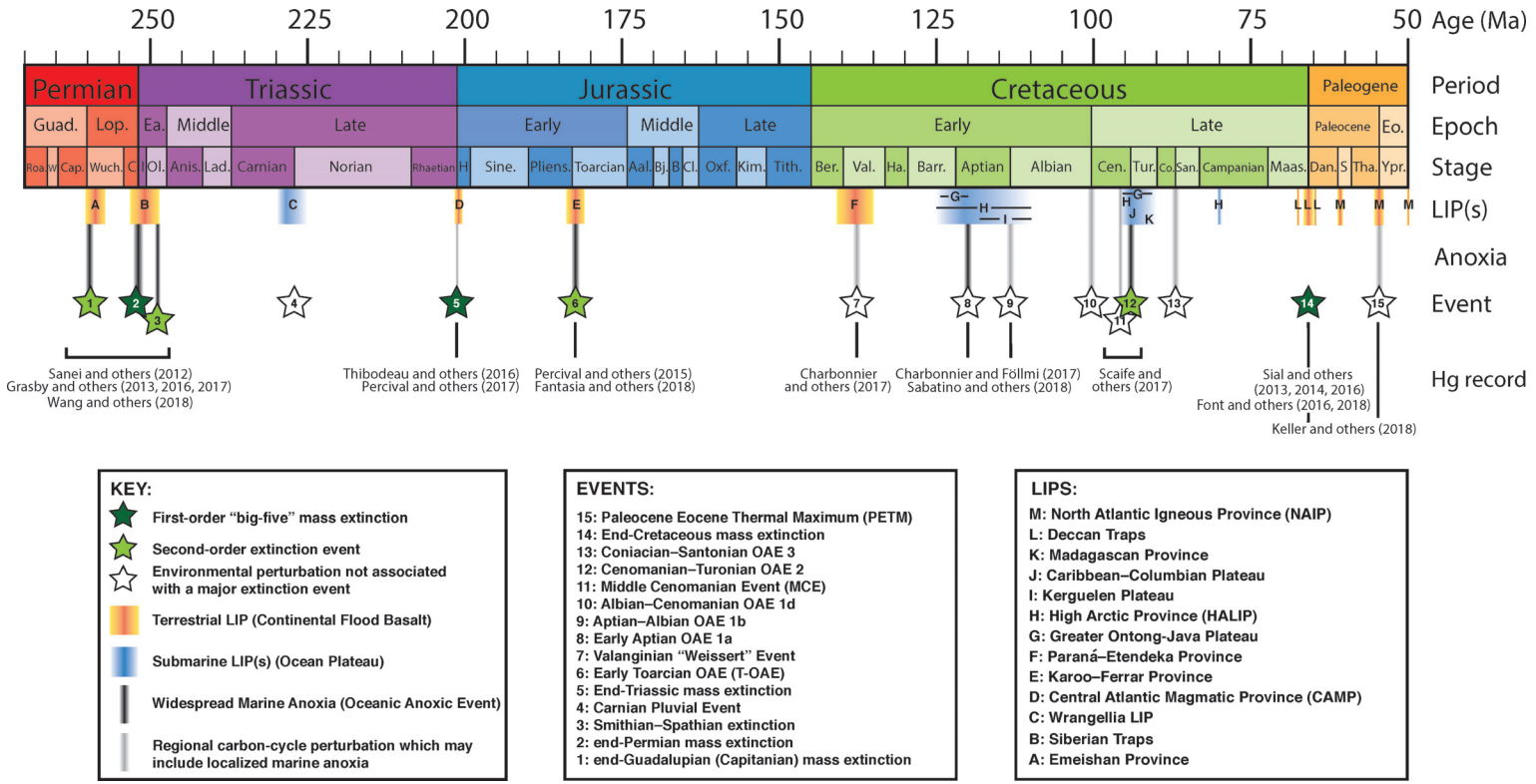

Fig. 1. An illustration of the Middle Permian to Eocene timescale, showing the respective ages of major Mesozoic environmental perturbations, LIP emplacements, and episodes of marine anoxia and carbon-cycle perturbations (taken from the reviews of Jenkyns, 2010; Bond and Wignall, 2014; Ernst and Youbi, 2017). Previous mercury studies are noted via references under the events. Mercury enrichments have also been reported from the Ordovician–Silurian boundary (Gong and others, 2017; Jónes and others, 2017), and Frasnian–Famennian boundary (Racki and others, 2018), although there is currently no clear candidate LIP for the earlier event. The ages of stage boundaries are taken from the 2016 Geological Timescale (Ogg and others, 2016). Ea. = Early. Abbreviated Epoch and Stage names are as follows: Guad. = Guadalupian; Lop. = Lopingian; Eo. = Eocene; Roa. = Roadian; W = Wordian; Cap. = Capitanian; Wuch. = Wuchiapingian; C = Changhsingian; I = Induan; Ol. = Olenekian; Anis. = Anisian; Lad. = Ladinian; H = Hettangian; Sine. = Sinemurian; Pliens. = Pliensbachian; Aal. = Aalenian; Bj = Bajocian; B = Bathonian; Cl. = Callovian; Oxf. = Oxfordian; Kim. = Kimmeridgian; Tith. = Tithonian; Ber. = Berriasian; Val. = Valanginian; Ha. = Hauterivian; Barr. = Barremian; Cen. = Cenomanian; Tur. = Turonian; Co. = Coniacian; San. = Santonian; Maas. = Maastrichtian; Dan. = Danian; S. = Selandian; Tha. = Thanetian; Ypr. = Ypresian.

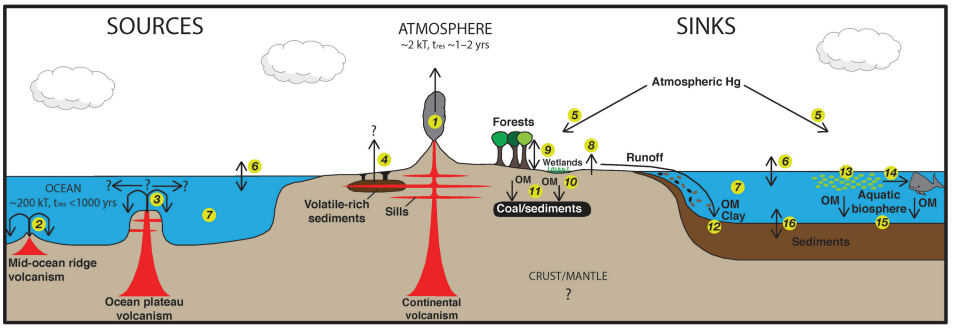

Fig. 2. Simplified illustration of the global mercury cycle, adapted from Percival and others (2015). Processes affecting the source, sink, and transportation of mercury through the ocean–atmosphere system are indicated as follows: **1** – Volcanic emission of mercury, chiefly as inert gaseous elemental mercury (Hg^0) to the atmosphere; **2** – Hydrothermal emission of Hg to the ocean at mid-ocean ridges; **3** – Presumed equivalent release of hydrothermal Hg to the ocean from submarine ocean plateau volcanism, similar to that at mid-ocean ridges; **4** – Possible emission of thermogenic Hg to the atmosphere following heating of organic-rich sediments by intruding sills; **5** – Deposition of atmospheric Hg to land, water, or forest canopy, either as particulate Hg (dry deposition) or soluble oxidized mercury (Hg^{2+}) following interaction between atmospheric Hg^0 and atmospheric oxidizing agents such as halogen, nitrile, ozone, and hydroxyl radicals (wet deposition); **6** – Air–water interchange of Hg^0; **7** – Conversion of mercury species between Hg^0, Hg^{2+}, MMHg (monomethylmercury) and DMHg (dimethylmercury) through multiple biotic and abiotic reactions in aquatic environments (for example, Fitzgerald and others, 2007; Selin, 2009; Bowman and others, 2015; summarized in Munthe and others, 2009); **8** – Reduction of soil Hg to Hg^0, which is subsequently re-emitted to the atmosphere; **9** – Interchange of mercury between soil and forest canopy through emission of soil Hg and decay of leaves that have taken up Hg; **10** – High abundance of sulfate- and/or iron-reducing bacteria in reduced wetland environments promoting methylation of Hg^{2+} to organophilic MMHg, which can adsorb onto organic matter; **11** – Deposition of sediments in Hg–OM complexes to soils, peats, or coals; **12** – Riverine runoff (and potentially deposition) into lacustrine or marine environments of detrital Hg bound to either organic matter or clay minerals; **13** – Uptake of Hg^{2+} or MMHg by aquatic biota; **14** – Bioaccumulation of organophilic MMHg up the food chain; **15** – Deposition of bioaccumulated Hg into sediments as Hg–OM complexes; **16** – Potential remobilization and release of sedimentary Hg into the aquatic realm. Atmospheric and oceanic residence times of Hg are indicated (Slemr and others, 1985; Gill and Fitzgerald, 1988).

Turgeon and Creaser, 2008; Tegner and others, 2011; Kingsbury and others, 2018). The Deccan Traps were emplaced during the latest Cretaceous and earliest Paleogene, overlapping with the time of the end-Cretaceous extinction (for example, Courtillot and others, 1986; Chenet and others, 2007, 2008, 2009; Renne and others, 2015; Schoene and others, 2015).

LIPs may be emplaced onto/into either continental or oceanic crust. For some provinces, volcanism was predominantly subaerial (Continental Flood Basalts), whereas for others eruptions were largely submarine (Oceanic Plateaus). The Cretaceous–Paleogene Deccan Traps represent a continental LIP emplaced subaerially, whereas all four LIPs that have been associated with OAE 2 are Oceanic Plateaus, where much of the volcanism would have occurred below the sea surface. However, Aptian age (~120 Ma) phreatomagmatic deposits documented from the Ontong-Java Plateau demonstrate that submarine Ocean Plateaus can become emergent and generate subaerial volcanic products (Chambers and others, 2004; Thordarson, 2004), and there is evidence for at least some subaerial volcanism on the LIPs associated with OAE 2 (for example, Storey and others, 1995; Buchs and others, 2018), although the volume and precise timing of those eruptions with respect to the OAE remains unclear. Additionally, the country rock intruded by LIP magmas may play a key role in the volatile budget of a specific LIP. Some LIPs, such as the end-Permian Siberian Traps and Pliensbachian–Toarcian Karoo–Ferrar Province, intruded volatile-rich sediments such as organic-rich shales, coals, and evaporites (for example, McElwain and others, 2005;

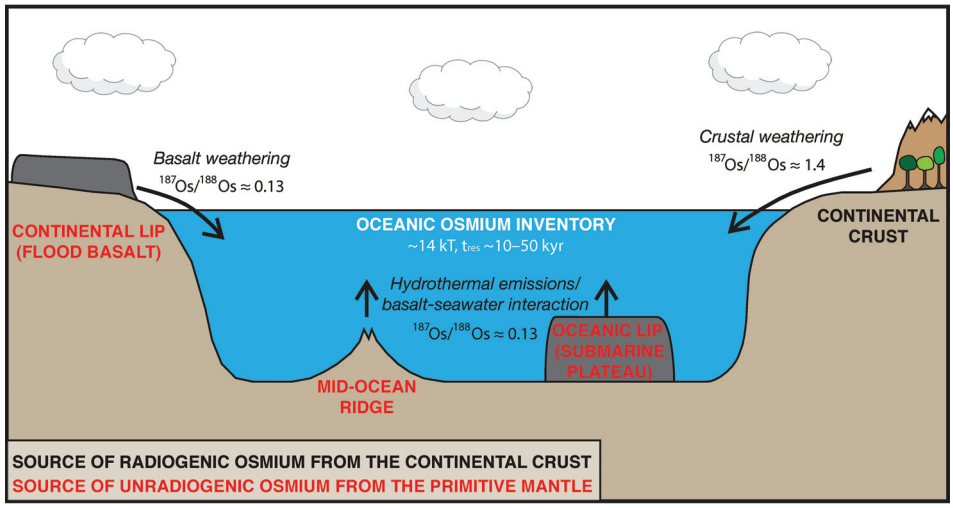

Fig. 3. Simplified illustration of the terrestrial inputs of osmium to the global ocean. Radiogenic osmium input is dominated by the flux from weathering of the continental crust. Unradiogenic osmium input is dominated by hydrothermal output from mid-ocean ridges and intra-plate oceanic volcanism, and weathering/alteration of basalts derived from partial melting of the primitive mantle. The relative input of these sources determines the isotopic composition of the oceanic osmium inventory, due to Os being well mixed in the open ocean. The approximate isotopic compositions from each source and oceanic residence time of Os are indicated (reviewed in Peucker-Ehrenbrink and Ravizza, 2000).

Svensen and others, 2009). Thermal metamorphism of these lithologies by LIP magmas may have produced additional thermogenic volatiles, supplementing magmatic emissions (for example, Svensen and others, 2004; Ganino and Arndt, 2009). These thermogenic emissions may also explain observed negative carbon-isotope ($\delta^{13}C$) excursions in both organic and inorganic carbon that are documented in records of numerous events associated with LIPs, but might potentially be of too great a magnitude to have been produced by magmatic carbon alone (for example, Dickens and others, 1995; Hesselbo and others, 2000; Beerling and Berner, 2002; compare Saunders, 2016; Gutjahr and others, 2017). However, the LIPs associated with OAE 2 and the latest Cretaceous interval are not thought to have intruded such volatile-rich country rocks conducive to the production of thermogenic volatiles (Ganino and Arndt, 2009).

In addition to a strong temporal association between LIP volcanism and Mesozoic events, a causal link between the two phenomena is indicated by proxy evidence for volcanism in stratigraphic horizons recording the onset of environmental change. Osmium (Os) isotopes (specifically $^{187}Os/^{188}Os$ ratios) of mudrocks have previously been used extensively as stratigraphic markers of LIP volcanism (for example, Cohen and Coe, 2002; Ravizza and Peucker-Ehrenbrink, 2003; Turgeon and Creaser, 2008; Tejada and others, 2009). Osmium has a relatively short ocean residence time (10–50 kyr at the present day) that permits recording of geologically rapid changes to the oceanic Os-isotope composition whilst still being well mixed throughout the global ocean (Peucker-Ehrenbrink and Ravizza, 2000). The $^{187}Os/^{188}Os$ composition of primitive mantle-derived basalt is very unradiogenic, typically <0.15 (Horan and others, 1995; Allègre and others, 1999; Gibson and others, 2016), compared to a much more radiogenic composition of the continental crust, typically ~1.4 (fig. 3; Peucker-Ehrenbrink and Jahn, 2001). There is also a cosmogenic influx of unradiogenic

osmium, but it is probably too continuous to rapidly alter the Os-isotope composition of oceans and sediments, except potentially following a large bolide impact event.

Therefore, weathering of subaerial LIP basalts, hydrothermal activity associated with submarine LIP volcanism, and/or low-temperature alteration of mafic material within the ocean, is expected to cause a decrease in the $^{187}Os/^{188}Os$ ratios of sediments deposited at that time ($Os_{(i)}$: Cohen and others, 1999). $Os_{(i)}$ indicates the calculated $^{187}Os/^{188}Os$ ratio of seawater at the time the analyzed sedimentary rocks were deposited, corrected for the post-depositional decay of ^{187}Re to ^{187}Os. Both OAE 2 and the latest Cretaceous have been linked to LIP emplacement through sedimentary records of osmium isotopes (Ravizza and Peucker-Ehrenbrink, 2003; Turgeon and Creaser, 2008; Robinson and others, 2009; Du Vivier and others, 2014, 2015), allowing comparison of Hg concentrations and Os isotopes as volcanic proxies.

Additionally, increased sedimentary abundances of specific trace metals such as scandium, chromium, cobalt, copper, and zirconium have been interpreted to result from hydrothermal output from subaqueous LIP volcanism, or weathering of juvenile basalts in a subaerial LIP (for example, Orth and others, 1993; Snow and others, 2005; Pujol and others, 2006; Pálfy and Zajzon, 2012; Erba and others, 2015). Numerous isotope systems have also been proposed to be indicative of LIP volcanism and/or weathering, including strontium, lead, neodymium, sulfur, chromium, and zinc isotopes (for example, Jones and Jenkyns, 2001; Kuroda and others, 2007; Zheng and others, 2013; Holmden and others, 2016; Jenkyns and others, 2017; Liu and others, 2017; Sweere and others, 2018). However, the application of most of these proxies remains in its early stages; many have yet to be tested on multiple records or events, or are known to respond to additional surface processes besides volcanic activity (for example, continental weathering, or changes in marine oxygenation). Additionally, strontium has a relatively long seawater residence time of >2 million years (Palmer and Edmond, 1989), making strontium-isotope (specifically $^{87}Sr/^{86}Sr$) ratios less suitable for recording geologically rapid events.

Mercury as a Proxy for Volcanism

An advantage of mercury over other proxies is that this element has the potential to be a uniquely volcanic marker, less impacted by changes in continental weathering rates than strontium or osmium isotopes, or by marine redox chemistry than many other metals. Figure 2 shows a simplified summary of the natural Hg cycle. Mercury is emitted as a volcanic trace gas in the modern environment (Pyle and Mather, 2003), and has an atmospheric residence time of 0.5 to 2 years, allowing global distribution (Schroeder and Munthe, 1998; Blum and others, 2014). An ice-core record of the historical atmosphere from a Wyoming glacier has highlighted episodes of abruptly elevated atmospheric Hg content proposed as following major eruptions in the last two centuries, although these correlations remain debated (Schuster and others, 2002; Chellman and others, 2017). Mercury is also emitted from hydrothermal activity associated with subaqueous volcanism (Lamborg and others, 2006; Bagnato and others, 2017). Hydrothermal Hg has a shorter oceanic residence time than the mixing-time of the oceans (<1000 yrs: Gill and Fitzgerald, 1988), and recent data have highlighted a limited range of Hg dispersal from hydrothermal plumes in the marine realm at the present-day (Bowman and others, 2015). Thus, the distribution of sedimentary Hg enrichments following mercury emissions from subaqueous volcanism would likely be relatively localized compared to those of emissions to the atmosphere from subaerial eruptions.

Most atmospheric gaseous elemental mercury is removed from the atmosphere via oxidation reactions (Selin, 2009), allowing the resultant Hg^{2+} to be precipitated in aqueous compounds, with a portion also deposited as particulate matter. In the terrestrial realm, both particulate and dissolved mercury can be adsorbed by tree

canopies or soils, with reduction and re-emission allowing for substantial interchange between the two reservoirs (reviewed in Munthe and others, 2009). Notably, vegetation type can play a significant role in the extent of mercury drawdown in the terrestrial realm, with coniferous trees thought to take up more of the element into both foliage and woody tissues than deciduous species (Obrist and others, 2012). Ultimately, terrestrial mercury may either be deposited into soils or peats, or carried into the aquatic realm as runoff.

In both marine and reducing freshwater (for example, lakes and wetlands) aquatic realms, mercury can be influenced by both biotic and abiotic processes, several of which result in the conversion of oxidized mercury to monomethyl-mercury or dimethyl-mercury (Benoit and others, 2001; Ravichandran, 2004; Emili and others, 2011). These geochemical species have a considerable affinity for organic matter. Consequently, Hg is typically transferred into sediments in organo-Hg complexes, resulting in a relatively consistent sedimentary Hg/TOC ratio at any one location under stable conditions (for example, Outridge and others, 2007; Liu and others, 2012; Ruiz and Tomiyasu, 2015). As a result, mercury concentrations in the sedimentary record are typically normalized against the total organic carbon (TOC) content of the sediment, so that relatively elevated Hg/TOC may point to the Hg present being derived from an external source such as volcanism, rather than simply an increased flux of organic matter drawing-down additional Hg to sediments (Sanei and others, 2012; Grasby and others, 2013; Percival and others, 2015). Additional sinks, in particular those involving reactions of Hg with sulfides or clay minerals, may also influence the deposition of mercury under certain conditions (Krupp, 1988; Benoit and others, 1999; Kongchum and others, 2011; Jin and Liebezeit, 2013). Examples of such environments are euxinic basins characterized by the presence of a sulfidic water column, or areas dominated by alluvial runoff.

Environmental and Volcanic Influences on the Sedimentary Record of Atmospheric Hg

Despite the promise of sedimentary Hg/TOC as a tracer of large-scale volcanism, it has been suggested that specific sedimentological processes might impact the mercury archive. In well-oxygenated environments where there is little organic matter, sulfide, or clays, mercury drawdown is likely to be limited (Mason and others, 2000; Percival and others, 2015). Conversely, sediments that record an abrupt transition to very organic-rich facies may result in TOC contents rising more than available Hg concentrations, overprinting the mercury signal and creating an apparent decrease in Hg/TOC ratios (Percival and others, 2015; Charbonnier and Föllmi, 2017). Sedimentary mercury also appears to have been relatively enriched in terrestrial or near-shore sediments compared to fully marine sediments during latest Triassic and early Toarcian times, both in terms of background values and in the magnitude of perturbations (Percival and others, 2015, 2017).

Recently, the importance of local processes and paleoenvironmental context on Hg records has also been indicated by mercury-isotope records. Two end-Permian sedimentary records, both with excursions in Hg/TOC ratios attributed to Siberian Trap volcanism, were found to record significantly different trends in Hg isotopes (Grasby and others, 2017). The marked contrasts in paleoenvironment inferred from the two sedimentary records were suggested to be the cause of the differences in the observed Hg-isotope trends, with one record dominated by atmospheric deposition of mercury, the other by mercury influx from terrestrial runoff and/or detrital input of ash from wildfires (Grasby and others, 2017; Thibodeau and Bergquist, 2017).

In addition to uncertainties in the depositional processes governing sedimentary Hg concentrations, the influence of processes at the volcanic source on delivering Hg to the oceans and atmosphere also remains unclear. LIPs show considerable variability in terms of their tectonic setting, intruded country rock, and style of volcanism

associated with emplacement (Bryan and others, 2010). It is not known whether certain volcanic processes might influence the extent to which LIP eruptions will perturb the global Hg inventory. Given the large variation in tectonic and volcanic contexts across individual LIPs, such information is crucial in understanding their influence on the Hg cycle. Three major factors operating at the volcanic source that are likely to influence the sedimentary Hg record are discussed here: (i) the importance of subaerial *vs* submarine volcanism (and associated emissions); (ii) the fraction of explosive *vs* effusive eruptions during LIP formation and its impact on the dispersal of volcanic mercury; (iii) the possibility of thermogenic mercury release from heating of organic-rich country rocks by intruding LIP magmas.

Gaining insight into which volcanic processes are important for increasing mercury emission and dispersion, and which sedimentary controls influence the stratigraphic record of such fluxes, represents a crucial step in the understanding of the element as a potential proxy of LIP volcanism. Here, Hg records from multiple sedimentary archives recording OAE 2 and the K–Pg, encompassing a range of sedimentary facies, are presented and compared with each other and with published Hg trends from other geological events. The OAE 2 and K–Pg mercury records will be compared directly to the sedimentary $Os_{(i)}$ records of the same events, to assess the differences between the two volcanic proxies. Through these analyses, the importance of specific volcanic processes in producing a (volcanogenic) perturbation of the Hg cycle, and how local paleoenvironmental factors might influence a sedimentary record of the global mercury inventory, are investigated. Of particular interest is: (i) whether certain sedimentary facies, with or without lithological variations, impede reconstruction of changes to the global Hg cycle; and (ii) whether all LIP eruptions manifestly produce major Hg emissions, or if the ability to perturb the global Hg cycle depends on a specific style of volcanism such as those outlined above.

STUDIED EVENTS AND RECORDS

End-Cretaceous Extinction

The end of the Cretaceous Period (66.0 Ma) marked the conclusion of the Mesozoic Era and witnessed the extinction of up to two-thirds of species, including, most famously, the non-avian dinosaurs (reviewed in Brusatte and others, 2015). The majority of extinctions appear to have occurred abruptly at the end of the Cretaceous, coincident with the impact of an extra-terrestrial object, as well as an apparent increase in the volcanic activity of the Deccan Traps (Alvarez and others, 1980; Hildebrand and others, 1991; Smit, 1999; Renne and others, 2015). However, there have also been claims for more gradual climate degradation and extinctions (Li and Keller, 1998a; Abramovich and Keller, 2002) supported by evidence for climate warming and changes to climate sensitivity throughout the final 300 to 400 kyr of the Maastrichtian (for example, Li and Keller, 1998b; Tobin and others, 2012; Batenburg and others, 2012, 2014; Woelders and others, 2017).

Latest Cretaceous warming has been linked to the main phase of emplacement of the Deccan Traps, dated to have begun at ~66.3 Ma, 300 kyr prior to the K–Pg boundary and approximately coincident with the C30N/C29R paleomagnetic reversal (for example, Wellman and McElhinny, 1970; Courtillot and others, 1986; Duncan and Pyle, 1988; Chenet and others, 2007, 2008, 2009; Jay and others, 2009; Renne and others, 2015; Schoene and others, 2015; Barnet and others, 2017). A decrease in $^{187}Os/^{188}Os$ ratios beginning at the C30N/C29R boundary in multiple stratigraphic records has been interpreted as being caused by weathering of juvenile Deccan basalts, supporting an onset of Deccan volcanism significantly prior to the extinction (Ravizza and Peucker-Ehrenbrink, 2003; Robinson and others, 2009). However, there is evidence of a substantial increase in volcanic intensity and erupted basalt volume

coincident with the end-Cretaceous extinction itself (Renne and others, 2015). Significant excursions in Hg/TOC around the K–Pg boundary at Bidart (France) and Elles (Tunisia) may reflect this phenomenon (Font and others, 2016; Keller and others, 2018). Hg/TOC increases have also been reported from other records of the K–Pg (Sial and others, 2016; Font and others, 2018; Keller and others, 2018), but are often either less clear or occur in sedimentary archives missing part of the K–Pg sequence. Most crucially however, no end-Cretaceous Hg study has interrogated the C30N/C29R boundary to establish whether the global mercury cycle was perturbed by the onset of the Deccan Trap volcanism, in addition to the potentially more intense eruptive phase around the time of the extinction.

Four uppermost Cretaceous sedimentary records were analyzed for Hg concentrations and Hg/TOC ratios (fig. 4A): Seymour Island (Antarctica), ODP Leg 174AX Bass River Site (New Jersey, USA), Zumaia (Spain), and the Hell Creek Formation at East Gilbert Creek (Montana, USA).

Seymour Island (Antarctica).—Seymour Island samples for this study derive from the British Antarctic Survey composite sections D5, D6, and D9 of the López de Bertodano Formation, described by Bowman and others (2012) and Witts and others (2016). The López de Bertodano Formation records an extremely expanded and lithologically consistent record of latest Maastrichtian to earliest Paleogene time, deposited in a back-arc basin (Crame and others, 1991). The facies consist chiefly of very fine (mud–silt) siliciclastics with negligible carbonate (Macellari, 1988; Crame and others, 2004), and low TOC contents (0.2–0.4 wt%; fig. 5A). An excellent organic-walled dinoflagellate cyst record, a documented spike in iridium concentration, and a detailed magnetostratigraphy with a well-established C30N/C29R boundary allows good temporal correlation with other uppermost Cretaceous records (Elliot and others, 1994; Bowman and others, 2012; Tobin and others, 2012). Oxygen-isotope and clumped-isotope data indicate a warming event at the C30N/C29R reversal that has been linked to Deccan volcanic activity (Tobin and others, 2012; Petersen and others, 2016). However, this warming appears to have had a limited impact on Antarctic fauna, with no significant changes observed in uppermost Maastrichtian taxa up until the end-Cretaceous extinction horizon (Witts and others, 2016).

ODP Leg 174AX Bass River (New Jersey, USA).—ODP Leg 174AX cored Cretaceous–Neogene sediments following drilling at Bass River State Forest (New Jersey, USA), including the Cretaceous–Paleogene transition and end-Cretaceous extinction horizon. The Maastrichtian sediments are lithologically homogeneous, typically consisting of glauconitic sands and clays, and containing ~1 weight percent TOC (Miller and others, 1998; this study). The K–Pg boundary marks the base of a spherule-rich layer, as well as a spike in iridium concentrations (Olsson and others, 2002). In the uppermost 2 m of the Cretaceous strata there are also records of changes in the planktonic foraminiferal community and excursions in $\delta^{18}O$ and Mg/Ca values, which are all suggestive of warming, interpreted as caused by Deccan Trap volcanism (Olsson and others, 2002). Temporal constraints on the Bass River record are poor, but the *M. prinsii* nannofossil Zone extends to at least 385.5 m depth, indicating that the C29R strata extend to at least that level on the basis of the lowest occurence of *M. prinsii* within C29R strata at other locations (Gardin and others, 2012; Thibault and others, 2012). A recovery gap at 385.5 m depth introduces stratigraphic uncertainty, but by comparing the pattern of warming deduced from oxygen isotopes at Bass River with records from other K–Pg sequences (Tobin and others, 2012; Birch and others, 2016; Petersen and others, 2016), the C30N/C29R boundary is tentatively positioned at approximately 386 m (see full correlation in Appendix fig. A1). Consequently, it is likely that the lower samples analyzed in this study are from C30N strata.

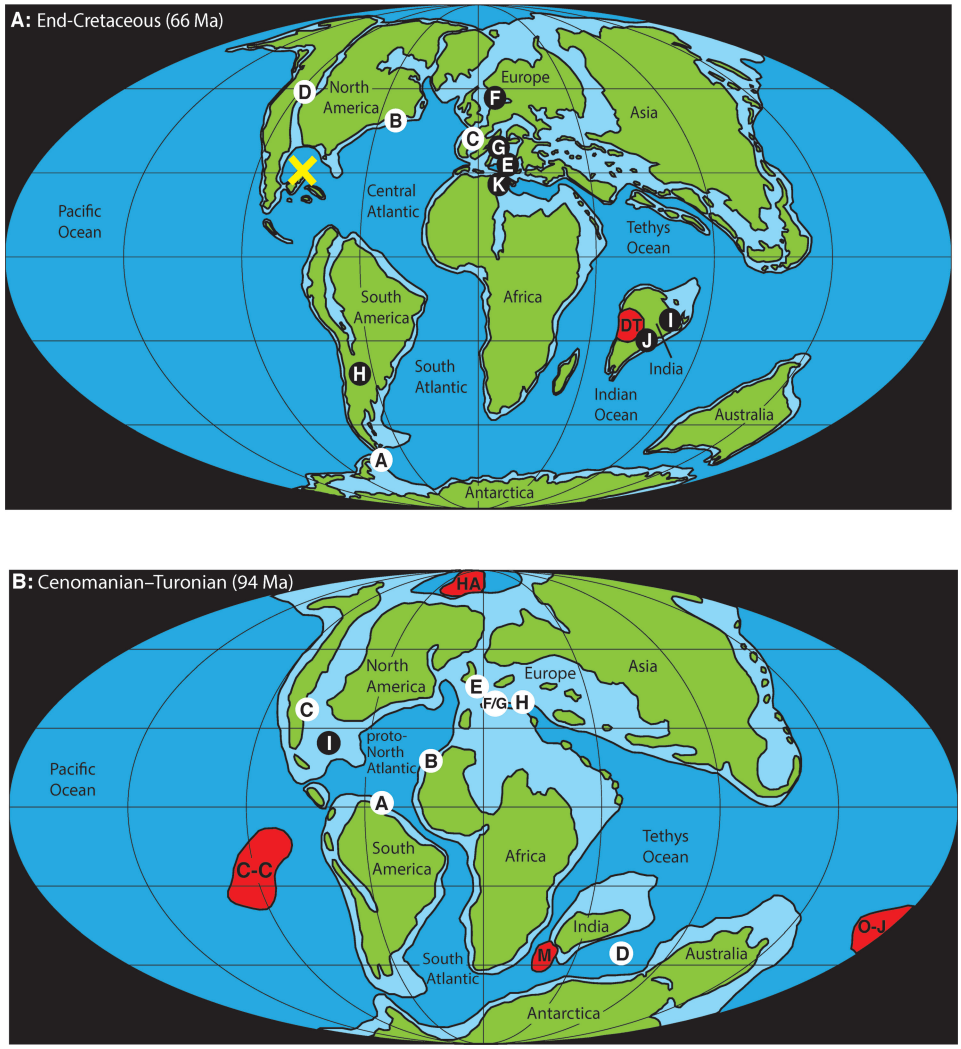

Fig. 4. Paleogeographic maps of the end-Cretaceous and Cenomanian–Turonian worlds, indicating the geographical position of LIPs emplaced at those times, and the locations of sedimentary records analyzed for mercury in this study (white circles), or previously published studies (black circles). (A) Paleogeographic map of the end-Cretaceous world. Sedimentary records studied for mercury are indicated as follows: A – Seymour Island (Antarctica); B – ODP Leg 174AX Bass River (New Jersey, USA); C – Zumaia (Spain: also marks the location of the French Bidart section studied in Font and others, 2016); D – Montana (USA); E: Bottaccione Gorge (Italy); F – Stevns Klint (Denmark); G – Padriciano (Italy); H – Bajada del Jäguel (Argentina); I – Meghalaya (India); J – Jhilmili (India); K – El Kef and Elles (Keller and others, 2018). All of the records E–J are documented in Sial and others (2016). The positions of the Deccan Traps (DT) and Chicxulub impact crater (X) are also indicated. (B) Paleogeographic map of the Cenomanian–Turonian world, indicating the location of the sedimentary records studied for mercury, and the Large Igneous Provinces dated to approximately equivalent age. The sedimentary records are indicated as follows: A – ODP Site 1260 (Demerara Rise: also the location of ODP Site 1258 studied in Scaife and others, 2017); B – Tarfaya (Morocco); C – Utah (USA); D – IODP Site 1138 (Kerguelen Plateau); E – Eastbourne (UK); F – Pont d'Issole and Vergons (south-east France); G – Clot Chevalier (south-east France); H – Furlo (Italy); I – Maverick Basin (Texas, USA) studied by Scaife and others (2017). Cenomanian–Turonian Igneous Provinces are indicated as follows: C-C – Caribbean–Columbian Plateau; HA – High Arctic LIP; M – Madagascan Province; O-J – Ontong Java Plateau. Both paleogeographical reconstructions are based on those of Ron Blakey (http://cpgeosystems.com).

Zumaia (Spain).—The coastal section below the town of Zumaia (also Zumaya), on the northeastern coast of Spain, is a reference section for the K–Pg interval. This study uses samples described by Batenburg and others (2012). The uppermost Cretaceous sediments consist of reddish-gray to purple marls and marly limestones with a minor amount of intercalated calcareous turbidites. These marine sediments were deposited in a hemipelagic setting in the relatively narrow Basque-Cantabric Basin (Pujalte and others, 1995). The rhythmic alternation of lithologies likely reflects the pacing of late Maastrichtian climate by eccentricity-modulated precession, which has been used to refine the geological time scale (Batenburg and others, 2012). The astrochronology provides ages for planktonic foraminifera and calcareous nannofossil events, bulk carbonate carbon-isotope variations, as well as the base of magnetochron C29R, which has been correlated based on individual limestone-marl alternations (Batenburg and others, 2012, 2014) and is consistent with other estimates (for example, Schoene and others, 2015; Barnet and others, 2017; Woelders and others, 2017). The K–Pg boundary itself is marked by both a clear biostratigraphic change and a clay layer characteristic of this stratigraphic horizon (Pujalte and others, 1995; Molina and others 2009).

A recent study documented sporadic peaks in mercury content in the uppermost 5 m of Cretaceous strata (Font and others, 2018). However, the strata investigated by Font and others (2018) represent only the last 100 kyr of the Cretaceous Period according to the timescale of Batenburg and others (2012), and thus do not necessarily demonstrate a clear enrichment in sedimentary Hg content compared to pre-Deccan times. For this study, samples up to 25 m below the K–Pg boundary are investigated, allowing sedimentary Hg content to be compared across strata deposited both prior to (within C30N) and during Deccan Trap emplacement.

East Gilbert Creek (Garfield County, Montana, USA).—The uppermost Cretaceous Hell Creek Formation is preserved across Montana, North Dakota, and South Dakota, and provides a terrestrial (fluvial/flood plain) record of the latest Cretaceous interval, with a number of widespread, stratigraphically continuous coal beds. In the uppermost part of the Hell Creek Formation the two main coal beds are the Null Coal and the Z Coal, with a small coal unit (the IrZ) just below the Z Coal (summarized in Sprain and others, 2015). The IrZ coal has been found to contain an iridium-rich clay, confirming that it marks the end-Cretaceous extinction (Alvarez, 1983; Smit and Van Der Kaars, 1984). Both the Null and IrZ coals contain tephras, which have been Ar-Ar dated to 66.289 Ma, and 66.052 Ma, respectively (Sprain and others, 2015, 2018). The uppermost Hell Creek Formation also records a negative excursion in carbon isotopes of organic matter of approximately 2 permil, thought to be equivalent with the $\delta^{13}C$ negative excursion documented at the end-Cretaceous extinction horizon in marine records (Arens and Jahren, 2000; Arens and others, 2014). The 66.289 Ma age of the Null Coal tephra matches the U-Pb date of a volcanic ash deposited within C29R strata in Colorado (Clyde and others, 2016), suggesting that the C30N/C29R boundary lies slightly below the Null Coal. A recent study has positioned the C30N/C29R boundary ~2 m below the Null Coal in sections 15 to 20 km to the east of East Gilbert Creek (Sprain and others, 2018), confirming that C29R strata extend stratigraphically from the Cretaceous–Paleogene boundary down to the Null Coal and slightly lower.

New samples for this study were collected from between 2 m below the Null Coal to 2 m above the Z Coal at East Gilbert Creek (47°40'03"N; 106°30'27"W), encompassing the uppermost Hell Creek Formation and lowermost Fort Union Member above (see Appendix fig. A2). These strata also include the K–Pg boundary but, at the time of sampling (August 2014), the C30N/C29R boundary was thought to be positioned above the Null Coal in a thick sand unit (LeCain and others, 2014). Thus, only six samples were taken from below the Null Coal and, based on more recent magnetostrati-

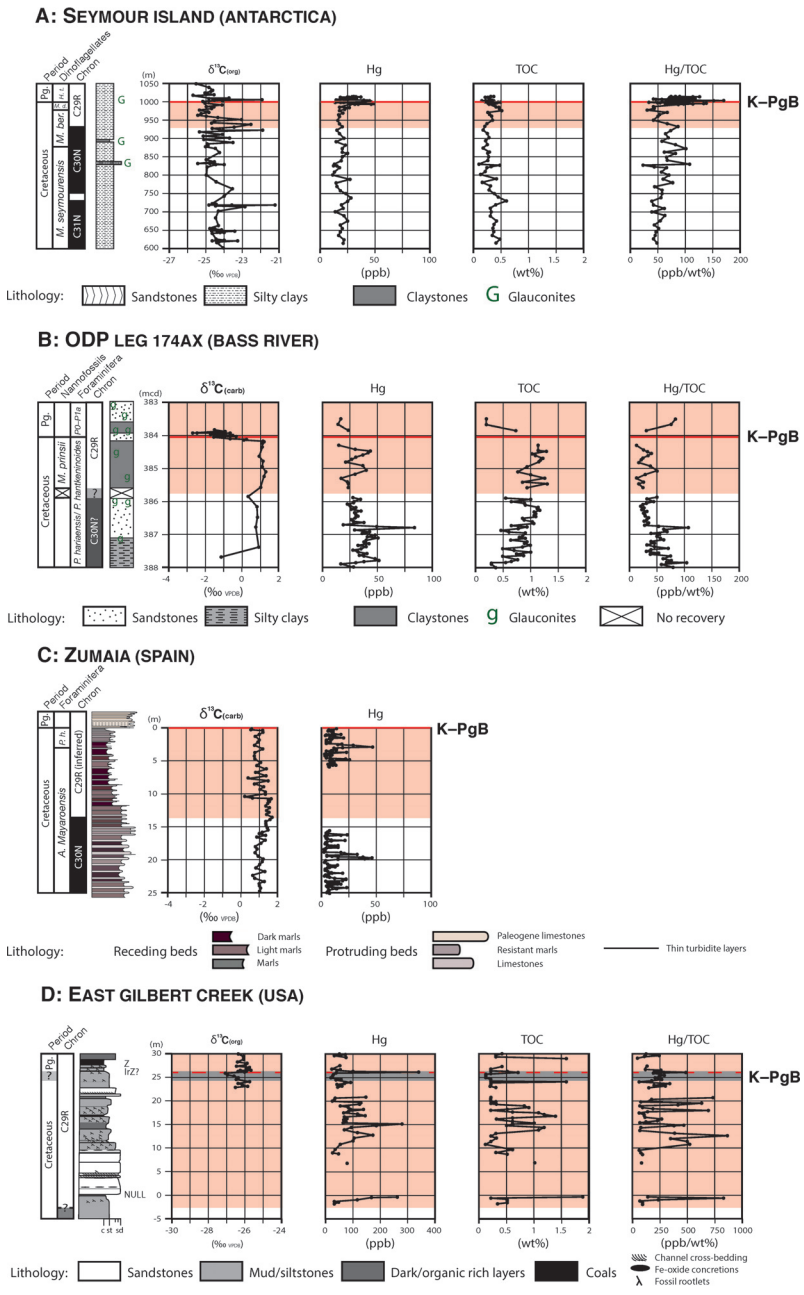

Fig. 5. Raw data plots for $\delta^{13}C$, Hg and TOC abundances, and Hg/TOC ratios, from the 4 sedimentary records of the K–Pg transition investigated in this study. Note the expanded Hg/TOC scale for East Gilbert Creek. Red shading indicates the stratigraphic extent of sediments deposited coevally with Deccan volcanism (assuming commencement at the C30N/C29R paleomagnetic reversal). The bold red line indicates the stratigraphic position of the K–Pg boundary at Seymour Island, Bass River, and Zumaia (marked K–PgB). The gray shading with dashed red line marks the stratigraphic uncertainty of the K–Pg boundary at East Gilbert Creek (the dashed red line marks the stratigraphic position of the assumed IrZ coal that marks the K–Pg boundary elsewhere in Montana). All vertical scales are in meters. Lithological data are sourced as follows: Seymour Island from Witts and others (2015); Bass River adapted from Miller and others (1998); Zumaia from Batenburg and others (2012); East Gilbert Creek from this study. Biostratigraphic data are

graphic interpretations (Clyde and others, 2016; Sprain and others, 2018), they do not include sediments from below the C30N/C29R boundary.

OAE 2

The Cenomanian–Turonian boundary (~94 Ma) witnessed the development of anoxic–euxinic conditions in numerous marine basins across the globe, particularly in the Atlantic and Tethyan realms. The development of anoxic–euxinic conditions is typically recorded by the abrupt appearance of meter-thick millimeter-laminated black shale units intercalated between less organic-rich lithologies (reviewed in Jenkyns, 2010). Global-scale organic-carbon burial at that time is supported by a large (up to 6‰) positive excursion in $\delta^{13}C$ in organic matter ($\delta^{13}C_{org}$), with a somewhat smaller positive excursion recorded in carbonates ($\delta^{13}C_{carb}$) (Schlanger and Jenkyns, 1976; Tsikos and others, 2004; Erbacher and others, 2005; Jarvis and others, 2011). Sedimentary enrichment of numerous redox-sensitive trace metals further indicates widespread anoxic conditions that would permit such high levels of organic-matter burial (for example, Turgeon and Brumsack, 2006; Jenkyns and others, 2007, 2017; Jenkyns, 2010; Westermann and others, 2014; Dickson and others, 2016, 2017).

There is geochemical evidence for substantial warming during OAE 2 (for example, Voigt and others, 2004, 2006; Forster and others, 2007), and enhanced rates of continental weathering leading to an influx of nutrients to the marine shelf (for example, Mort and others, 2007; Blättler and others, 2011; Pogge von Strandmann and others, 2013; Charbonnier and others, 2018b), assumed to be responses to LIP volcanic activity. However, at least one global cooling and re-oxygenation episode also took place during the OAE, dubbed the Plenus Cold Event (Gale and Christensen, 1996; Pearce and others, 2009; Jarvis and others, 2011; Jenkyns and others, 2017).

The Caribbean–Columbian Plateau, High Arctic LIP, Ontong-Java Plateau, and Madagascan Province have all been dated as being volcanically active around the time of OAE 2 (Storey and others, 1995; Neal and others, 1997; Courtillot and Renne, 2003; Snow and others, 2005; Turgeon and Creaser, 2008; Tegner and others, 2011; Kingsbury and others, 2018). A decrease in sedimentary $^{187}Os/^{188}Os$ ratios observed across the globe is further evidence for LIP emplacement during OAE 2 (Turgeon and Creaser, 2008; Du Vivier and others, 2014, 2015), and mercury enrichments have also been reported from the southern part of the Western Interior Seaway and ODP Site 1258 on Demerara Rise (Scaife and others, 2017). Large-scale volcanism during OAE 2 has also been inferred from an increased concentration of trace metals associated with hydrothermal activity in the interval of the Plenus Cold Event in some records (Orth and others, 1993; Snow and others 2005; Eldrett and others, 2014; Jenkyns and others, 2017), as well as studies of sedimentary neodymium, chromium, and zinc isotopes (Zheng and others, 2013; Holmden and others, 2016; Sweere and others, 2018).

Eight sedimentary records of OAE 2 were analyzed for Hg/TOC trends (fig. 4B): two from the Atlantic (ODP Site 1260 on the Demerara Rise, and Tarfaya, Morocco); three from the margins of the Tethys (Clot Chevalier, a composite record of Pont d'Issole and Vergons, all from south-east France, and Furlo, Umbria-Marche, Italy);

Fig. 5 (continued). sourced as follows: Seymour Island from Witts and others (2015); Bass River from Miller and others (1998) and Esmeray-Senlet and others (2015); Zumaia from Batenburg and others (2012). Magnetostratigraphic data for Seymour Island is sourced from Tobin and others (2012); and for Zumaia from Batenburg and others (2012). Magnetostratigraphic data for Montana is inferred from data in Clyde and others (2016) and Sprain and others (2018) (see also section introducing East Gilbert Creek). Bass River magnetostratigraphic data are inferred in this study (see section introducing Bass River). Carbon-isotope data are sourced as follows: Seymour Island from Hall and others (2018); Bass River from Esmeray-Senlet and others (2015); Zumaia from Batenburg and others (2012); East Gilbert Creek from this study.

and three others: a composite terrestrial record from Utah, USA; IODP Site 1138 on the Kerguelen Plateau (Indian Ocean); and Eastbourne, UK.

ODP Site 1260 (Demerara Rise, equatorial Atlantic).—Site 1260 sampled a deep pelagic paleoenvironment on the western side of the Atlantic, with the Cenomanian–Santonian interval dominated by organic-rich shales. OAE 2 is recorded by a positive excursion in $\delta^{13}C_{org}$ across a 2-m-thick interval (Erbacher and others, 2005). Numerous other geochemical studies have been conducted on the 1260 core, including osmium, neodymium, sulfur, and oxygen isotopes, TEX_{86}, and sedimentary trace-metal concentrations, from which climate warming, changes to ocean redox chemistry, and coeval volcanism have been inferred (Forster and others, 2007, 2008; Turgeon and Creaser, 2008; MacLeod and others, 2008; Hetzel and others, 2009; Martin and others, 2012). Intriguingly, the decline in sedimentary Os-isotope ratios occurs slightly below the onset level of elevated $\delta^{13}C_{org}$ values (Turgeon and Creaser, 2008), consistent with the hypothesis that Ocean Plateau emplacement and associated volcanism/basalt-seawater interactions were the trigger for OAE 2 (for example, Turgeon and Creaser, 2008; Jenkyns and others, 2017).

Tarfaya core S57 (Morocco).—The S57 core from Tarfaya preserves an expanded record of a somewhat shallower-water marine environment, predominantly consisting of marls with variable carbonate and organic-matter content (1–25 wt% TOC) deposited beneath an anoxic–euxinic watermass (Tsikos and others, 2004; Kolonic and others, 2005; Mort and others, 2008; Poulton and others, 2015; Dickson and others, 2016). Strong cyclostratigraphic signals are recorded, initially attributed to 20-kyr precession and 40-kyr obliquity forcing (Kuhnt and others, 1997), but later reinterpreted as the effect of obliquity and 100-kyr eccentricity (Meyers and others, 2012a). An abrupt positive excursion is recorded in the $\delta^{13}C$ composition of co-existing carbonates and organic matter (Tsikos and others, 2004; Kuhnt and others, 2017).

Utah composite record (USA).—The composite section of the Dakota Formation established by Barclay and others (2010) in southwestern Utah preserves a record of the coastal and terrestrial environments along the western edge of the Western Interior Seaway, and has long been attributed to the Upper Cenomanian and Lower Turonian (Averitt, 1962; Peterson, 1969). Subsequent work focused on creating a detailed correlation of the landward limit of Cenomanian–Turonian strata in southwestern Utah to the marine global stratotype of the stage boundary in central Colorado (Meyers and others, 2012b). This correlation, first achieved using limestone and bentonite marker beds and ammonite and bivalve biostratigraphy (Elder and others, 1994), has subsequently been improved using a combination of higher resolution outcrop and well-log data that allowed correlation at the bed scale (Laurin and Sageman, 2001, 2007). The presence of an OAE 2 record in SW Utah was confirmed by recognition of a 4 permil positive $\delta^{13}C$ excursion in dispersed organic matter within the *Sciponoceras gracile* biozone, consistent with the organic-matter $\delta^{13}C$ record in the Colorado GSSP (Barclay and others, 2010). Stomatal index data from plant fossils were used to reconstruct atmospheric pCO_2 during the Late Cenomanian in these sections (Barclay and others, 2010), which suggest an overall increase in pCO_2, peaking just before the onset of the $\delta^{13}C$ positive excursion (Barclay and others, 2015). Several second-order decreases in pCO_2 superimposed on this overall rise mirror changes in the $\delta^{13}C$ record, supporting a carbon-cycle perturbation coincident with OAE 2 (Barclay and others, 2010).

Importantly, the paralic nature of these sediments means that the organic matter present is predominantly terrestrial in origin, the only known record of OAE 2 where this is the case. Therefore, if the atmospheric Hg inventory was perturbed during OAE 2, it should have been recorded at this location.

IODP Site 1138 (Kerguelen Plateau, Indian Ocean).—Site 1138 sampled one of the few known southern hemisphere records of OAE 2. The site is located on the Kerguelen Plateau, which was largely emplaced on the Indian Ocean crust during the Early Cretaceous, though with some further emplacement in the Late Cretaceous and Cenozoic (Frey and others, 2002; Mohr and others, 2002). The sediments record a marine environment, with a transition from shallow- to deep-marine deposits through the Upper Cretaceous. However, the presence of terrestrial organic matter including pollen, spores and wood fragments in parts of the core indicates the proximity of land for part of the depositional history (Frey and others, 2002; Meyers and others, 2009). A positive excursion in the $\delta^{13}C$ composition of organic matter marks the second half of OAE 2, with foraminiferal and nannofossil biostratigraphy indicating a hiatus that includes the lower part of the OAE record, up to the top of the predicted level of the Plenus Cold Event (Dickson and others, 2017). Elevated TOC abundances generally occur throughout the OAE 2 interval, although the onset level of TOC enrichment is half-a-meter higher than that of the $\delta^{13}C$ excursion. This $\delta^{13}C$ shift also correlates with changes in trace-metal concentrations and molybdenum-isotope ratios (Dickson and others, 2017), indicating increased marine anoxia (although not euxinia) on the Kerguelen Plateau during OAE 2.

Eastbourne (S.E. England, UK).—The Cenomanian–Turonian succession at Eastbourne consists predominantly of foraminiferal-nannofossil chalk, and OAE 2 is marked by a clear lithological change to the more argillaceous Plenus Marls (for example, Jefferies, 1963; Tsikos and others, 2004). The Plenus Marls record a broad increase in $\delta^{13}C_{carb}$, continuing into the immediately overlying chalk, with a smaller negative excursion superimposed upon it (Gale and others, 1993; Tsikos and others, 2004). $\delta^{18}O$ data indicate warming during the onset of OAE 2, with two phases of subsequent cooling during the Plenus Cold Event before the mid-point of the OAE (Paul and others, 1999; Pearce and others, 2009; Jenkyns and others, 2017). Calcium and lithium isotopes suggest increased rates of weathering during the OAE, with a consequential influx of nutrients indicated by phosphorus enrichment (Mort and others, 2007; Blättler and others, 2011; Pogge von Strandmann and others, 2013). Neodymium-isotope data suggest the invasion of a boreal watermass at the onset of OAE 2, with a radiogenic shift during the Plenus Cold Event, possibly carrying the mafic signature of the High Arctic LIP (Zheng and others, 2013).

Pont d'Issole and Vergons composite record (S.E. France).—Sediments at Pont d'Issole and the stratigraphically underlying Vergons sections were deposited in the Vocontian Basin on the north-western margin of the Tethys, and are dominated by limestone-marl alternations reflecting a fluctuating hemipelagic environment (Crumière and others, 1990; Grosheny and others, 2006). For this study, the two sections were combined to give a composite record with the bottom of the 'Niveau Thomel' organic-rich strata at the base of Pont d'Issole assumed to be equivalent to the same organic-rich sediments at the top of the Vergons sequence. These laminated organic-rich black shales mark the OAE 2 interval, and document an increase in TOC content from 0.2 to 0.3 weight percent below the OAE level to 2 to 3 weight percent within them (Jarvis and others, 2011). A 2 permil positive excursion is recorded in the $\delta^{13}C$ compositions of both carbonate and bulk organic matter but, intriguingly, the base of both excursions lies markedly above the base of the black shales (Jarvis and others, 2011). The position of the Plenus Cold Event is also indicated at Pont d'Issole by a relative decrease in $\delta^{13}C$ values of both organic matter and carbonate in the middle of the positive $\delta^{13}C$ excursion characteristic of the OAE. As at ODP Site 1260, an abrupt decline in sedimentary $Os_{(i)}$ is recorded below the $\delta^{13}C$ positive excursion (Du Vivier and others, 2014). However, the more expanded nature of the Pont d'Issole–Vergons record highlights the offset between the shifts in C- and Os-isotope values much more

clearly than the record at Site 1260, strongly indicating that the onset of submarine volcanism/basalt-seawater interaction predated OAE 2 (Du Vivier and others, 2014).

Clot Chevalier (S.E. France).—Clot Chevalier also records a hemipelagic environment from the Vocontian Basin, on the northwestern margin of the Tethys, described by Falzoni and others (2016). The succession consists of alternating limestones and marlstones, with OAE 2 indicated by the transition from organic-lean (0.1–0.2 wt% TOC) limestones to more organic-rich marls (1–2 wt% TOC) and a broad, positive excursion in $\delta^{13}C_{carb}$ (Falzoni and others, 2016; Gale and others, 2018). The positive excursion in $\delta^{13}C$ is punctuated by multiple small negative excursions.

Furlo (Italy).—The abandoned quarry at Furlo (Umbria–Marche Apennines) records uppermost Cenomanian to lowest Turonian sediments deposited on the southern margin of the Tethys, and has been described by Beaudoin and others (1996) and Gambacorta and others (2015). The sediments consist of regularly bedded pelagic limestones and marls with thin to very thin (<1–10 cm) sporadic layers of black heterogeneous cherts and organic-rich shales, which are locally discontinuous. A much thicker (~1 m) band of organic-rich shales records the Bonarelli Level, marking OAE 2 and documenting a positive excursion in organic-matter $\delta^{13}C$. As for ODP Site 1260, numerous other geochemical studies have been conducted on samples from Furlo, with phosphorus and iron speciation, and nitrogen-, sulfur-, iron-, osmium- and molybdenum-isotope data all showing perturbations at the Bonarelli Level, supporting the influence of distal volcanism, and nutrient influx and marine anoxia, at that location during OAE 2 (Turgeon and Brumsack, 2006; Jenkyns and others, 2007; Mort and others, 2007; Turgeon and Creaser, 2008; Du Vivier and others, 2014; Westermann and others, 2014; Owens and others, 2017).

METHODS

Mercury analyses were performed on a RA-915 Portable Mercury Analyzer with PYRO-915 Pyrolyzer, Lumex, at the University of Oxford, based on the methods described in Percival and others (2017). New TOC content data were measured using either a Strohlein Coulomat 702 (methodology in Jenkyns, 1988) or Rock-Eval VI (following the methods in Espitalié and others, 1977, and Behar and others, 2001) at the University of Oxford. Reproducibility of the Hg concentrations was within ±10 percent.

New end-Cretaceous carbon-isotope data for bulk organic matter were generated on samples from East Gilbert Creek (Montana, USA) that were decarbonated with 3M HCl in a 80 °C water bath for 5 hours, before being rinsed and centrifuged at least three times to reach a neutral pH. The isotopic analyses were performed on a SERCON 20-22 IRMS, coupled to a SERCON GLS, in the School of Archaeology, University of Oxford. An internal Alanine standard was used, with a $\delta^{13}C_{org}$ value of −27.1 permil. Five standards were analyzed at the beginning of a sample-set run, with an additional two standards measured after each set of seven sample determinations. Twenty-six measured standards averaged −27.09 permil, with a standard deviation of 0.15 permil. New carbonate carbon-isotope data for Vergons samples from the Pont d'Issole and Vergons composite record were generated using a VG mass Isocarb device and Prism mass spectrometer at the University of Oxford, following the methods laid out in Jenkyns and others (1994). Reproducibility of replicate analyses and internal standards was generally better than 0.1 permil. The Al_2O_3 content of samples from Zumaia was determined by X-Ray Fluorescence of pressed-powder pellets at the School of Science, University of Greenwich, United Kingdom.

Carbon-isotope, TOC, Hg, and Hg/TOC results from the uppermost Cretaceous sections are displayed in figure 5, and those from the OAE 2 level in figure 6.

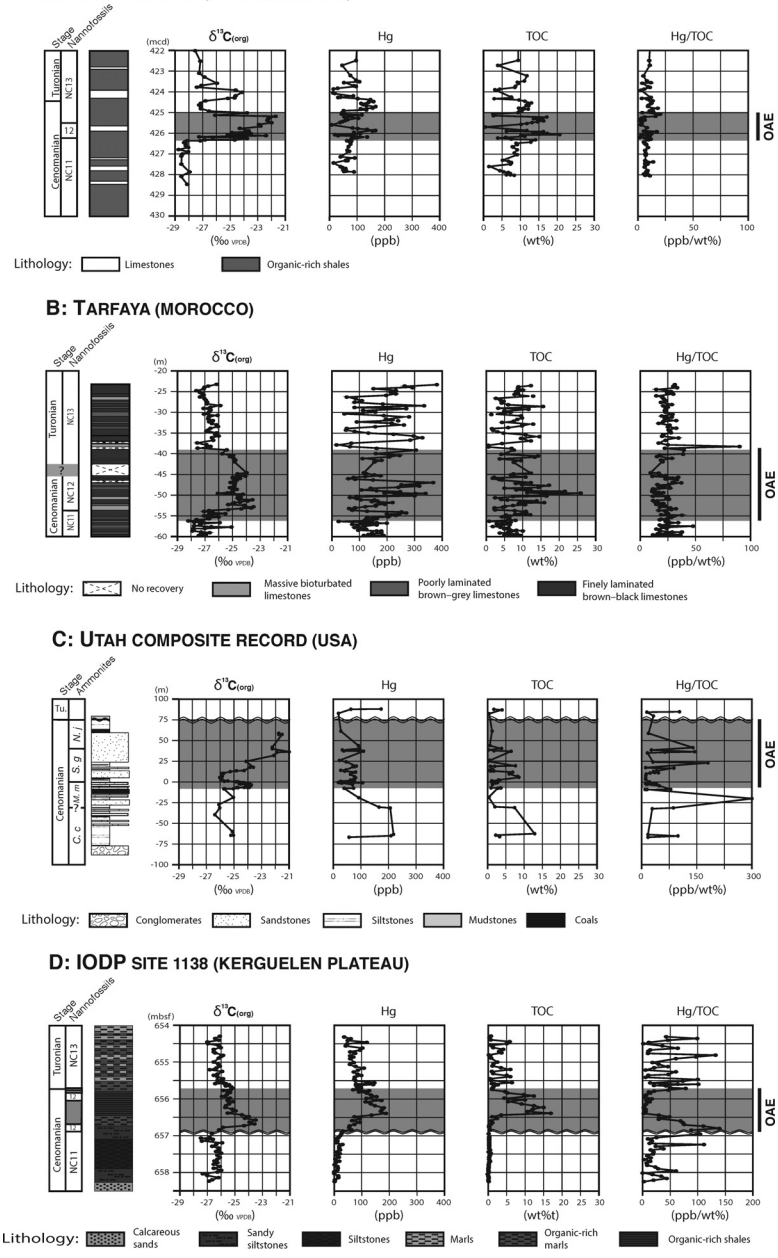

Fig. 6. Raw data plots for $\delta^{13}C$, Hg and TOC abundances, and Hg/TOC ratios, from the 8 sedimentary records of OAE 2 investigated in this study. Note the changed scales for Hg concentrations for Eastbourne and Furlo, for TOC content for the Pont d'Issole and Vergons composite record and Clot Chevalier, and variable scales for Hg/TOC ratios. Gray shaded areas indicate the stratigraphic extent of the OAE as indicated by the positive excursion in carbon isotopes, typically beginning at the base of more organic-rich lithologies. All vertical scales are in meters. Tu., *R. cu.*, *H. h.*, *C. c.*, *M. m.*, *S. g.*, *and N. j.*, and 12 indicate the Turonian Stage, *R. cushmani* and *H. helvetica* foraminiferal Zones, *C. canitaurinum*, *M. mosbyense*, *S. gracile*, and *N. juddii* ammonite Zones, and NC12 calcareous nannofossil Zone, respectively. Statigraphic logs are sourced as follows: ODP Site 1260 from Forster and others (2007); Tarfaya and Eastbourne from Tsikos and others (2004); Utah from Barclay and others (2010); IODP Site 1138 and the Pont d'Issole and Vergons composite from this study; Clot Chevalier from Falzoni and others (2016); Furlo from Jenkyns and others

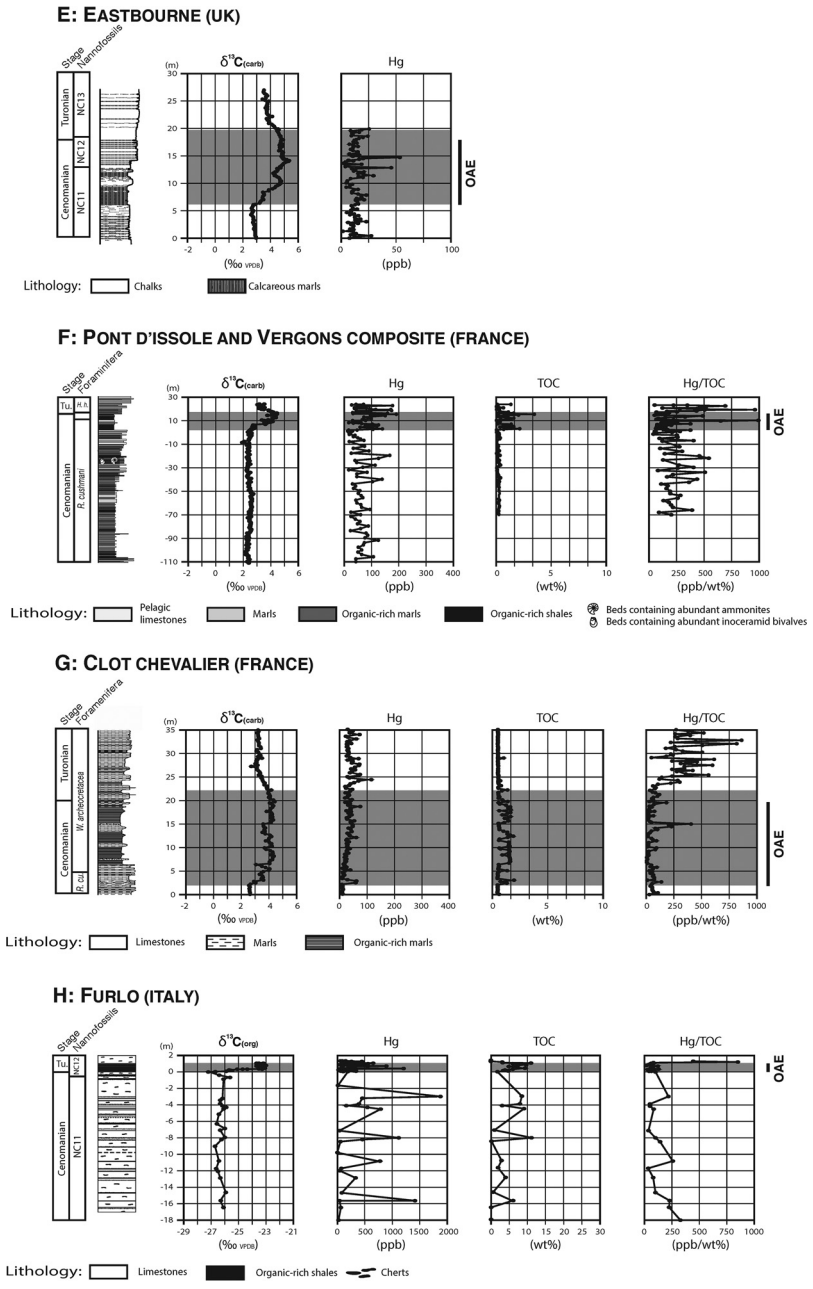

Fig. 6 (continued). (2007). Biostratigraphy is sourced as follows: ODP Site 1260 based on the correlations of Erbacher and others (2005), and Hardas and Mutterlose (2006); Tarfaya and Eastbourne from Tsikos and others (2004); Utah from Barclay and others (2010); IODP Site 1138 from Dickson and others (2017); Pont d'Issole and Vergons composite from Jarvis and others (2011); Clot Chevalier from Falzoni and others (2016); Furlo from Tsikos and others (2004), and Lanci and others (2010). Carbon-isotope data are sourced as follows: ODP Site 1260 from Forster and others (2007); Tarfaya and Eastbourne from Tsikos and others (2004); Utah from Barclay and others (2010); IODP Site 1138 from Dickson and others (2017); Clot Chevalier from Falzoni and others (2016); Furlo from Jenkyns and others (2007). Tarfaya TOC data are from Tsikos and others (2004); IODP Site 1138 TOC data are from Dickson and others (2017). Clot Chevalier TOC data are from Gale and others (2018). Pont d'Issole and Vergons composite lithology and carbon data are from Jarvis and others (2011) and this study. All other TOC data are new for this study.

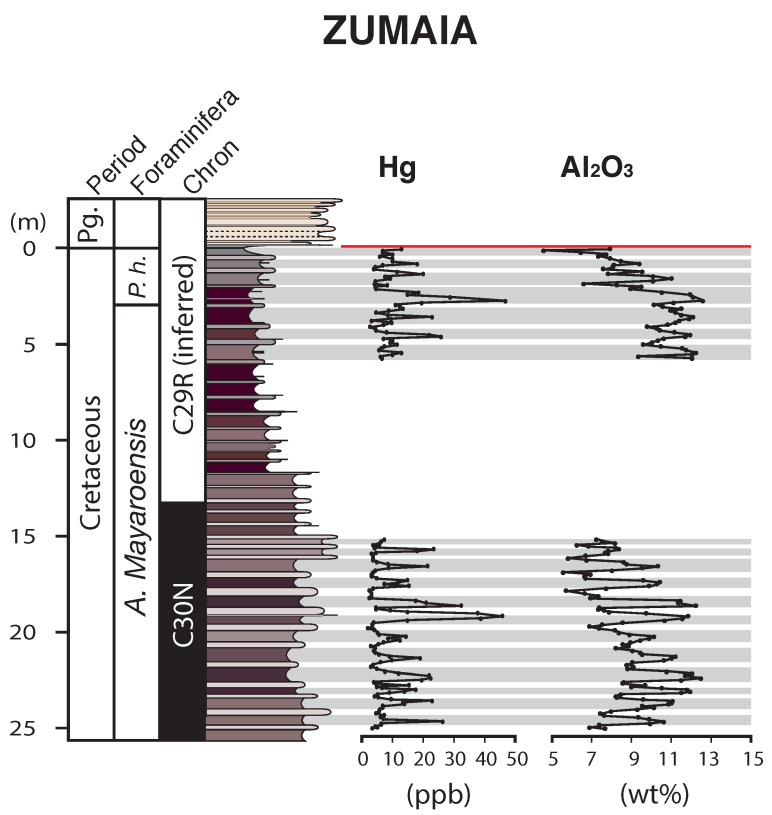

Fig. 7. Lithology, Hg concentration, and Al_2O_3 content data for Zumaia. The red line indicates the stratigraphic position of the K–Pg boundary. Gray bands indicate the marl beds, and highlight the correlation of the marly lithologies with Hg and Al_2O_3 peaks. Lithological, magnetostratigraphic, biostratigraphic data for Zumaia are from Batenburg and others (2012), see also fig. 5C; Hg and Al_2O_3 data are from this study.

Lithological and, where available, biostratigraphic data are shown, with magnetostratigraphic information also indicated for uppermost Cretaceous records. Zumaia and Eastbourne lack TOC and Hg/TOC data due to the negligible organic-matter content of samples from those locations. Where TOC content is negligible, the Hg contents were compared to aluminium (see separate fig. 7 and Appendix fig. A3). The presence or absence of mercury excursions in sedimentary records of both events (and other Phanerozoic events) is also summarized in table 1.

RESULTS

End-Cretaceous Results

A clear increase in sedimentary Hg and Hg/TOC is observed at and just below the end-Cretaceous extinction horizon at Seymour Island (fig. 5A). However, sediments from the rest of C29R show no enrichment compared to the strata in C30N and below. The Bass River extinction horizon was not available for analysis. Whilst there are variations in Hg content and Hg/TOC ratios in the inferred C29R strata at Bass River, these again do not represent a clear enrichment compared to the values from C30N strata (fig. 5B).

TABLE 1

Presence or absence of Hg records depending on location with respect to coincident LIP

				Distance of sedimentary Hg record from coincident LIP								
				TERRESTRIAL RECORDS				MARINE RECORDS				
Event	**Age (Ma)**	**Large Igneous Province (location)**	**Coverage of Hg records**	**<500km**	**500–2000 km**	**2000–5000 km**	**>5000 km**	**<500 km**	**500–2000 km**	**2000–5000 km**	**>5000 km**	**Hg references**
PETM	55	North Atlantic Province (high latitude; subaerial)	SINGLE: N. Africa							**Dababiya**		Keller and others (2018)
K–Pg (EXTINCTION RATHER THAN ENTIRETY OF C29R)	66	Deccan Traps (mid-latitude subaerial)	GLOBAL: Europe, N. America, S. America, India, Antarctica, N. Africa	Meghalaya Jhilmili			**East Gilbert Creek**		**Elles** **Bidart** *Zumaia* *El Kef* **Bottaccione** **Stevns Klint** Padriciano	Bass River Bajada del Jäguel **Seymour Island**		Font and others (2016, 2018) Sial and others (2016) Keller and others (2018) *this study*
OAE 2	94	Caribbean-Columbian Plateau Madagascan Province High Arctic Province Ontong-Java Plateau (widespread; largely submarine)	GLOBAL: Europe, N. America, Indian Ocean, Central Atlantic Ocean			*Utah*			**Maverick Basin** **Kerguelen Plateau**	**Demerara Rise**	*Eastbourne* *Pont d'Issole* *Clot Chevalier* *Tarfaya* *Furlo*	Scaife and others (2017) *this study*
OAE 1a	121	Ontong-Java Plateau (low latitude; largely submarine) ? High Arctic Province?	TETHYAN ONLY: Switzerland, France								**La Bédoule** **Glaise** **Roter Sattel**	Charbonnier and Föllmi (2017)
Valanginian	134	Paraná-Etendeka Province (mid latitude; subaerial)	TETHYS AND EUROPE Switzerland, France, Poland								**Angles** **Orpierre** *Wawal* **Breggia**	Charbonnier and others (2017)
T-OAE	183	Karoo-Ferrar Province (high latitude; subaerial)	WIDESPREAD: Europe, S. America						**Arroyo Lapa** **El Peñon**		**Peniche** *Sancerre* *Velebit* *Hawsker Bottoms* **Mochras** **Bornholm**	Percival and others (2015) Fantasia and others (2018)
T–J	201	Central Atlantic Province (low latitude; subaerial)	GLOBAL: Europe, N. America, S. America, N. Africa	**Partridge Island** Igounane		**Astartekløft**			**St Audries Bay** **Kuhjoch**	**New York Canyon** **Arroyo Malo**		Thibodeau and others (2016) Percival and others (2017)
P–T	252	Siberian Traps (high latitude; subaerial)	WIDESPREAD: Arctic, S. China						**Buchanan Lake** **Spitsbergen**		**Meishan** **Daxiakou** **Shangsi**	Sanei and others (2012) Grasby and others (2013, 2016, 2017) Wang and others (2018)
Capitanian	260	Emeishan Province (low latitude; subaerial)	SINGLE: Arctic								**Spitsbergen**	Grasby and others (2016)
Frasnian–Famennian	372	Viluy Traps (high latitude; subaerial)	WIDESPREAD: Morocco, Germany, Russia						**Syv'yu**		**Lahmida** **Kahlleite**	Racki and others (2018)
Ordovician–Silurian	444	*UNKNOWN*	WIDESPREAD: S. China, N. America					*UNKNOWN*				Gong and others (2017) Jones and others (2017)

Green bold text signifies clear Hg enrichments at that location, red italic text signifies no such clear Hg signal. Gray regular text indicates that the event horizon is missing at that location. Information on LIPs from Bryan and Ferrari (2013) and Self and others (2014).

At Zumaia (where results are limited to Hg contents only due to the paucity of sedimentary organic matter), there is no spike recorded at or just below the extinction horizon in the same pattern as Seymour Island, but several peaks in Hg content are documented in the uppermost 5 m of Cretaceous strata (fig. 5C), in agreement with the findings of Font and others (2018). However, analyses of (pre-Deccan) C30N strata also document numerous peaks in Hg of equivalent magnitude to those from C29R strata (fig. 5C). Both C29R and C30N Hg peaks at Zumaia show a marked correlation with more clay-rich beds and associated increases in Al_2O_3 content (fig. 7), both of which have been attributed to cyclical variations in terrigenous runoff to the area driven by orbital climatic forcing (Batenburg and others, 2014). Since the Hg peaks from pre-Deccan C30N strata cannot have resulted from Deccan volcanism, it is concluded that the mercury peaks in C30N, and therefore likely also C29R, strata at Zumaia result from cyclical increases in clastic influx to the basin, following the trends in Al_2O_3 content. The lack of Hg enrichment in C29R strata compared to C30N at Bass River and Zumaia is confirmed by histogram plots of the mercury contents at those localities (see Appendix fig. A4).

The new $\delta^{13}C_{org}$ data from East Gilbert Creek samples show a negative excursion across strata that include the IrZ coal unit (fig. 5D). This excursion is assumed to be equivalent to those previously reported at the K–Pg boundary from other archives of the Hell Creek Formation (Arens and Jahren, 2000; Arens and others, 2014), and thus to include the extinction horizon. However, because there is an offset between the IrZ and base of the negative $\delta^{13}C_{org}$ excursion at East Gilbert Creek, the precise stratigraphic position of the K–Pg boundary within the negative excursion is not clear. A spike in Hg and Hg/TOC is documented from within the stratigraphic uncertainty of the K–Pg boundary, but this is one of several Hg peaks throughout the entire studied stratigraphy at East Gilbert Creek (fig. 5D). Local arc volcanism is known to have occurred proximally to this deposition area (for example, Swisher and others, 1993). Thus, the multiple Hg and Hg/TOC peaks observed in C29R strata might have resulted from local volcanic activity rather than Deccan eruptions, although Hg analyses of C30N sediments from Montana are required to confirm or refute this hypothesis.

In summary, the Hg peaks at the extinction horizons of Seymour Island and East Gilbert Creek (figs. 5A and 5D) match results from Bidart, France (Font and others, 2016), Elles, Tunisia (Keller and others, 2018), Bottaccione Gorge, Italy and Stevns Klint, Denmark (Sial and others, 2016), supporting the possibility of a volcanically induced Hg-cycle perturbation at or just before the end-Cretaceous extinction, although it should be noted that both the Bottaccione Gorge and Stevns Klint Hg peaks coincide with profound changes in lithology from carbonates to clays. However, it is apparent from the new compilation of results presented here that the uppermost Cretaceous mercury record shows substantial variation between individual localities (tables 1 and 2), suggesting that many sedimentary locations may not unambiguously record Deccan volcanism. These differences are particularly the case for C29R strata below the extinction horizon. Crucially, aside from a possible peak at the extinction horizon, the comparisons of Hg content in C29R strata compared to C30N strata in this study do not show any overarching enrichment in sediments deposited during the time of Deccan emplacement compared to those formed in pre-Deccan times, suggesting that the global mercury cycle might not have been perturbed during (and, therefore, may not record) a large part of the history of Deccan volcanism.

OAE 2 Results

A small increase in Hg/TOC (increasing from 10 up to 20 ppb/wt%) is recorded at the base of OAE 2 strata from ODP Site 1260 (fig. 6A). This low-magnitude

TABLE 2

Presence or absence of Hg records within specific sedimentary contexts

Event	Age (Ma)	RELATIVELY CONSISTENT REDOX THROUGH EVENT							Records of abrupt redox changes as TOC increases	Hg references
		Terrestrial	Coastal/shoreface	Nearshore Shallow marine	Hemipelagic	Pelagic	Carbonate reef	Persistently anoxic environment		
PETM	55				**Dababiya**					Keller and others (2018)
K–Pg (EXTINCTION RATHER THAN ENTIRETY OF C29R)	66	**East Gilbert Creek** Meghalaya Jhilmili		**Elles** **Bidart** **Seymour Island** Bass River *Zumaia* Bajada del Jäguel	*El Kef*	**Bottaccione** **Stevns Klint**	Padriciano			Font and others (2016, 2018) Sial and others (2016) Keller and others (2018) *this study*
OAE 2	94	Utah			**Maverick Basin**	*Eastbourne*		**Demerara Rise**	*Pont d'Issole* *Clot Chevalier* *Tarfaya* *Furlo* **Kerguelen Plateau**	Scaife and others (2017) *this study*
OAE 1a	121								**La Bédoule** **Glaise** **Roter Sattel**	Charbonnier and Föllmi (2017)
Valanginian	134				**Angles** **Orpierre** *Wawal*	**Breggia**				Charbonnier and others (2017)
T-OAE	183		**Bornholm**	**Arroyo Lapa** **Mochras**	**Peniche** **El Peñon**		*Velebit*		*Hawsker Bottoms* *Sancerre*	Percival and others (2015) Fantasia and others (2018)
T–J	201	**Partridge Island** **Astartekløft** Igounane		**New York Canyon** **St Audries Bay** **Arroyo Malo**	**Kuhjoch**					Thibodeau and others (2016) Percival and others (2017)
P–T	252			**Meishan**		**Buchanan Lake** **Spitsbergen** **Daxiakou** **Shangsi**				Sanei and others (2012) Grasby and others (2013, 2016, 2017)
Capitanian	260					**Spitsbergen**				Grasby and others (2016)
Frasnian–Famennian	372					**Lahmida** **Kahlleite** **Syv'yu**				Racki and others (2018)
Ordovician–Silurian	444					**Monitor Range**		**Wangjiawan** **Dingjiapo**		Gong and others (2017) Jones and others (2017)

Green bold text signifies clear Hg enrichments at that location, red italic text signifies no such clear Hg signal. Gray regular text indicates that the event horizon is missing at that location.

excursion is similar to those reported from ODP Site 1258 and the Maverick Basin (southern Western Interior Seaway: Texas, USA) by Scaife and others (2017). Elevated Hg/TOC is also recorded in OAE 2 strata at IODP Site 1138 (fig. 6D) but, because the onset of the OAE is not recorded at that location due to a hiatus, the temporal relationship between the mercury perturbation and onset of OAE 2 is not clear.

There is no good evidence at any of the other studied locations for significant perturbations of the global mercury cycle during OAE 2. Some records do document sporadic Hg/TOC peaks in sediments deposited during OAE 2 (for example, Utah, Pont d'Issole, and Clot Chevalier: figs. 6C, 6F, and 6G) but these peaks correlate with a decreased TOC content rather than with elevated Hg concentrations, and thus likely do not record mercury enrichment sourced externally from volcanism. Minor increases in Hg concentrations are observed in OAE 2 strata from Eastbourne (fig. 6E), but there is insufficient TOC against which the mercury can be reasonably normalized, and these peaks appear in the more clay-rich Plenus Marls (where Al content is also higher: see Appendix fig. 3); thus, they may result from a change in lithology rather than volcanic output. None of the Tethyan records of Pont d'Issole, Furlo, and Clot Chevalier show an increase in Hg/TOC ratios based on elevated Hg (as opposed to reduced TOC) in OAE 2 strata (figs. 6F–6H). There is also no clear increase in sedimentary Hg/TOC at Tarfaya, potentially due to the large increase in TOC abundance in OAE 2 strata (fig. 6B).

In summary, most records of OAE 2 do not show clear peaks in Hg and Hg/TOC, with excursions recorded in OAE 2 strata from only a few locations (figs. 4 and 6), namely in the proto-North Atlantic, on the Kerguelen Plateau, and in the Maverick Basin at the southern end of the Western Interior Seaway (Texas: Scaife and others, 2017). There are no clear Hg/TOC peaks related to elevated Hg concentrations in sediments from the Tethyan or boreal European realms. These observations are supported by histogram plots of Hg/TOC values from OAE *vs* pre-OAE samples (see Appendix fig. 4). Significantly, there is no good record of perturbed mercury in the paralic deposits from Utah (fig. 6C), which would have been influenced chiefly by the atmospheric Hg inventory.

DISCUSSION

Stratigraphic records of the global mercury inventory likely vary depending on factors such as lithological changes, the nature of the prevailing paleoenvironment recorded by the sedimentary archive, and the geographical location of deposition. Volcanic Hg signatures might be masked by correlative increases in TOC or cyclical variations in lithology resulting from local climatic forcing, hindering interpretation of Hg data in such settings. Additionally, the considerable variation documented between different LIPs in terms of emplacement and eruptive style (Bryan and others, 2010) means that certain volcanogenic processes (for example, submarine *vs* subaerial volcanism, explosive *vs* effusive eruptions, and additional thermogenic emissions) during the emplacement of individual LIPs are likely to have different impacts on the global Hg cycle. These issues are addressed here through comparison of the mercury trends reported above with each other, with published Hg data from stratigraphic records of other events, and other markers of LIP volcanism such as Os isotopes (fig. 8).

Impact of the Depositional Environment on the Mercury Record

Links between mercury records and sedimentary facies.—Previous studies have noted that a large increase in the TOC content of strata that record a major event can overprint any increase in Hg content, resulting in a lowering of Hg/TOC ratios even if a volcanically caused sedimentary Hg enrichment were present. Examples of such overprinting by excess TOC are known from both the Early Toarcian OAE (T-OAE:

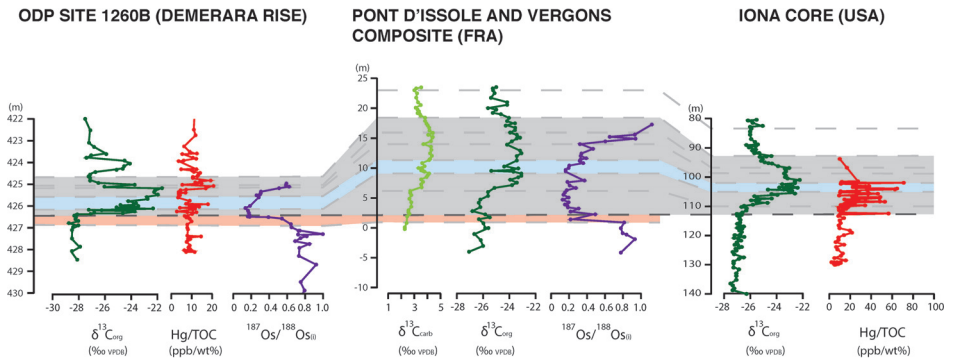

Fig. 8. Correlation of carbon- and osmium-isotope data and Hg/TOC ratios from ODP Site 1260, the Pont d'Issole and Vergons composite record, and the Iona core. All vertical scales are in meters; note the variable Hg/TOC scales. Gray shading indicates the stratigraphic extent of OAE 2, based on carbon isotopes; the bold dashed line indicates the horizon marking the onset of OAE 2. Blue shading indicates the assumed stratigraphic extent of the Plenus Cold Event. Red shading indicates the stratigraphic gap between the onset horizon of OAE 2, and the base of the decrease in $Os_{(i)}$. Carbon-isotope data are sourced as follows: ODP Site 1260 from Forster and others (2007); Pont d'Issole and Vergons from Jarvis and others (2011) and this study; Iona from Eldrett and others (2014). Osmium-isotope data are sourced as follows: ODP Site 1260 from Turgeon and Creaser (2008); Pont d'Issole and Vergons from Du Vivier and others (2014). Hg/TOC data from the Iona core are sourced from Scaife and others (2017); all other data are from this study.

Hawsker Bottoms, UK and Sancerre, France: Percival and others, 2015), and Early Aptian OAE (OAE 1a: Roter Sattel, Switzerland: Charbonnier and Föllmi, 2017). The Tethyan and Atlantic records of OAE 2 in this study also illustrate this phenomenon, with Hg enrichments within OAE 2 strata documented at Tarfaya (fig. 6B), Pont d'Issole and Vergons (fig. 6F), and Clot Chevalier (fig. 6G) overprinted by higher magnitude excursions in TOC content, resulting in an apparent decrease in Hg/TOC ratios at that stratigraphic level. Sedimentary records that document sudden changes towards oxygen-depleted seawater conditions, particularly if anoxic or euxinic, are likely to be significantly impacted by major increases in TOC and the potential overprinting of any Hg/TOC signal (table 2).

Lithologically controlled variations in Hg content may also be observed in organic-lean sedimentary records that feature changes from carbonate-rich lithologies to clay-rich marls or shales. In such oxygenated depositional settings, burial and preservation of organic matter might be limited (for example, the T-OAE record at Velebit, Croatia: table 2 and Percival and others, 2015), and mercury fixation may be predominantly controlled by clay content. At Zumaia, Hg concentrations closely follow those of Al_2O_3 (fig. 7) and Hg peaks typically occur in the more marly layers, suggesting that the mercury content in this archive is lithologically controlled. Sediments with higher Hg contents at Eastbourne (fig. 6E) are documented within the Plenus Marls, and correlate with a change in lithology from chalks to clay-rich marls, an increase in both Al/Ca ratios and Al_2O_3 (both proxies for clay content: see Appendix fig. 3; Pearce and others, 2009; Sweere and others, 2018). It cannot, however, be ruled out that the Hg enrichments in the Eastbourne OAE 2 record were associated with volcanic emissions.

Similarly, the Hg peaks in the inferred C29R strata at Zumaia may have originally derived from Deccan gas emissions containing mercury that were subsequently transferred to the depositional environment via terrigenous influx. However, although an originally volcanic source cannot be totally excluded, the fact that levels of relatively elevated Hg correlate with peaks in Al_2O_3 and more clay-rich sediment, both in C29R and C30N strata, suggests that the main control on variations in mercury concentra-

tions measured in this record was changes in orbitally forced input of fine-grained fluvially derived clastic material.

It is noteworthy that Hg/TOC values in uppermost Cretaceous strata at East Gilbert Creek (fig. 5D) and the OAE 2 record in Utah (fig. 6C) are significantly higher than other records of the same age with similar TOC contents (for example, Bass River or Seymour Island in the case of East Gilbert Creek). This pattern indicates a greater uptake of Hg by organic matter in these two locations compared to fully marine records of the same age, even though neither East Gilbert Creek nor Utah document a clear excursion in Hg during a time of LIP volcanism (although the multiple spikes at East Gilbert Creek might have been volcanic in origin). Previous studies have also noted an apparent trend towards higher magnitude Hg/TOC ratios in sedimentary records containing predominantly terrestrial organic matter (for example, Bornholm, Denmark, T-OAE: Percival and others, 2015; Astartekløft, Greenland, end-Triassic extinction: Percival and others, 2017). This apparent enrichment of mercury in terrestrial organic matter compared to marine might reflect processes such as direct adsorption of atmospheric Hg by the tree canopy. Alternatively, higher-plant organic matter may have a greater structural affinity for mercury than other types of organic matter. Crucially, this pattern raises the possibility that a change in sedimentary organic-matter type from predominantly marine to mainly terrestrial could increase the Hg/TOC ratio of those sediments without any volcanic forcing. Thus, constraints on the type of organic matter present in a sedimentary record may be vital in interpreting mercury trends.

Finally, the impact of post-depositional processes on sedimentary Hg records remains unclear. The removal of porewater during compaction will result in some chemical changes within the sediment, but it is not thought likely that such processes will greatly impact Hg due to its complexion on to organic compounds. Oxidation of organic matter during the early stages of diagenesis or thermal maturation of sediments will alter the sedimentary TOC content, but it is not clear how such processes will impact Hg and whether the Hg/TOC ratio of those sediments will be significantly altered. Further work is required to improve understanding of how post-depositional processes might alter the sedimentary mercury record. However, it is worth noting that broadly similar Hg enrichments have been reported from numerous stratigraphic records of other events, such as the end-Triassic and Toarcian OAE, which span a range of facies types and diagenetic/maturation histories (Percival and others, 2015, 2017; Thibodeau and others, 2016; Fantasia and others, 2018). This trend would be less likely to be the case if post-depositional processes always had a major impact on sedimentary Hg.

Geographic disparity in mercury records.—It is also possible that sedimentary mercury trends of different sections within a single sedimentary basin might show significant variations, due to contrasting input fluxes of mercury to that area. Subtle variations in sedimentary mercury records of the same depositional age in the same sedimentary basin have been observed previously in records of OAE 2 from the Maverick Basin (Texas, USA; Scaife and others, 2017) and OAE 1a records from the Vocontian Basin (S.E. France; Charbonnier and Föllmi, 2017). Similarly, the two OAE 2 records from the Vocontian Basin in this study (Clot Chevalier and the Pont d'Issole–Vergons composite) show noticeably different Hg trends. In particular, the Hg content in sediments from Pont d'Issole and Vergons is typically more than double that in strata from Clot Chevalier, despite the comparable lithology and not dissimilar TOC content of those records (figs. 6F–6G). This disparity in sedimentary mercury content is suggestive of a variable mercury supply to different areas of the Vocontian Basin, possibly caused by proximity to (minor) local volcanic systems or a riverine supply of terrigenous mercury.

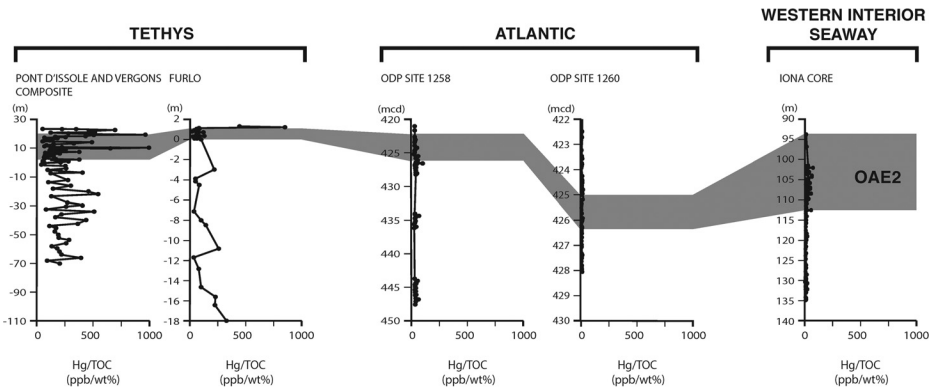

Fig. 9. Comparison of the magnitude of Hg/TOC ratios in sediments from the Tethyan (Pont d'Issole and Vergons composite record and Furlo), Atlantic (ODP Sites 1258 and 1260), and Western Interior Seaway (Iona) localities. All vertical scales are in meters. Gray shading indicates the stratigraphic extent of OAE 2 at each location on the basis of carbon-isotope data. Hg/TOC data from ODP Site 1258 and the Iona core are sourced from Scaife and others (2017); all other data are from this study.

The importance of considering possible terrestrial influxes of Hg to marine sediments is consistent with the cyclical pattern of Hg deposition documented in uppermost Cretaceous strata from Zumaia in this study, compared to the absence of such a correlation between Hg and phyllosilicate contents at a time-equivalent, but more distal from the paleoshoreline, record from the same marine basin (Bidart, France; Font and others, 2016). This issue is also highlighted by isotopic evidence for the input of terrestrial Hg to end-Permian near-shore sediments, compared to a predominantly atmospherically derived flux of Hg to sediments deposited at the same time, but more distally from the paleoshoreline (Grasby and others, 2017).

In addition to local intra-basinal variations, there appears to be variability in sedimentary mercury content in markedly dispersed geographical areas. For example, the Hg/TOC ratio of sediments deposited prior to and during OAE 2 is notably higher in Tethyan records such as Vergons and Furlo compared to proto-North Atlantic or Western Interior Seaway records like Site 1260 or the Iona core (fig. 9). This discrepancy does not appear to result just from different TOC contents of the sediments, since the Hg content of sediments stratigraphically below the OAE at Furlo is up to an order of magnitude higher than in time-equivalent strata from the proto-North Atlantic or Western Interior Seaway, despite having a TOC content comparable to or higher than the other locations. One possibility is that localized volcanism, hydrothermal activity, or supply from terrestrial runoff, resulted in a larger mercury influx to the Tethyan area prior to OAE 2 compared to the proto-North Atlantic. Significant volcanic activity in the Tethyan realm during the later Cretaceous has been inferred from the widespread preservation of Late Cretaceous ophiolites (Robertson, 2002; Dilek and Furnes, 2011). However, bentonite layers in the Iona core are also suggestive of local volcanism proximal to that area in the run-up to OAE 2 (Eldrett and others, 2014), but there is no indication that they supplied extra mercury to those sediments. An alternative explanation is that variability in the mercury content of individual deep-water bodies (as seen in the modern environment: Bowman and others, 2015) might have caused the difference in Tethyan and Atlantic/Western Interior Seaway Hg levels.

In summary, it appears that the paleogeographic setting can be a major influence on the Hg content of sediments. Combined with the varying lithological suitability of sedimentary archives as recorders of global Hg, there is a high potential for local processes to influence and/or overprint any global mercury signal. These findings

reaffirm the importance of investigating numerous sedimentary records in order to account for potential local sedimentological variations, ideally including lithologically homogeneous sedimentary records.

Impact of Specific Volcanogenic Processes on Perturbing the Hg Cycle

Subaerial volcanism.—The results from analyses of uppermost Cretaceous records in this study support the findings of Font and others (2016), Sial and others (2016) and Keller and others (2018) for a perturbed mercury cycle during the end-Cretaceous extinction. However, geochronological evidence and sedimentary $Os_{(i)}$ records from around the world suggest that the onset of Deccan volcanism (or weathering of Deccan basalts) began at least 300 kyr prior to that event, during the C30N/C29R paleomagnetic reversal (fig. 10A). The absence of any overarching increase in sedimentary Hg concentrations and Hg/TOC ratios at that horizon, or in any C29R strata until close to the end-Cretaceous extinction horizon, indicates that Deccan volcanism did not produce sufficient mercury emissions to perturb the global Hg cycle for much of its history.

The Hg-cycle perturbation documented at or near the K–Pg boundary might be linked to a highly intense/voluminous episode of Deccan volcanism thought to have occurred just prior to the extinction (Renne and others, 2015). An alternative hypothesis could be made that the Hg spikes at or near the extinction horizon were produced by the Chicxulub impact, and that Deccan volcanism did not perturb the global mercury cycle at any point during its emplacement. However, such a circumstance is considered unlikely here as the Hg enrichment typically appears noticeably below the boundary and associated iridium anomaly, suggesting that the recorded Hg-cycle perturbation commenced prior to the impact and can, therefore, be attributed to Deccan volcanism (see also Sial and others, 2013).

In comparing these findings to Hg trends from other major events, it is noteworthy that the Deccan Traps are not the only LIP where volcanism is documented as occurring prior to any recorded perturbation of the global Hg cycle (see table 3). In end-Permian records, a clear enrichment in sedimentary mercury is observed at the extinction horizon, with Hg concentrations remaining elevated above pre-extinction values higher up the stratigraphic sequence (Sanei and others, 2012; Grasby and others, 2013, 2016, 2017). However, Siberian Trap basalts have been precisely dated to older than the end-Permian extinction, with the extinction itself specifically coincident with the onset of sill intrusions into volatile-rich country rocks (fig. 10B; see also Burgess and Bowring, 2015; Burgess and others, 2017). Moreover, Os- and Zn- isotope data both indicate that Siberian Trap volcanism had commenced prior to the extinction, albeit based on analyses of one sedimentary record for each proxy (Schoepfer and others, 2013; Georgiev and others, 2015; Liu and others, 2017).

Similarly, lower Valanginian strata record a sedimentary mercury enrichment correlative with the onset of the Valanginian 'Weissert' Event, indicating a short spell of mercury release from LIP volcanism, in this case from the Paraná–Etendeka LIP (Charbonnier and others, 2017). However, paleomagnetic studies of Paraná–Etendeka basalts indicate a much more prolonged eruptive history for at least the Etendeka part of the province (4–5 Myr: Dodd and others, 2015), although Ar-Ar and U-Pb geochronology suggests that the Paraná volcanics may have been emplaced more rapidly (~1 Myr: Thiede and Vasconcelos, 2010; Pinto and others, 2011). This short episode of mercury enrichment within a much longer history of LIP volcanism is confirmed by comparing the magnetostratigraphic records of the Etendeka basalts with those of Valanginian sediments (fig. 10C).

A recent correlation of lower Toarcian strata with coeval Karoo basalt emplacement noted volcanism associated with that LIP was likely continuous throughout the early Toarcian Stage, but only two distinct enrichments in sedimentary Hg had been recorded (Xu and others, 2018). Thus, the Karoo–Ferrar LIP likely also did not

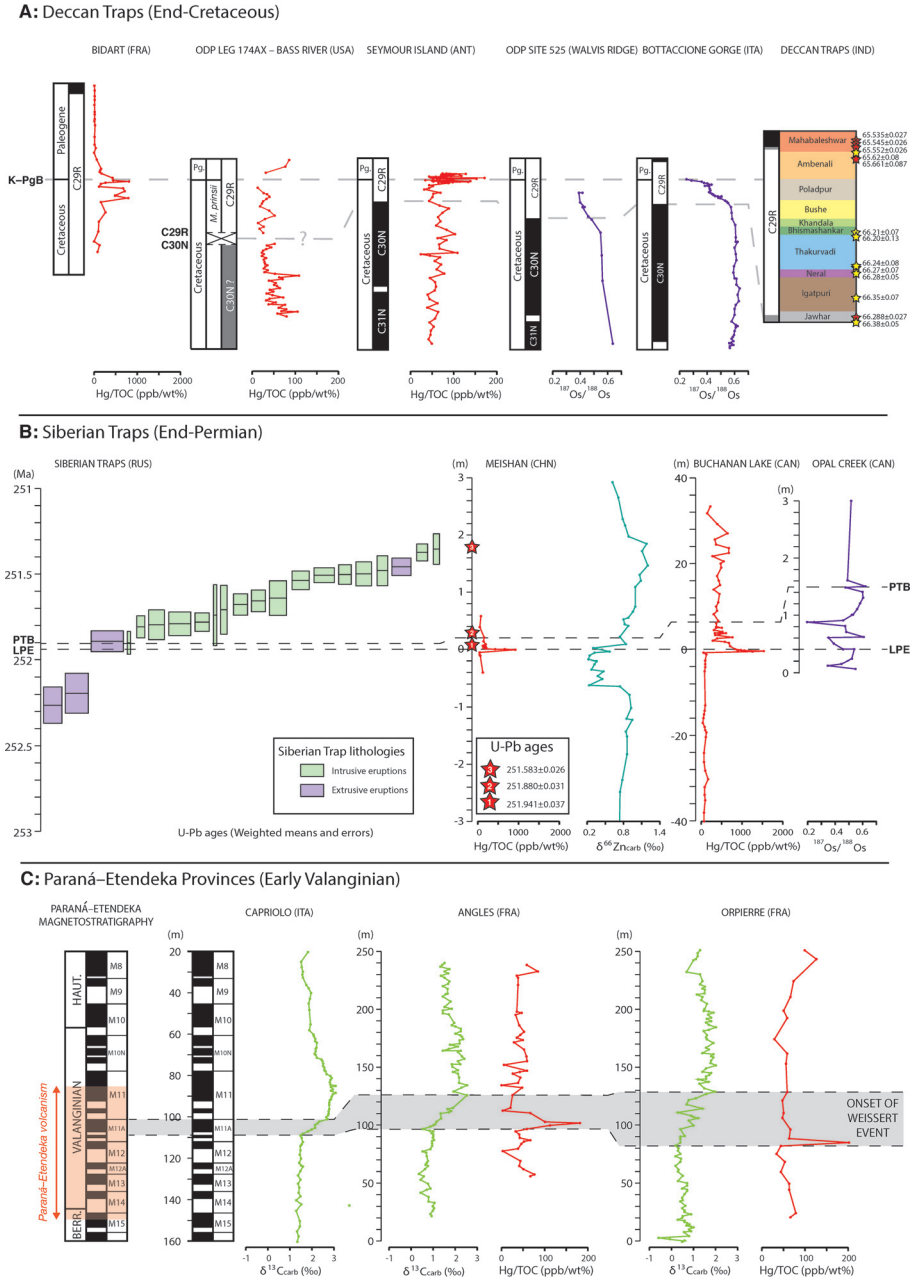

Fig. 10. Temporal correlation of mercury records with other indicators of Large Igneous Province volcanism. (A) Correlated end-Cretaceous records of Hg/TOC and $Os_{(i)}$ data. Temporal correlation achieved using paleomagnetic records of the sedimentary successions and also Deccan basalts, as well as Deccan geochronological dating. $Os_{(i)}$ data are from Robinson and others (2009). Hg/TOC data from Bidart are sourced from Font and others (2016); all other Hg/TOC data are from this study. The Deccan basalt formations and ages shown are from the Western Gnats, following Schoene and others (2015) and Renne and others (2015). The end-Cretaceous extinction horizon (marked K–PgB) and C30N/C29R chron reversal are indicated. Biostratigraphic data at Bass River sourced from Miller and others (1998). Magnetostratigraphic data are sourced as follows: Bidart from Galbrun and Gardin (2004); Bass River inferred in this study (see Appendix fig. A2 and section introducing Bass River); Seymour Island from Tobin and others (2012); ODP Site 525 and Bottaccione Gorge from Robinson and others (2009); Deccan Traps from Chenet

perturb the global Hg cycle throughout the entirety of its emplacement history (Percival and others, 2016).

Mercury trends from sediments deposited during the emplacement of these four LIPs (Deccan, Siberian, Paraná–Etendeka, and Karoo–Ferrar) strongly suggest that not all individual volcanic events during LIP emplacement will perturb the global Hg cycle. This conclusion poses the question of which processes associated with LIP volcanism and emplacement are key for producing major Hg emissions that have a global-scale impact. Extensive pyroclastic eruptions are known to have occurred during the emplacement of both of the Siberian Traps and the Karoo–Ferrar LIP (for example, Ross and others, 2005; McClintock and White, 2006; Burgess and Bowring, 2015; Burgess and others, 2017), possibly allowing for an important role of explosive volcanism in causing global Hg perturbations, although the precise temporal relationship between the Karoo pyroclastics and the Early Toarcian Hg enrichments is unclear (Percival and others, 2015). This hypothesized effect may have resulted from the ability of more explosive eruptions to inject mercury into the stratosphere and/or upper troposphere, prolonging its atmospheric lifetime and, therefore, likely increasing dispersal of the element. Evidence for explosive volcanism during the emplacement of continental LIPs has also been reported for the Emeishan Traps (Capitanian), Central Atlantic Magmatic Province (end Triassic), Paraná–Etendeka (Valanginian), and North Atlantic Igneous Province (Paleocene–Eocene) (for example, Ross and others, 2005; Pinto and others, 2011, and references therein, Olsen and others, 2017), all LIPs associated with events where sedimentary Hg enrichments have been documented (see fig. 11).

Additionally, all of the Emeishan, Siberian, Central Atlantic, Karoo–Ferrar, and North Atlantic LIPs have been hypothesized to result in the release of additional, thermogenic, volatile emissions following baking of surrounding volatile-rich country rocks by intrusive magmatism (reviewed in Ganino and Arndt, 2009). Thus, these LIPs may also have emitted an unusually large quantity of mercury if and when Hg-rich coals/organic shales were intruded by magmas, compared to volcanic events where only magmatic Hg was produced. In this context, it is noteworthy that the onset of Siberian Trap sill emplacement and proposed thermogenic emissions apparently coincided with the end-Permian extinction and the observed onset of global Hg-cycle perturbation (fig. 10B; also Burgess and others, 2017).

Further work is needed on LIP lithologies and processes to investigate the impact of explosive *vs* effusive eruptions and thermogenic emissions. Returning to the uppermost Cretaceous records for example, given that there is currently no record of explosive volcanism associated with the Deccan Traps, the Hg enrichment documented at or near the K–Pg boundary cannot be attributed to specifically explosive eruptions, instead possibly resulting from highly intense/voluminous effusive volcanism (Renne and others, 2015; Font and others, 2016). In this context, it should be noted that the eruption dynamics of neither effusive nor explosive LIP eruptions are

Fig. 10 (continued). and others (2009). (B) Correlated end-Permian records of Hg/TOC, $Os_{(i)}$, and zinc-isotope data. Correlation achieved using the indicated end-Permian extinction (marked LPE) horizon and Permian–Triassic boundary (marked PTB). Further correlation with the Siberian Traps achieved using U-Pb geochronology (Burgess and Bowring, 2015). U-Pb data are sourced as follows: Siberian Traps from Burgess and Bowring (2015); Meishan from Burgess and others (2014). Hg/TOC data are sourced as follows: Meishan from Grasby and others (2017: *corrected following personal communication with Steve Grasby*); Buchanan Lake from Sanei and others (2012). Meishan zinc-isotope data are from Liu and others (2017). Opal Creek $Os_{(i)}$ data are from Georgiev and others (2015). (C) Temporal correlation of Valanginian Hg/TOC records with the record of emplacement of the Paraná-Etendeka LIP. Correlation achieved on the basis of carbon-isotope stratigraphy and magnetostratigraphy. The magnetostratigraphic history of the Paraná-Etendeka is from Dodd and others (2015). All Capriolo data are from Channell and others (1993). Other carbon-isotope data are sourced as follows: Angles from Duchamp-Alphonse and others (2007); Orpierre from Charbonnier and others (2013). Hg/TOC data are from Charbonnier and others (2017).

TABLE 3

Mercury vs other indicators of LIP volcanism

Event	Age (Ma)	Large Igneous Province (location)	Evidence for thermogenic emissions?	Hg/TOC excursion	Hg/TOC comparison with other indicators of LIP volcanism	Hg references	Other references
PETM	55	North Atlantic Province (high latitude; subaerial)	YES	1 RECORD: Peak during main event, no Hg peak at base of event.	Ashes linked to North Atlantic Province and $Os_{(i)}$ shift to unradiogenic values at onset of PETM. Hg/TOC excursion lags both.	Keller and others (2018)	Larsen and others (2003); Ross and others 2005); Wieczirek and others (2013); Dickson and others (2015)
K–Pg (EXTINCTION RATHER THAN ENTIRETY OF C29R)	66	Deccan Traps (mid latitude subaerial)	NO	13 RECORDS: 5 missing K–Pg boundary data, 6 of other 8 have a peak at boundary. No clear enrichment throughout C29R vs C30N.	Sedimentary $Os_{(i)}$ values, U-Pb, Ar-Ar, and magnetochronology indicates Deccan volcanism throughout C29R. Thus, main Hg/TOC peak occurs 200–300 kyr after onset of Deccan volcanism.	Font and others (2016, 2018) Sial and others (2016) Keller and others (2018) *this study*	Ravizza and Peucker-Ehrenbrink (2003); Chenet and others (2007); Robinson and others (2009); Renne and others (2015); Schoene and others (2015)
OAE 2	94	Caribbean-Columbian Plateau Madagascan Province High Arctic Province Ontong-Java Plateau (widespread; largely submarine)	NO	11 RECORDS: 4 with low magnitude increases, all proximal to LIP. No clear Hg/TOC record of volcanism in more distal records although high TOC may overprint signal.	Where present, Hg/TOC excursions begin at onset of OAE, $Os_{(i)}$ values begin to fall just below OAE strata. No clear peak correlative with other markers of volcanism in Plenus Cold Event strata. Hg signal therefore regional and lags other volcanic tracers.	Scaife and others (2017) *this study*	Snow and others (2005); Kuroda and others (2007); Turgeon and Creaser (2008); Du Vivier and others (2014, 2015); Holmden and others (2016); Jenkyns and others (2017); Sweere and others (2018)
OAE 1a	121	Ontong-Java Plateau (low latitude; largely submarine) ? High Arctic Province ?	yes?	3 RECORDS: All show increase during event, 2 at low magnitude (maybe muted by TOC increase)	Hg/TOC peaks match fall in sedimentary $Os_{(i)}$ values in OAE strata. No published correlation with trace metal/Pb-isotope perturbations below OAE strata.	Charbonnier and Föllmi (2017)	Tejada and others (2009); Kuroda and others (2011); Bottini and others (2012); Erba and others (2015)
Valanginian	134	Paraná-Etendeka Province (mid latitude; subaerial)	NO	4 RECORDS: At least 3 excursions, but peaks only seen at onset of event, not throughout event.	Hg/TOC evidence for short volcanic pulse at onset of Valanginian event, but does not match evidence for much longer (>4 Myr) duration of volcanism.	Charbonnier and others (2017)	Thiede and Vasconcelos (2010); Pinto and others (2011); Dodd and others (2015)
T-OAE	183	Karoo-Ferrar Province (high latitude; subaerial)	YES	8 RECORDS: 5 clear excursions, 2 of the other 3 may be overprinted by TOC increase. Peaks in 3 records of precursor Pl–To event.	2 Hg/TOC peaks within 1 Myr of LIP volcanism. Exact correlation hindered by lack of a precise age for the T-OAE.	Percival and others (2015) Fantasia and others (2018)	Svensen and others (2012); Sell and others (2014); Burgess and others (2015); Xu and others (2018)
T–J	201	Central Atlantic Province (low latitude; subaerial)	YES	7 RECORDS: 6 clear excursions at Triassic extinction horizon, 4 with additional peaks above.	Hg/TOC peaks match early CAMP volcanic pulses. No published Hg data from sediments deposited during Late CAMP volcanism, but $Os_{(i)}$ values suggest weathering of CAMP throughout T-J interval.	Thibodeau and others (2016) Percival and others (2017)	Cohen and Coe (2002, 2007); Kuroda and others (2010); Pálfy and Zajzon (2012); Blackburn and others (2013); Davies and others (2017)
P–T	252	Siberian Traps (high latitude; subaerial)	YES	5 RECORDS: 5 excursions all beginning at the extinction horizon. One record shows another peak at subsequent Smithian crisis.	Hg/TOC lags the onset of Siberian volcanism, as indicated by U-Pb geochronology and Os and Zn isotopes. Hg/TOC peaks match onset of explosive eruptions and potential thermogenic emissions.	Sanei and others (2012) Grasby and others (2013, 2016, 2017) Wang and others (2018)	Schoepfer and others (2013); Burgess and others (2014, 2017); Burgess and Bowring (2015); Georgiev and others (2015); Liu and others (2017)
Capitanian	260	Emeishan Province (low latitude; subaerial)	YES	1 RECORD: Excursion documented at extinction horizon.	N/A	Grasby and others (2016)	N/A
Frasnian–Famennian	372	Viluy Traps (high latitude; subaerial)	*UNKNOWN*	3 RECORDS: 3 excursions all within the Upper Kellwasser 'extinction' level.	Zr/Al_2O_3 enrichments inferred as volcanic in origin also present in Upper Kellwasser horizons, but may have also resulted from non-volcanic processes.	Racki and others (2018)	Racki and others (2002); Pujol and others (2006)
Ordovician–Silurian	444	*UNKNOWN*	*UNKNOWN*	2 RECORDS: Peaks broadly correlative with first O–S extinction pulse.	N/A	Gong and others (2017) Jones and others (2017)	N/A

Information on LIPs as for table 1, with evidence for thermogenic emissions summarized in Svensen and others (2004, 2007, 2009), and Ganino and Arndt (2009).

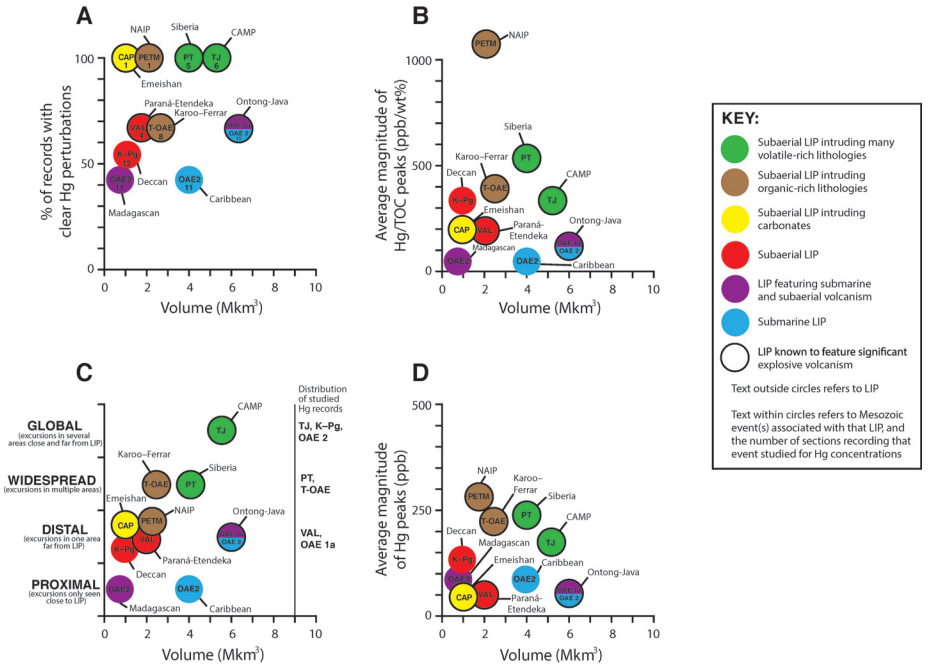

Fig. 11. Plots showing the relationship of LIP volume with (A) the consistency of Hg excursions (that is, for the T-OAE, 8 sections have been studied for Hg, but only 5 show clear Hg/TOC perturbations); (B) the magnitude of observed excursions in sedimentary Hg/TOC ratios (see also table 1); (C) the distribution of documented sedimentary Hg excursions with respect to LIP volcanism; and (D) the magnitude of observed excursions in sedimentary Hg concentrations. The subaerial *vs* submarine nature of LIP volcanism, presence *vs* absence of evidence for significant explosive eruptions, and the country rock intruded, are also shown for each LIP. The distribution plot shows the distribution of clear sedimentary enrichment compared to the LIP, with the total distribution of all sections analyzed for mercury also shown (that is, a global distribution of OAE 2 records has been analyzed for mercury, but Hg enrichments are only recorded in records proximal to a LIP). The plots are based on data from the LIP reviews of Ganino and Arndt (2009); Bond and Wignall (2014); and Marzoli and others (2004: CAMP only), and the Hg records of Sanei and others (2012); Grasby and others (2013, 2016, 2017); Percival and others (2015, 2017); Font and others (2016); Sial and others (2016); Thibodeau and others (2016); Charbonnier and Föllmi (2017); Charbonnier and others (2017); Scaife and others (2017); Keller and others (2018); Wang and others (2018); Fantasia and others (2018) and this study. Ordovician–Silurian and Frasnian–Famennian data are not shown here due to the limited knowledge of the LIPs potentially associated with those events.

well understood, and it is possible that some effusive LIP eruptions might have been capable of injecting volatiles into the stratosphere with an efficiency approaching that of explosive events (Glaze and others, 2017). Interestingly, for the Mesozoic-style events (Capitanian through to Paleocene–Eocene), the highest-magnitude and most consistently observed Hg and Hg/TOC enrichments in studies to date are associated with sedimentary records of the end-Permian and end-Triassic extinctions and Toarcian OAE, all linked to continental LIPs featuring explosive eruptions and possible thermogenic emissions (see fig. 11). Such comparisons of the magnitudes of sedimentary mercury enrichments must be made very cautiously however, due to the likely importance of other dispersion, sedimentation, or diagenetic factors in determining the magnitude of these concentrations.

Submarine volcanism.—Elevated Hg concentrations and Hg/TOC ratios appear in only a few records of OAE 2, with a low magnitude of perturbation if present (fig. 6). The clear absence of a global-scale elevation in sedimentary Hg concentrations suggests that the atmospheric mercury inventory was not perturbed by volcanism

during OAE 2, and that most volcanic mercury from LIPs was likely emitted directly into the ocean. This conclusion is also suggestive that the subaerial volcanism inferred for some of the Cenomanian–Turonian LIPs (for example, Storey and others, 1995; Buchs and others, 2018) might have played only a minor role in the emplacement of the Oceanic Plateaus associated with OAE 2. The absence of a Hg/TOC perturbation in OAE 2 strata from Utah (fig. 6C), where the bulk of deposited organic matter is terrestrial and would have carried Hg sourced chiefly from the atmosphere rather than the oceans, further indicates that the atmospheric Hg inventory was not perturbed during OAE 2. However, unless the oceanic residence time of mercury was greater during OAE 2 than it is today, a global-scale impact on the Hg-cycle would have required a perturbation of the atmospheric mercury inventory. Thus, the lack of evidence for any atmospheric or global-scale Hg perturbation during OAE 2 suggests that any submarine Hg emissions were only regional in their impact.

It is noteworthy that the Hg/TOC peaks that are documented in OAE 2 strata are all at locations relatively proximal to submarine volcanic sources. The IODP Site 1138 strata were deposited on to the Kerguelen Plateau itself, and were also not far from the Madagascan LIP (fig. 4B). The records from the Maverick Basin (Texas, southern Western Interior Seaway) and Demerara Rise (proto-North Atlantic) were likely both relatively proximal to the Caribbean–Columbian Plateau, based on tectonic reconstructions assuming that this Plateau was sourced from the modern Galápagos plume (Thompson and others, 2004; Seton and others, 2012; Nerlich and others, 2014), although strata from the Maverick Basin have also been proposed as showing the influence of volcanic material from the High Arctic LIP (Eldrett and others, 2014). Regional Hg perturbations proximal to LIPs are consistent with the near-field impact and short residence time of mercury in the modern ocean (<1 kyr: Gill and Fitzgerald, 1988; Bowman and others 2015). It is possible that the lack of Hg/TOC perturbations in Tethyan sites results from lithological changes (from limestones to organic-rich shales) masking a true signal of volcanism at those localities. However, such a circumstance is deemed unlikely as the distance of the Tethyan records from any LIP emplaced during OAE 2 would decrease the likelihood of their recording a volcanic Hg signal, assuming most/all LIP emissions of Hg during this OAE occurred subaqueously.

The apparently heterogeneous nature of submarine Hg distribution during OAE 2 stands in contrast to the globally recorded $Os_{(i)}$ signature of extremely enhanced volcanism and/or basalt-seawater interactions recorded in marine sedimentary records of OAE 2 (Turgeon and Creaser, 2008; Du Vivier and others, 2014, 2015). The disparity between the two proxies may be attributed to the different oceanic residence times of the two elements, assuming that most LIP activity during OAE 2 was submarine in nature. In contrast to the short lifetime of Hg in the ocean, the oceanic residence time of osmium (~10–50 kyr at present: Peucker-Ehrenbrink and Ravizza, 2000) is sufficient for the element to be relatively well mixed in the global ocean, which today has a mixing time of ~1 kyr.

In addition to the contrasting distribution of Os-isotope and Hg records of volcanism, there appears to be a lag recorded between the onset of perturbations to the marine Os and Hg inventories. The decline in sedimentary $Os_{(i)}$ values is known to begin in strata noticeably below those that document the onset of the $\delta^{13}C$ excursion in most records (Du Vivier and others, 2014, 2015), indicating that the marine osmium perturbation began prior to OAE 2 (by up to 80 kyr). ODP Site 1260 is the only record where anomalies in both Hg/TOC and $Os_{(i)}$ have been documented, and illustrates the onset of Hg/TOC elevation as occurring stratigraphically above the level of initial decrease in sedimentary $Os_{(i)}$, but correlative with the base of the $\delta^{13}C$ excursion (fig. 8). Hg/TOC excursions observed in sediments from the Maverick Basin also begin in

the same strata that record the commencement of the global carbon-cycle perturbation. Unfortunately, strata that record the onset of OAE 2 are missing from the Kerguelen Plateau record of IODP Site 1138, and thus the timing of the onset of Hg enrichment cannot be constrained at that site.

These trends might indicate a diachronous onset of mercury and osmium perturbations during OAE 2. It is possible that the mercury perturbation was achieved only when global-scale changes in ocean-redox chemistry began at the onset of the OAE itself, but this is not consistent with the enrichment of mercury in both sediments that record oxygenation during OAE 2 (Maverick Basin: Scaife and others, 2017), and those that record de-oxygenation during OAE 2 (Demerara Rise: Scaife and others, 2017; fig. 6A of this study). A more plausible explanation for a change in the oceanic Os inventory being recorded as happening earlier than the marine Hg perturbation during OAE 2 may be linked to the emplacement of multiple LIPs around the time of the OAE. Under these circumstances, the decrease in recorded $Os_{(i)}$ values just below OAE 2 strata could have been caused by a submarine LIP at any location, due to the capacity of osmium to be distributed throughout the global ocean, whilst a sedimentary Hg enrichment would not have been recorded until a subsequent LIP was emplaced proximally to that stratigraphic record (for example, the Caribbean–Columbian Plateau for Demerara Rise or the Maverick Basin). Alternatively, the dispersal pattern of volcanic mercury during OAE 2 may also have been impacted by a change in eruption style (from submarine to subaerial if an oceanic LIP became emergent), or the well-documented change in ocean circulation at that time (for example, MacLeod and others, 2008; Zheng and others, 2013), allowing Hg emissions from specific volcanic sources to be dispersed to sedimentary environments previously not influenced by that eruptive center.

The conclusion that hydrothermal mercury emissions from submarine LIPs can only influence Hg concentrations in sediments deposited relatively proximally to that LIP has important implications for the volcanic processes that took place during OAE 1a. Tethyan sedimentary archives record elevated Hg/TOC during that event, albeit of a smaller magnitude than mercury excursions associated with most other Mesozoic events (table 1; fig. 11; Charbonnier and Föllmi, 2017). Volcanism is also indicated by a clear decline in $Os_{(i)}$ to unradiogenic values recorded in both Tethyan and Pacific sediments (Tejada and others, 2009; Bottini and others, 2012).

Volcanism during OAE 1a is usually attributed to the Ontong-Java Plateau (for example, Tejada and others, 2009; Bottini and others, 2012; Erba and others, 2015; Charbonnier and Föllmi, 2017), but this LIP was emplaced far from the Tethys in a predominantly submarine manner. Therefore, it is possible that the appearance and stratigraphic position of Hg/TOC peaks documented in OAE 1a strata depended on the subaerial (phreatomagmatic) volcanic phases reported as being associated with this LIP (Chambers and others, 2004; Thordarson, 2004). Alternatively, the occurrence of OAE 1a sedimentary Hg/TOC peaks may have been caused by magmatic processes associated with the High Arctic LIP during the Aptian (Polteau and others, 2016). Mercury studies of additional OAE 1a and OAE 2 records from new localities and paleoenvironments, both proximal and distal from LIPs, are needed to resolve the impact of submarine LIPs on the global mercury cycle.

CONCLUSIONS

This study has expanded on previous investigations into mercury enrichments in the sedimentary records of Oceanic Anoxic Event 2 and the latest Cretaceous. There is little evidence for a global-scale perturbation of the mercury cycle during OAE 2, or that the atmospheric mercury inventory was impacted. Likewise, no broad enrichment of mercury is found in the majority of uppermost Cretaceous sediments deposited during Deccan volcanism, except at or just below the extinction horizon itself. Zumaia

represents an exception to this pattern and records Hg peaks in sediments deposited both prior to and during Deccan volcanism, which are likely to have resulted from local sedimentological processes. The absence of a clear volcanic signal in mercury for these two events is in contrast to osmium-isotope records of those times, which clearly document LIP volcanism and/or basalt-seawater interaction.

It is concluded that certain LIP volcanic processes, such as subaerial rather than submarine volcanism, explosive rather than effusive eruptions, and the production of thermogenic volatiles, are important for perturbing the global mercury cycle. Consequently, the lack of sedimentary Hg peaks in records of OAE 2 and the end-Cretaceous likely resulted from the comparative absence of subaerial volcanism (for OAE 2) and explosive eruptions and/or thermogenic emissions (for the end-Cretaceous) during much of the volcanic history of the LIPs associated with those events. Comparison of these results with Hg trends reported from other records of mass extinction and environmental change supports the hypothesis that not all LIP eruptions manifestly result in major perturbations to the global mercury cycle.

Comparison of the mercury records in this study with those from other events has also highlighted the importance of sedimentary processes for the recording of any mercury-cycle perturbation in the sedimentary record, particularly major changes in sedimentary lithology. Abrupt increases in sedimentary organic-carbon content might mute any signal of increased mercury deposition by impacting the Hg/TOC ratio. The effect of minor volcanic eruptions on the mercury content of local sedimentary records remains unclear but may be important in terrestrial settings such as latest Cretaceous Montana.

It is apparent that numerous surface processes can influence the deposition of mercury in sediments at any one site, demonstrating the need to evaluate multiple sedimentary archives from locations around the globe, ideally including records with a relatively consistent lithology and organic-carbon content. Further investigations are needed to gain insight into the influence of different dispersal, sedimentary, and diagenetic processes on the recording of atmospheric Hg signals in strata. Additionally, comparing trends of Os-isotopes and Hg contents as proxies of volcanism, the importance of subaerial *vs* submarine volcanism, and explosive eruptions and thermogenic emissions related to LIP emplacement for perturbing the mercury cycle, need to be explored further. These open questions highlight the need for future work to clarify the many nuances in interpretation of this geochemical proxy.

ACKNOWLEDGMENTS

We greatly appreciate reviews by Jiří Laurin and Wang Zheng that have improved this manuscript, and must also thank Steve Grasby for discussions on the Meishan end-Permian mercury record. We gratefully acknowledge Alistair Crame and the British Antarctic Survey for their loan of samples from Seymour Island (Antarctica), the GTSnext project for support in collecting samples from Zumaia, Bill Simpson and Adrienne Stroup for access to the Utah samples, and Greg Wilson, Dave de Mar Jr., Denver Fowler, Regan Dunn, Jack Horner, Harold and Jean Isaacs, the Hell Creek III project, the University of Washington, the Museum of the Rockies, and the Montana Bureau of Land Management for their support and permission for sampling at East Gilbert Creek (Montana, USA). We must thank John Farmer and the University of Edinburgh for provision of geochemical standard material. We thank David Wray at the University of Greenwich for performing XRF analyses. We acknowledge the UK Natural Environment Research Council Grant NE/G01700X/1 (to Tamsin Mather), Ph. D. studentship NE/L501530/1 (to Lawrence Percival), Grant NE/H020756/1 (to Ian Jarvis), the European Commission (FP7/2007–2013 grant number 215458), National Science Foundation Grant EAR0643290 (to Bradley Sageman and Jennifer McElwain), Shell International Exploration and Production Inc., and the Leverhulme Trust for funding.

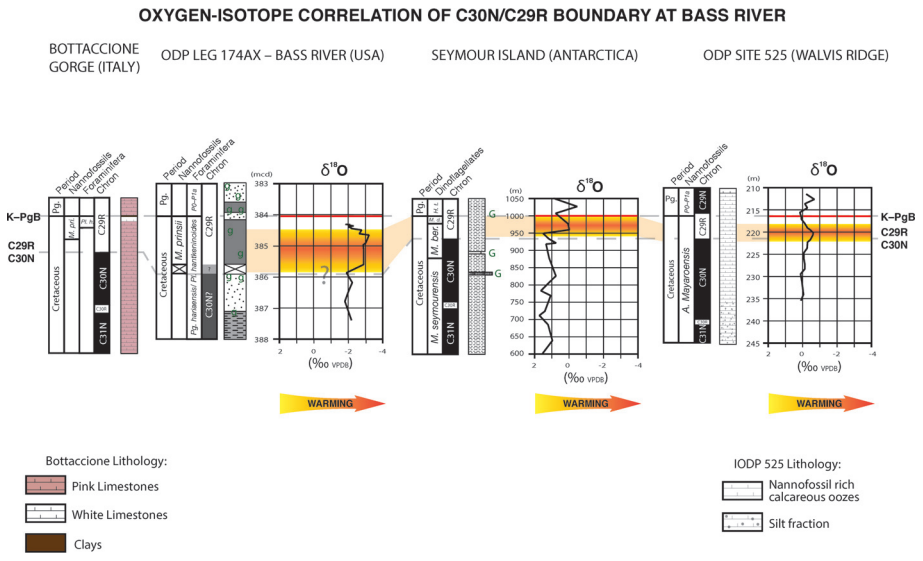

Fig. A1. Bottaccione Gorge biostratigraphy from Gardin and others (2012); Bass River lithology and biostratigraphy from Miller and others (1998) and Esmeray-Senlet and others (2015); Seymour Island lithology and biostratigraphy from Witts and others (2015); Walvis Ridge lithology and biostratigraphy from Moore and others (1983, GSA Bulletin, https://doi.org/10.1130/0016-7606(1983)94<907:TWRTDS>2.0.C0;2). Oxygen-isotope trend lines based on data from Olsson and others (2002: Bass River); Tobin and others (2012: Seymour Island); and Birch and others (2016: Walvis Ridge). Bottaccione Gorge paleomagnetic data from Gardin and others (2012); Seymour Island paleomagnetic data from Tobin and others (2012); Walvis ridge paleomagnetic data from Robinson and others (2009). The K–Pg boundary and C30N/C29R boundaries are indicated. Bass River magnetostratigraphy reconstructed on the basis of the relationship between the C30N/C29R boundary and changes in nannofossil species and oxygen-isotope compositions recorded at these locations.

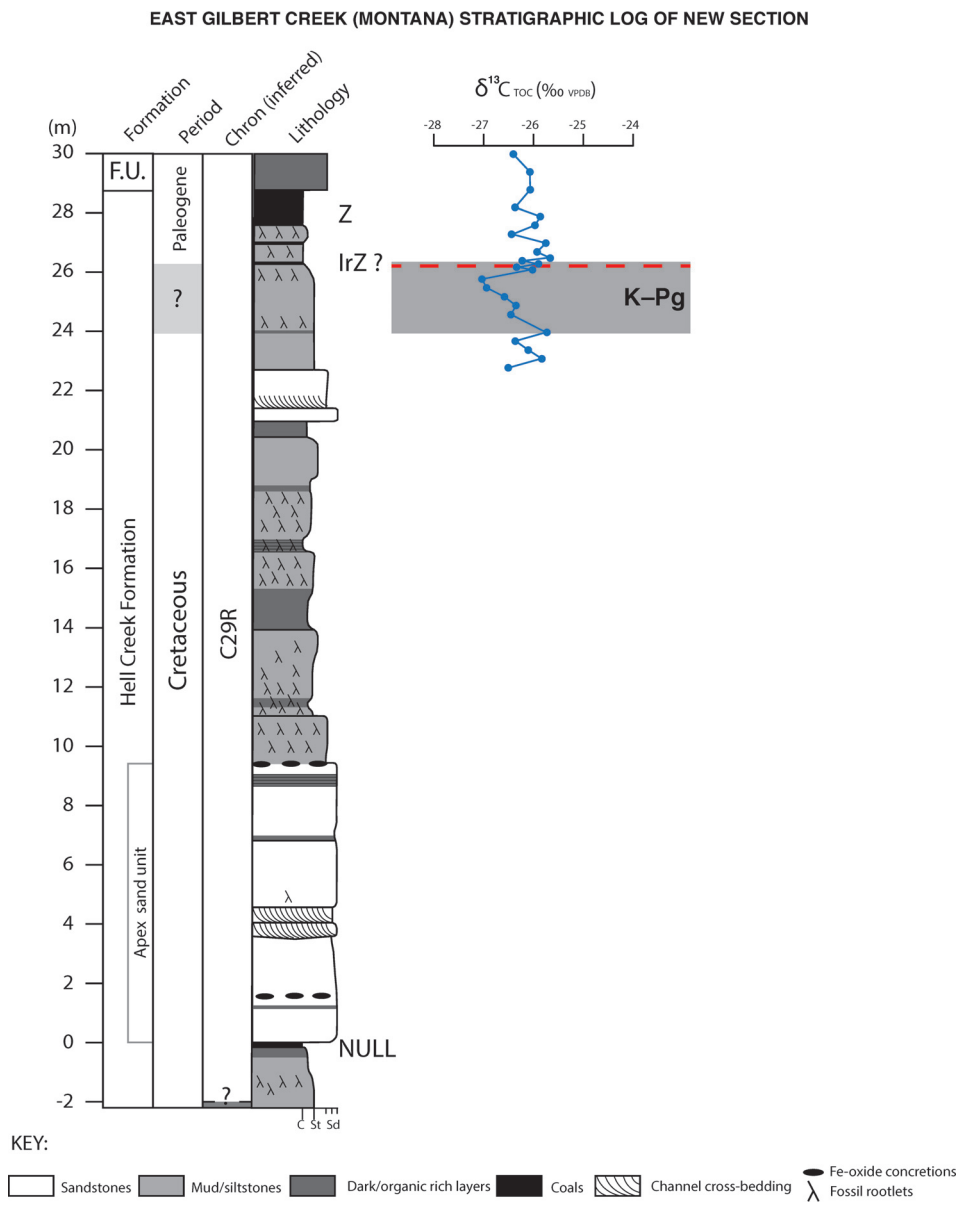

Fig. A2. Magnetostratigraphy inferred from data in Clyde and others (2016) and Sprain and others (2018). "F.U." denotes "Fort Union Member". NULL, IrZ, and Z indicate the stratigraphic position of their respective coal units.

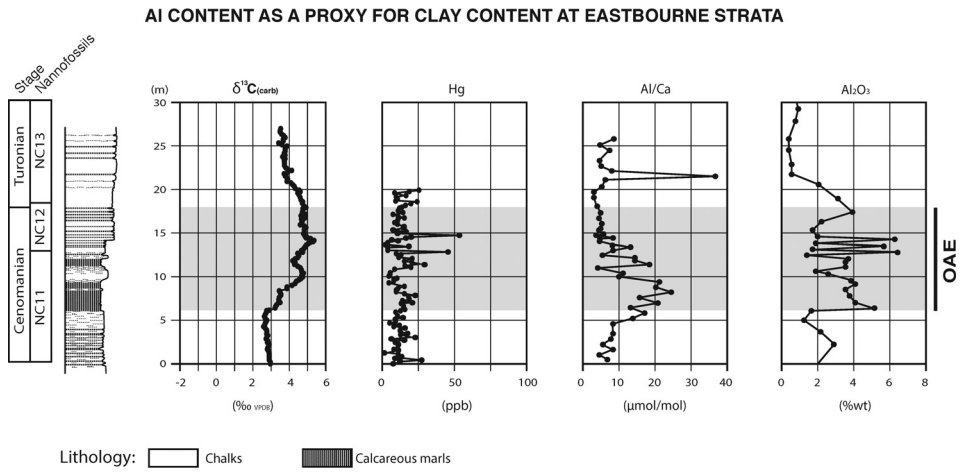

Fig. A3. Al/Ca data from supplementary information in Sweere and others (2018). Al_2O_3 data from Pearce and others (2009). Hg data from this study. Carbon-isotope data, biostratigraphy, and lithology from Tsikos and others (2004).

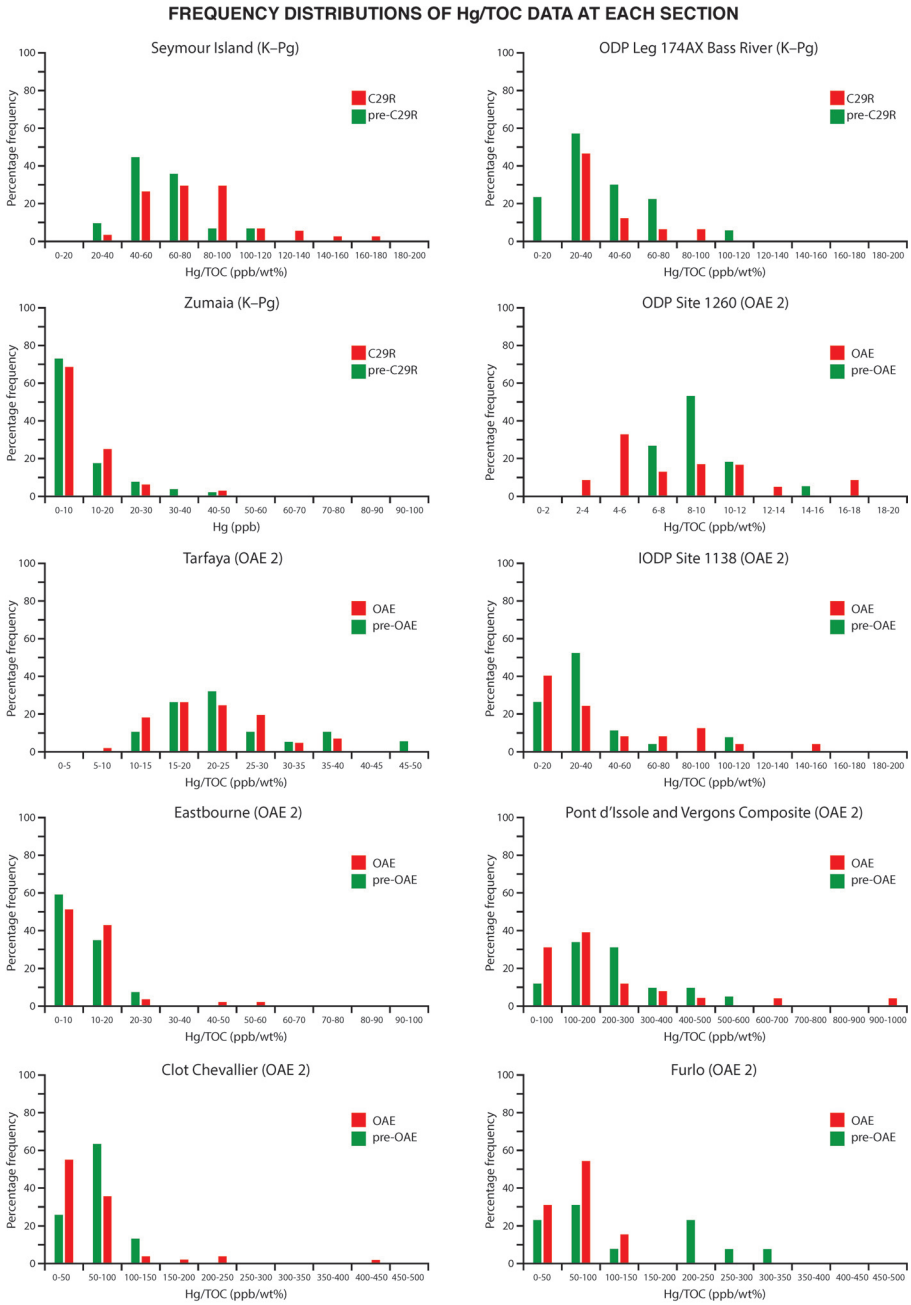

East Gilbert Creek (Montana, USA: K–Pg) and Utah Composite (OAE 2) are not presented due to insufficient pre-event data.

Fig. A4. East Gilbert Creek (Montana, USA: K–Pg) and Utah Composite (OAE 2) are not presented due to insufficient pre-event data.

TABLE A1

K–Pg Data: Seymour Island

Sample	Height (m)	Hg (ppb)	TOC (wt%)	Hg/TOC	Sample	Height (m)	Hg (ppb)	TOC (wt%)	Hg/TOC
D6.004.44	14.8	32.5	0.390	83.27	D6.004.4	-5.3	31	0.315	98.40
D6.004.43	14.3	29.5	0.394	74.89	D6.004.3	-5.8	24.5	0.377	65.03
D6.004.42	13.8	30.5	0.338	90.25	D9.007.1	-5.85	27	0.42	64.29
D6.004.41	13.3	36.5	0.286	127.56	D6.004.2	-6.3	34	0.379	89.79
D6.004.40	12.8	31.5	0.275	114.38	D6.004.1	-6.8	31.5	0.359	87.77
D6.004.39	12.3	18	0.235	76.62	D5.1279.1	-13.5	18	0.430	41.86
D6.004.38	11.8	26	0.353	73.68	D9.006.1	-14.85	25.5	0.49	52.04
D6.004.37	11.3	29	0.296	98.11	D5.1253.1	-19.5	22	0.500	44
D6.004.36	10.8	20	0.276	72.35	D5.1268.1	-23.5	17.5	0.540	32.41
D6.004.35	10.3	24	0.320	74.09	D5.1248.1	-29.5	20	0.29	68.97
D6.004.34	9.8	27.5	0.296	93.05	D5.1258.1	-33.5	17	0.32	53.13
D6.004.33	9.3	33	0.279	118.48	D5.1242.1	-39.5	17.5	0.35	50
D6.004.32	8.8	28	0.301	93.15	D5.1237.1	-49.5	16	0.37	43.24
D6.004.31	8.3	26	0.335	77.58	D5.1230.1	-59.5	17.5	0.26	67.31
D6.004.30	7.8	23.5	0.289	81.29	D5.1225.1	-67.5	19.5	0.22	88.64
D9.035.1	7.65	14	0.32	43.75	D5.1120.1	-77.5	15	0.2	75
D6.004.29	7.3	24	0.345	69.58	D5.1215.1	-87.5	17.5	0.27	64.81
D6.004.28	6.8	24	0.309	77.67	D5.1210.1	-97.5	21.5	0.31	69.35
D6.004.27	6.3	17	0.359	47.42	D5.1205.1	-107.5	14	0.24	58.33
D6.004.26	5.8	15.5	0.263	59.02	D5.1198.1	-117.5	22.5	0.27	83.33
D6.004.25	5.3	16.5	0.252	65.36	D5.1192.1	-127.5	19.5	0.19	102.63
D6.004.24	4.8	25.5	0.305	83.54	D5.1187.1	-137.5	19.5	0.31	62.90
D6.004.23	4.3	39.5	0.230	171.52	D5.1184.1	-141.5	24	0.29	82.76
D6.004.22	3.8	38.5	0.400	96.21	D5.1179.1	-151.5	20	0.3	66.67
D6.004.21	3.3	25	0.323	77.28	D5.1174.1	-161.5	19	0.28	67.86
D6.004.20	2.8	45	0.295	152.65	D5.1168.1	-171.5	13	0.12	108.33
D9.032.1	2.65	16.5	0.17	97.06	D5.1165.1	-174.5	12	0.51	23.53
D6.004.19	2.3	19	0.310	61.26	D5.1162.1	-177.5	15.5	0.35	44.29
D6.004.18	1.8	16	0.310	51.63	D5.1160.1	-181.5	17.5	0.26	67.31
D6.004.17	1.3	27	0.299	90.29	D5.1155.1	-191.5	13	0.23	56.52
D6.004.16	0.8	20	0.360	55.58	D5.1151.1	-199.5	10.6	0.15	70.67
D6.004.15	0.3	30	0.300	99.90	D5.1147.1	-211.5	26.5	0.44	60.23
D9.029.1	-0.15	20.5	0.37	55.41	D5.1142.1	-221.5	14	0.18	77.78
D6.004.14	-0.3	16	0.232	68.92	D5.1137.1	-231.5	15	0.33	45.45
D5.1292.1	-0.5	13.5	0.390	34.62	D5.1132.1	-241.5	18	0.31	58.06
D6.004.13	-0.8	46.5	0.518	89.75	D5.1128.1	-251.5	23.5	0.4	58.75
D9.009.1	-1.05	19	0.38	50	D5.1121.1	-261.5	27.5	0.49	56.12
D6.004.12	-1.3	43	0.477	90.14	D5.1116.1	-271.5	24.5	0.63	38.89
D9.028.1	-1.35	19.5	0.36	54.17	D5.1106.1	-281.5	18.5	0.43	43.02
D6.004.11	-1.8	39.5	0.372	106.23	D5.1096.1	-291.5	20.5	0.33	62.12
D6.004.10	-2.3	37.5	0.440	85.25	D5.1086.1	-301.5	13.5	0.34	39.71
D6.004.9	-2.8	48.5	0.350	138.68	D5.1077.1	-311.5	21	0.33	63.64
D9.026.1	-2.85	31	0.30	103.33	D5.1061.1	-326.5	24.5	0.44	55.68
D9.008.1	-2.85	18	0.36	50	D5.1051.1	-336.5	18	0.4	45
D6.004.8	-3.3	31	0.404	76.75	D5.1040.1	-346.5	19.5	0.37	52.70
D5.1289.1	-3.5	23	0.430	53.49	D5.1032.1	-356.5	18.5	0.39	47.44
D6.004.7	-3.8	30	0.357	84.07	D5.1021.1	-366.5	17	0.37	45.95
D6.004.6	-4.3	46	0.343	133.98	D5.1011.1	-376.5	21.5	0.51	42.16
D6.004.5	-4.8	35.5	0.310	114.57	D5.1001.1	-386.5	21	0.43	48.84

All data generated in this study.

TABLE A2

K–Pg Data: ODP Leg 174AX (Bass River)

Top (ft)	Bottom (ft)	Top (m)	Bottom (m)	Hg (ppb)	TOC (wt%)	Hg/TOC
1258.2	1258.25	383.499	383.515	17	0.2	85
1258.75	1258.8	383.667	383.682	14.5	0.19	76.32
1259.35	1259.4	383.850	383.865	23.5	0.74	31.76
1260.8	1260.85	384.292	384.307	15	1.14	13.16
1261.25	1261.3	384.429	384.444	30	1.14	26.32
1261.4	1261.45	384.475	384.490	44	1.29	34.11
1261.6	1261.65	384.536	384.551	42	1.04	40.38
1261.8	1261.85	384.597	384.612	36.5	1.09	33.49
1262.05	1262.1	384.673	384.688	30.5	1.22	25
1262.25	1262.3	384.734	384.749	27	1.19	22.69
1262.5	1262.55	384.810	384.825	21	1.16	18.10
1262.9	1262.95	384.932	384.947	37	0.95	38.95
1263.4	1263.45	385.084	385.100	40	0.77	51.95
1263.7	1263.75	385.176	385.191	29.5	1.01	29.21
1264.1	1264.15	385.298	385.313	17	1.26	13.49
1264.45	1264.5	385.404	385.420	22.5	0.85	26.47
1264.65	1264.7	385.465	385.481	23.5	1.31	17.94
1265.05	1265.1	385.587	385.602	23.5	0.94	25
1266.05	1266.1	385.892	385.907	28	0.55	50.91
1266.2	1266.25	385.938	385.953	34.5	1.02	33.83
1266.4	1266.45	385.999	386.014	29	0.66	43.94
1266.55	1266.6	386.044	386.060	28.5	0.89	32.02
1266.7	1266.75	386.090	386.105	22.5	0.9	25
1266.9	1266.95	386.151	386.166	26	1.15	22.61
1267.05	1267.1	386.197	386.212	30.5	1.13	26.99
1267.2	1267.25	386.243	386.258	26.5	1.18	22.46
1267.4	1267.45	386.304	386.319	35	1.07	32.71
1267.55	1267.6	386.349	386.364	29.5	1.1	26.82
1267.75	1267.8	386.410	386.425	30.5	1.06	28.77
1267.9	1267.95	386.456	386.471	32.5	1.1	29.55
1268.05	1268.1	386.502	386.517	30	0.85	35.29
1268.25	1268.3	386.563	386.578	26.5	0.88	30.11
1268.4	1268.45	386.608	386.624	28.5	1.04	27.40
1268.55	1268.6	386.654	386.669	38	1.06	35.85
1268.75	1268.8	386.715	386.730	19	0.66	28.79
1268.9	1268.95	386.761	386.776	50	0.94	53.19
1269.05	1269.1	386.806	386.822	84	0.78	107.69
1269.2	1269.25	386.852	386.867	29.5	0.47	62.77
1269.4	1269.45	386.913	386.928	43	0.61	70.49
1269.55	1269.6	386.959	386.974	36	0.91	39.56
1269.75	1269.8	387.020	387.035	47.5	0.86	55.23
1269.9	1269.95	387.066	387.081	41	0.8	51.25
1270.05	1270.1	387.111	387.126	51	0.9	56.67
1270.25	1270.3	387.172	387.187	40.5	0.64	63.28
1270.4	1270.45	387.218	387.233	38	0.93	40.86
1270.6	1270.7	387.279	387.309	42.5	0.89	47.75
1270.75	1270.8	387.325	387.340	32.5	0.99	32.83
1270.9	1270.95	387.370	387.386	40	0.86	46.51
1271.1	1271.15	387.431	387.447	35	0.49	71.43
1271.25	1271.3	387.477	387.492	28	0.7	40
1271.4	1271.45	387.523	387.538	32.5	1.02	31.86
1271.6	1271.65	387.584	387.599	40.5	0.75	54
1271.75	1271.8	387.629	387.645	33.5	0.87	38.51
1271.85	1271.9	387.660	387.675	37	0.49	75.51
1272.1	1272.15	387.736	387.751	47.5	0.77	61.69
1272.25	1272.3	387.782	387.797	51.5	0.66	78.03
1272.4	1272.45	387.828	387.843	38	0.56	67.86
1272.5	1272.55	387.858	387.873	30.5	0.29	105.17
1272.65	1272.7	387.904	387.919	17	0.29	58.62
1272.9	1272.95	387.980	387.995	28.5	0.36	79.17

All data generated in this study.

TABLE A3

K–Pg Data: Zumaia

Sample		Depth (cm)	Hg (ppb)	Al_2O_3	Sample		Depth (cm)	Hg (ppb)	Al_2O_3
ZK	1	-4.9	13	7.96	ZU	70	-1873.1	2.3	6.96
ZK	2	-14.6	6.9	4.64	ZU	69	-1886.2	17.5	11.51
ZK	3	-24.4	6.8	6.48	ZU	68	-1899.3	21	11.40
ZK	4	-34.1	10	7.79	ZU	67	-1912.4	32.5	12.28
ZK	5	-44.8	5.7	7.35	ZU	66	-1923.0	4.5	7.40
ZK	6	-56.3	10	7.98	ZU	65	-1931.0	4.5	7.36
ZK	7	-70.5	9.9	8.51	ZU	64	-1939.0	9.2	7.65
ZK	8	-83.3	18	9.45	ZU	63	-1947.0	15	7.91
ZK	9	-92.0	6.9	8.14	ZU	62	-1955.0	38	9.79
ZK	10	-100.7	4.3	8.13	ZU	61	-1969.6	46	11.88
ZK	11	-111.3	3.8	7.63	ZU	60	-1980.9	39	11.59
ZK	12	-123.8	11.5	9.58	ZU	59	-1992.1	15	10.71
ZK	13	-136.3	20	7.87	ZU	58	-2003.4	3.8	8.60
ZK	14	-149.0	7.5	10.12	ZU	57	-2014.3	3.4	7.59
ZK	15	-161.7	9.3	11.04	ZU	56	-2024.8	3.3	6.92
ZK	16	-175.3	4.4	10.14	ZU	55	-2035.4	1.9	7.40
ZK	17	-189.3	4.1	6.63	ZU	54	-2045.9	4.2	8.21
ZK	18	-198.3	8.2	8.31	ZU	53	-2056.5	5.1	8.41
ZK	19	-204.8	4.4	9.52	ZU	52	-2067.1	5.5	8.93
ZK	20	-219.0	4.7	8.99	ZU	51	-2077.6	14.5	10.18
ZK	21	-236.2	18.5	10.58	ZU	50	-2088.2	8.4	9.94
ZK	22	-248.5	15	11.98	ZU	49	-2098.7	12.5	9.47
ZK	23	-260.8	29	12.14	ZU	48	-2109.4	7	9.02
ZR	30	-281.0	47	12.63	ZU	47	-2120.1	5.3	8.61
ZR	29	-291.6	19.5	11.16	ZU	46	-2130.8	2.9	8.91
ZR	28	-302.3	11	10.18	ZU	45	-2141.5	4.4	8.25
ZR	27	-312.9	12.5	10.59	ZU	44	-2152.2	3.87	9.07
ZR	26	-323.5	13.5	11.53	ZU	43	-2162.9	4.23	9.51
ZR	25	-334.1	8.8	11.00	ZU	42	-2173.6	5.6	9.59
ZR	24	-344.8	4.6	11.24	ZU	41	-2184.3	8.9	11.24
ZR	23	-355.4	8.4	11.54	ZU	40	-2195.0	19	11.06
ZR	22	-366.0	23	12.16	ZU	39	-2205.7	9.7	10.67
ZR	21	-376.6	9.5	11.92	ZU	38	-2216.8	6.1	9.07
ZR	20	-387.3	3	11.43	ZU	37	-2228.5	3.5	8.82
ZR	19	-397.9	9.7	11.24	ZU	36	-2240.2	2.9	9.14
ZR	18	-408.5	7.1	10.88	ZU	35	-2251.8	4.9	8.86
ZR	17	-419.1	2.6	9.81	ZU	34	-2263.5	7.6	10.82
ZR	16	-429.8	4.3	10.32	ZU	33	-2275.2	12	12.08
ZR	15	-440.4	4.5	10.47	ZU	32	-2286.8	22	11.73
ZR	14	-451.0	7.9	11.20	ZU	31	-2298.5	22.5	12.53
ZR	13	-461.7	22	11.99	ZU	30	-2310.2	19.5	11.53
ZR	12	-472.3	26	11.73	ZU	29	-2320.1	3.8	8.63
ZR	11	-482.9	7.1	10.68	ZU	28	-2328.4	4.3	8.58
ZR	10	-493.5	10	10.35	ZU	27	-2336.6	15.5	9.72
ZR	9	-504.2	9.2	10.08	ZU	26	-2344.9	4.9	9.03
ZR	8	-514.8	11.5	9.65	ZU	25	-2353.1	6.5	10.55
ZR	7	-525.4	7.3	10.52	ZU	24	-2361.4	17.5	11.83
ZR	6	-536.0	6.4	11.57	ZU	23	-2369.6	14	11.98
ZU	92	-1628.6	4.6	7.73	ZU	22	-2377.9	9.1	11.56
ZU	91	-1636.9	3	7.84	ZU	21	-2386.4	5.1	8.48
ZU	90	-1646.5	3.57	6.76	ZU	20	-2395.2	4.2	8.24
ZU	89	-1657.5	3.5	5.84	ZU	19	-2403.9	5.4	8.31
ZU	88	-1668.5	3.5	6.80	ZU	18	-2412.7	9.4	9.64
ZU	87	-1679.5	4.8	8.63	ZU	17	-2421.5	23	11.12
ZU	86	-1690.5	8.5	8.78	ZU	16	-2430.3	13.5	11.05
ZU	85	-1701.5	21.5	10.38	ZU	15	-2439.1	14	10.90
ZU	84	-1712.5	8.7	9.60	ZU	14	-2447.8	6.9	9.59
ZU	83	-1723.5	4.4	8.05	ZU	13	-2456.6	6.8	10.19
ZU	82	-1734.3	3.7	5.61	ZU	12	-2466.4	5.9	9.34
ZU	81	-1744.9	3.2	6.97	ZU	11	-2477.1	5.5	8.02
ZU	80	-1755.6	3.2	6.67	ZU	10	-2487.9	4.7	7.45
ZU	79	-1766.2	4.8	6.72	ZU	9	-2498.6	7.3	7.66
ZU	78	-1776.8	15	9.62	ZU	8	-2509.4	6.1	9.36
ZU	77	-1787.4	12	10.46	ZU	7	-2520.1	7	9.92
ZU	76	-1798.1	7.4	10.31	ZU	6	-2530.9	26.5	10.67
ZU	75	-1808.7	15.5	9.93	ZU	5	-2541.6	6.3	9.98
ZU	74	-1820.6	3.7	7.75	ZU	4	-2550.1	6.4	7.42
ZU	73	-1833.7	2.3	5.76	ZU	3	-2556.4	4.4	7.44
ZU	72	-1846.8	3	6.68	ZU	2	-2562.6	5.1	6.93
ZU	71	-1859.9	3.03	7.35	ZU	1	-2568.9	3.3	7.71

All data generated in this study.

TABLE A4

K–Pg Data: East Gilbert Creek, Montana

Sample # (height in cm)	δ^{13}Corg (‰)	Hg (ppb)	TOC (wt%)	Hg/TOC
3000	-26.41	48.5	0.4	121.25
2970		72	0.3	240
2940	-26.08	32	0.3	106.67
2910		71.5	1.6	44.69
2880	-26.07	8	50.2	0.16
2820	-26.38	34	30.8	1.10
2760	-25.98	267.5	39	6.86
2730	-26.44	50.5	0.4	126.25
2700	-25.76	366.5	48.6	7.54
2670	-25.93	23	0.2	115
2650	-25.67	51	0.2	255
2640	-26.23	42	0.2	210
2630	-25.91	116.5	20.3	5.74
2620	-26.34	99.5	0.5	199
2610	-26.02	340	0.7	485.71
2580	-27.04	36.5	0.2	182.5
2550	-26.95	28.5	0.1	285
2520	-26.59	24.5	0.1	245
2490	-26.36	20	0.1	200
2460	-26.46	53.5	0.2	267.5
2430		34.5	0.2	172.5
2400	-25.74	92	1.6	57.5
2370	-26.37	67	0.2	335
2340	-26.11	38.5	0.2	192.5
2310	-25.84	59.5	0.2	297.5
2280	-26.51	43.5	0.3	145
2070		147.5	0.2	737.5
2040		34	0.2	170
2010		31	0.2	155
1980		23	0.3	76.67
1950		126.5	0.2	632.5
1920		124	0.3	413.33
1890		53.5	0.8	66.88
1860		79.5	0.9	88.33
1830		92.5	0.5	185
1800		138.5	0.2	692.5
1770		83.5	0.6	139.17
1740		65.5	1.1	59.55
1710		116.5	1.2	97.08
1680		145	1.4	103.57
1650		67	0.6	111.67
1620		77.5	0.3	258.33
1590		66.5	0.3	221.67
1560		74.5	0.6	124.17
1530		63.5	1	63.5
1500		277.5	0.6	462.5
1470		186.5	0.5	373
1440		92	1.2	76.67
1380		68.5	1.1	62.27
1320		115	0.3	383.33
1260		172.5	0.2	862.5
1200		102	0.3	340
1140		99.5	0.2	497.5
1080		52	0.1	520
960		34.5	0.6	57.5
900		22.5	0.3	75
870		46	0.5	92
690		79	1	79
-30		262.5	1.9	138.16
-60		165.5	0.2	827.5
-90		115	0.5	230
-120		30.5	0.5	61
-150		44	0.5	88
-180		31	0.34	91.18

All data generated in this study.

TABLE A5

OAE 2 Data: ODP Site 1260 (Demerara Rise)

mbsf (of top)	Hg (ppb)	TOC (wt%)	Hg/TOC		mbsf (of top)	Hg (ppb)	TOC (wt%)	Hg/TOC
415.31	163.5	4.6	35.54		420.99	59.5	13	4.58
416	135.5	10.7	12.66		421.05	48.5	11.6	4.18
416.41	111.5	9.2	12.12		421.095	38.5	10.1	3.81
417.995	103	9.3	11.08		421.23	4.7	0.5	9.4
418.25	46.5	3.8	12.24		421.38	88	11.6	7.59
418.74	79.5	11.7	6.79		421.41	109.5	6.1	17.95
419	101.5	11	9.23		421.445	146.5	16	9.16
419.065	115.5	9	12.83		421.505	181	13.3	13.61
419.105	54	9.4	5.74		421.53	169.5	17.2	9.85
419.27	93.5	8.7	10.75		421.57	94.5	20.5	4.61
419.295	103	8.4	12.26		421.61	120.5	10.1	11.93
419.39	27.5	4.2	6.58		421.645	117.5	11.1	10.59
419.43	11.9	3	3.97		421.715	17.5	5.9	2.97
419.625	10				421.735	30.5	3.8	8.03
419.65	17				421.77	94.5	7.4	12.77
419.78	92	7.4	12.43		421.825	148	13.9	10.65
419.82	39.5	7.5	5.27		421.94	84	12.7	6.61
419.855	30.5	2.9	10.52		422	65	8.8	7.39
419.91	109	9.5	11.47		422.02	74.5	8.8	8.47
419.96	160.5	11.1	14.46		422.055	81.5	9	9.06
420.05	172	12.8	13.44		422.17	80	7.7	10.39
420.11	153	11.8	12.97		422.19	80	7.9	10.13
420.15	122	11.5	10.61		422.31	73	9	8.11
420.21	131	12.2	10.74		422.47	67.5	8.2	8.23
420.25	143.5				422.55	76	9	8.44
420.31	182.5	9.4	19.41		422.805	40	5	8
420.36	170	12	14.17		422.855	97.5	6.6	14.77
420.41	121	10.2	11.86		422.905	68	7.4	9.19
420.46	144.5	9.7	14.90		422.96	65	7.6	8.55
420.5	52.5	9.3	5.65		422.98	70	7.3	9.59
420.575	51.5	2.5	20.6		423.01	60.5	7.2	8.40
420.59	49				423.11	10.8	1.4	7.71
420.66	44	2.6	16.92		423.31	40.5	4.4	9.20
420.71	126	17	7.41		423.36	47.5	5.4	8.80
420.76	74	15	4.93		423.41	61.5	6.5	9.46
420.81	55	13.4	4.10		423.46	49.5	7.3	6.78
420.87	113	15.9	7.11		423.51	62.5	6.1	10.25
420.91	66	16.2	4.07		423.535	54	7.3	7.40
420.955	68.5	14.5	4.72		423.56	95	8.2	11.59

All data generated in this study.

TABLE A6

OAE 2 Data: Tarfaya

Sample no.	mbs (top)	Hg (ppb)	TOC (wt%)	Hg/TOC	Sample no.	mbs (top)	Hg (ppb)	TOC (wt%)	Hg/TOC
S57-120	-23.41	381	12.240	31.13	S57-60	-48.08	241	14.360	16.78
S57-119	-23.79	264	8.850	29.83	S57-59	-48.31	140	5.236	26.74
S57-118	-24.16	291	8.720	33.37	S57-58	-48.5	145.5	12.040	12.08
S57-117	-24.51	152	10.060	15.11	S57-57	-48.69	110	8.351	13.17
S57-116	-24.9	232	8.280	28.02	S57-56	-48.92	161.5	12.140	13.30
S57-115	-25.29	214.5	8.736	24.55	S57-55	-49.13	248.5	21.580	11.52
S57-114	-25.69	235	7.909	29.71	S57-54	-49.36	192	11.340	16.93
S57-113	-26.09	197	12.850	15.33	S57-53	-49.57	303	15.050	20.13
S57-112	-26.48	55.5	2.730	20.33	S57-52	-49.8	227.5	15.550	14.63
S57-111	-26.87	86.5	4.024	21.50	S57-51	-49.51	340	25.930	13.11
S57-110	-27.27	110.5	4.796	23.04	S57-50	-50.16	301	16.610	18.12
S57-109	-27.65	84.5	4.368	19.345	S57-49	-50.35	91.5	7.511	12.18
S57-108	-28.07	184.5	6.320	29.19	S57-48	-50.56	67.5	2.696	25.04
S57-107	-28.49	333.5	15.640	21.32	S57-47	-50.76	91	3.881	23.45
S57-106	-28.89	85.5	3.408	25.09	S57-46	-51	104.5	4.373	23.90
S57-105	-29.24	268.5	11.600	23.15	S57-45	-51.13	156	5.875	26.55
S57-104	-29.62	114.5	5.061	22.62	S57-44	-51.36	167	13.820	12.08
S57-103	-30	156.5	6.818	22.95	S57-43	-51.55	146	9.306	15.69
S57-102	-30.47	44.5	1.540	28.90	S57-42	-51.75	218.5	15.960	13.69
S57-101	-30.87	188.5	9.635	19.56	S57-41	-51.92	171	10.510	16.27
S57-100	-31.27	279	9.772	28.55	S57-40	-52.11	192	9.031	21.26
S57-99	-31.67	195.5	8.666	22.56	S57-39	-52.3	161.5	10.840	14.90
S57-98	-32.07	240.5	7.500	32.07	S57-38	-52.51	157	7.367	21.31
S57-97	-32.41	91.5	4.351	21.03	S57-37	-52.7	121	5.283	22.90
S57-96	-32.77	217.5	13.010	16.72	S57-36	-52.92	84.5	4.566	18.51
S57-95	-33.16	262.5	9.961	26.35	S57-35	-53.12	63	2.308	27.30
S57-94	-33.57	156	6.171	25.28	S57-34	-53.33	80	2.455	32.59
S57-93	-33.92	54.5	1.692	32.21	S57-33	-53.52	75	2.613	28.70
S57-92	-34.31	51.5	1.975	26.08	S57-32	-53.73	127	7.879	16.12
S57-91	-34.61	83	3.082	26.93	S57-31	-54	253	10.910	23.19
S57-90	-35	132	4.835	27.30	S57-30	-54.16	270.5	10.960	24.68
S57-89	-35.41	223.5	10.890	20.52	S57-29	-54.35	247	10.310	23.96
S57-88	-35.8	296	14.440	20.50	S57-28	-54.53	202	8.093	24.96
S57-87	-36.26	328.5	9.643	34.07	S57-27	-54.76	231	12.080	19.12
S57-86	-36.78	282.5	12.300	22.97	S57-26	-54.95	209.5	5.534	37.86
S57-85	-37.52	71.5	4.393	16.28	S57-25	-55.13	205	6.561	31.25
S57-84	-37.94	17	0.671	25.34	S57-24	-55.34	127.5	4.560	27.96
S57-83	-38.34	67	0.755	88.74	S57-23	-55.51	164.5	5.938	27.70
S57-82	-38.75	160.5	7.090	22.64	S57-22	-55.71	153.5	6.277	24.45
S57-81	-39.17	303.5	7.708	39.37	S57-21	-55.89	122	6.387	19.10
S57-80	-40.07	161.5	4.200	38.45	S57-20	-56.08	146	8.040	18.16
S57-79	-40.44	246	14.240	17.28	S57-19	-56.29	25	1.018	24.56
S57-78	-40.8	210	13.310	15.78	S57-18	-56.49	162	6.841	23.68
S57-77	-41.22	112	3.818	29.33	S57-17	-56.72	200	5.868	34.08
S57-76	-41.63	179.5	9.562	18.77	S57-16	-56.87	75	2.982	25.15
S57-75	-42	153	7.661	19.97	S57-15	-57.07	162	6.611	24.50
S57-74	-44.61	115.5	12.160	9.50	S57-14	-57.25	118.5	6.621	17.90
S57-73	-44.81	126.5	7.625	16.59	S57-13	-57.42	87	3.888	22.38
S57-72	-45.15	153.5	6.913	22.20	S57-12	-57.59	91	1.931	47.13
S57-71	-45.32	177	7.592	23.31	S57-11	-57.77	83	4.001	20.74
S57-70	-45.54	120.5	10.840	11.12	S57-10	-58	119	6.100	19.51
S57-69	-45.74	79	2.335	33.83	S57-9	-58.16	124.5	5.243	23.75
S57-68	-45.94	60.5	2.071	29.21	S57-8	-58.36	96.5	6.647	14.52
S57-67	-46.13	87	3.709	23.46	S57-7	-58.57	164.5	8.326	19.76
S57-66	-46.32	148.5	4.485	33.11	S57-6	-58.69	177.5	9.903	17.92
S57-65	-47	367	12.280	29.89	S57-5	-58.91	178	6.166	28.87
S57-64	-47.19	310.5	8.415	36.90	S57-4	-59.12	145.5	3.828	38.01
S57-63	-47.46	253.5	9.906	25.59	S57-3	-59.35	132	8.493	15.54
S57-62	-47.61	274.5	17.350	15.82	S57-2	-59.52	188	5.209	36.09
S57-61	-47.84	314	14.700	21.36	S57-1	-59.68	117.5	9.309	12.62

TOC data from Tsikos and others (2004).

TABLE A7

OAE 2 Data: Utah composite

Sample	Height (m)	Hg (ppb)	TOC (wt%)	Hg/TOC
RSB0766	84.5	170.50	1.70	100.29
RSB0765	84.2	61.00	4.00	15.25
RSB0742	79.5	15.50	0.48	32.29
RSB0552-CDR2-58.68A	58.68	23.50	1.25	18.80
RSB0552-CDR2-41.6A	41.6	86.50	0.64	135.16
RSB0552-CDR2-38.43A	38.43	93.50	4.00	23.38
RSB0552-CDR2-36.8A	36.8	29.50	0.21	140.48
RSB0552-CDR2-36.0A	36	94.50	1.58	59.81
RSB0552-CDR2-35.55A	35.55	34.50		
RSB0556-KMT1-35.08	35.08	108.50	6.33	17.14
RSB0552-CDR2-24.25A	24.25	19.00	0.59	32.20
RSB0552-CDR2-22.8A	22.8	43.50	0.24	181.25
RSB0527-CDR4-17.62B	17.62	82.00	7.62	10.76
RSB0527-CDR4-17.0A	17	73.50	1.90	38.68
RSB0527-CDR4-16.9A	16.9	68.00	0.78	87.18
RSB0527-CDR4-13.2A	13.2	42.00	1.31	32.06
RSB0527-CDR4-12.4A	12.4	23.00	0.64	35.94
RSB0527-CDR4-12.0A	12	41.00	1.20	34.17
RSB0527-CDR4-11.6A	11.6	37.00	0.84	44.05
RSB0527-CDR4-11.2A	11.2	36.50	1.66	21.99
RSB0527-CDR4-10.2A	10.2	77.50	6.76	11.46
RSB0527-CDR4-08.0A	8	60.00	5.81	10.33
RSB0527-CDR4-05.2A	5.2	74.00	8.06	9.18
RSB0527-CDR4-03.7A	3.7	77.50	8.46	9.16
RSB0749-10.75	0.92	60.00	2.95	20.34
RSB0749-10.35	0.52	72.00	3.36	21.43
RSB0749-09.80	-0.23	24.00	1.12	21.43
RSB0749-08.63	-1.2	13.00	1.20	10.83
RSB0749-08.33	-1.5	29.00	1.12	25.89
RSB0749-08.03	-1.8	62.50	1.99	31.41
RSB0749-07.73	-2.1	20.00	1.52	13.16
RSB0543-CWC1-m2.1A	-2.1	103.00	2.72	37.87
RSB0749-07.43	-2.4	29.00	2.20	13.18
RSB0749-05.60	-4.23	66.00	1.42	46.48
RSB0749-01.43	-8.4	70.00	0.92	76.09
RSB0749-01.38	-8.45	35.50	3.43	10.35
RSB0749-01.28	-8.55	34.50	3.64	9.48
RSB0749-01.18	-8.65	36.50	2.65	13.77
CWC2-m19.5A	-19.5	90.00	0.30	300.00
RSB0731	-30.7	163.00	1.93	84.46
RSB0730	-31.6	205.50	7.33	28.04
BKM1-07.4A	-62.6	215.00	12.72	16.90
RSB0534-BKM1-05.6A	-64.4	207.00	2.18	94.95
BKM1-03.8A	-66.2	53.50	3.23	16.56

All data generated in this study.

TABLE A8

OAE 2 Data: IODP Site 1138 (Kerguelen Plateau)

Depth (mbsf)	Hg (ppb)	TOC (wt%)	Hg/TOC	Depth (mbsf)	Hg (ppb)	TOC (wt%)	Hg/TOC
654.31	39	0.783	49.82	656.24	179.5	14.916	12.03
654.36	61	0.590	103.35	656.285	175	12.166	14.38
654.41	50.5	0.958	52.74	656.34	170	10.700	15.89
654.465	119	5.909	20.14	656.39	188.5	16.987	11.10
654.51	50	4.997	10.01	656.44	136	3.670	37.05
654.56	43	0.986	43.62	656.49	72.5	1.308	55.45
654.62	101	1.450	69.63	656.54	93	2.416	38.49
654.665	97.5	4.168	23.39	656.59	69	0.910	75.79
654.725	65	3.214	20.22	656.64	93.5	1.176	79.49
654.76	73.5	3.724	19.74	656.69	73	0.900	81.10
654.82	65	0.477	136.19	656.74	59	0.514	114.78
654.86	69.5	0.677	102.71	656.79	59	0.414	142.53
654.905	65	0.974	66.76	656.84	61.5	0.655	93.93
655.01	70.5	2.561	27.53	656.89	32.5		
655.06	58.5	1.557	37.57	656.95	28	0.255	109.60
655.115	73.5	1.407	52.25	657	23.5		
655.16	108.5	3.610	30.06	657.05	17.5	0.517	33.84
655.21	87.5	5.998	14.59	657.08	9.5	0.498	19.081
655.265	76	1.140	66.65	657.1	10.1	0.416	24.25
655.32	82.5	1.530	53.91	657.14	10.9	0.424	25.68
655.36	99.5	5.186	19.19	657.19	9.4	0.428	21.94
655.41	78	6.049	12.89	657.24	31.5	0.272	115.85
655.465	76.5	0.734	104.27	657.29	14	0.430	32.54
655.51	80	0.996	80.31	657.34	20	0.440	45.45
655.56	148	6.512	22.73	657.39	15.5	0.625	24.81
655.595	80.5	1.134	70.99	657.44	10.3	0.361	28.55
655.595	140.5	1.326	105.97	657.49	21.5	0.781	27.54
655.6	80.5	1.672	48.14	657.54	10.5	0.616	17.06
655.63	80	2.767	28.91	657.59	13	0.562	23.14
655.65	96.5	1.920	50.26	657.64	7.4	0.597	12.41
655.685	82	1.417	57.88	657.69	14	0.624	22.44
655.71	98	1.168	83.87	657.74	7.9	0.476	16.59
655.75	70.5	1.318	53.49	657.79	4.4	0.258	17.05
655.78	128	4.362	29.35	657.84	10.8	0.340	31.73
655.81	92	4.620	19.91	657.89	11.9	0.322	36.90
655.84	120	5.319	22.56	657.95	10.3	0.153	67.20
655.89	137	9.775	14.02	657.99	1.5	0.270	5.55
655.94	152.5	12.353	12.35	658.04	3	0.112	26.71
655.99	118	4.481	26.33	658.09	12	0.289	41.54
656.04	174.5	9.962	17.52	658.15	16.5	0.326	50.58
656.08	115.5	5.458	21.16	658.2	7	0.249	28.16
656.14	136	9.074	14.99	658.24	3.1	0.268	11.55

TOC data from Dickson and others (2017).

TABLE A9

OAE 2 Data: Eastbourne

Sample	Height (m)	Hg (ppb)	Sample	Height (m)	Hg (ppb)
WC 6.0	19.9	24	PM 400	10	2.4
WC 5.8	19.7	17	PM 380	9.8	8.3
WC 5.6	19.5	7	PM 360	9.6	6.6
WC 5.4	19.3	15	PM 340	9.4	6.4
WC 5.2	19.1	8	PM 320	9.2	2.8
WC 5.0	18.9	8.6	PM 300	9	
WC 4.8	18.7	7.9	PM 280	8.8	13.5
WC 4.6	18.5	23	PM 260	8.6	9
WC 4.4	18.3	18	PM 240	8.4	7.9
WC 4.2	18.1	14	PM 220	8.2	8.1
WC 4.0	17.9	12	PM 200	8	13.5
WC 3.8	17.7	10.6	PM 180	7.8	21
WC 3.6	17.5	9	PM 160	7.6	16.5
WC 3.4	17.3	12.5	PM 140	7.4	17
WC 3.2	17.1	5.7	PM 120	7.2	12.2
WC 3.0	16.9	9.5	PM 100	7	19
WC 2.8	16.7	14	PM 80	6.8	11.1
WC 2.6	16.5	9.2	PM 60	6.6	13.5
WC 2.4	16.3	9.1	PM 40	6.4	13
WC 2.2	16.1	6.6	PM 20	6.2	14
WC 2.0	15.9	8.8	GC 0	6	11
WC 1.8	15.7	13.5	GC 20	5.8	7.7
WC 1.6	15.5	13	GC 40	5.6	
WC 1.4	15.3	5.4	GC 60	5.4	8.9
WC 1.2	15.1	14.5	GC 80	5.2	12
WC 1.0	14.9	8.2	GC 100	5	7.3
WC 0.8	14.7	52.5	GC 120	4.8	7.5
WC 0.6	14.5	18.5	GC 140	4.6	2.6
WC++40	14.4		GC 160	4.4	9.8
WC 0.4	14.3	14.5	GC 180	4.2	6.5
WC 0.2	14.1	4.4	GC 200	4	14
PM 800	14	8.6	GC 220	3.8	10.5
WC 0.0	13.9		GC 240	3.6	11
PM 780	13.8	2.5	GC 260	3.4	15.5
PM 760	13.6	0	GC 280	3.2	11
PM 740	13.4	16.5	GC 300	3	21
PM 720	13.2	1.6	GC 320	2.8	5
PM 700	13	2.1	GC 340	2.6	13
PM 680	12.8	44.5	GC 360	2.4	7.1
PM 660	12.6	7.8	GC 380	2.2	9.3
PM 640	12.4	11.3	GC 400	2	9
PM 620	12.2	9.6	GC 420	1.8	
PM 600	12	19.5	GC 440	1.6	6.3
PM 580	11.8	13.5	GC 460	1.4	10
PM 560	11.6	19.5	GC 480	1.2	0
PM 540	11.4	27.5	GC 500	1	9.4
PM 520	11.2	14	GC 520	0.8	11.7
PM 500	11	18.5	GC 540	0.6	7.4
PM 480	10.8	6.9	GC 560	0.4	25.5
PM 460	10.6		GC 580	0.2	11
PM 440	10.4	3.6	GC 600	0	5.9
PM 420	10.2	3.5			

All data generated in this study.

TABLE A10

OAE 2 Data: Pont d'Issole and Vergons Composite

Sample	Height (m)	Hg (ppb)	TOC (wt%)	Hg/TOC	Sample	Height (m)	Hg (ppb)	TOC (wt%)	Hg/TOC
isl51b	23.50	69	1.49	46.31	vgn429	-6.00	58	0.28	207.14
isl51a	23.30	41.5	0.19	218.42	vgn428	-7.00	71.5	0.32	223.44
isl51	23.00	24.5	0.07	350	vgn431	-4.00	29.5	0.17	173.53
isl50	22.50	177.5	0.26	682.69	vgn427	-8.00	16.5	0.14	117.86
isl49a	21.80	50	0.11	454.55	vgn423	-12.00	72.50	0.26	278.85
isl49	21.00	35.5	0.07	507.15	vgn421	-14.00	31.00	0.28	110.72
isl48	20.55	78.5	0.67	117.16	vgn419	-16.00	89.00	0.29	306.90
isl47	20.05	35.5	0.13	273.08	vgn417	-18.00	24.50	0.17	144.12
isl46	19.75	92.5	0.21	440.48	vgn415	-20.00	166.50	0.36	462.5
isl44	19.20	114.5	0.12	954.17	vgn413	-22.00	125.50	0.23	545.65
isl43	19.00	170	0.34	500	vgn411	-24.00	36.50	0.28	130.36
isl41	18.40	174	0.41	424.39	vgn409	-26.00	44.50	0.22	202.27
isl40	17.90	41.5	0.26	159.62	vgn407	-28.00	113.00	0.41	275.61
isl39	17.45	95	0.39	243.59	vgn405	-30.00	66.00	0.16	412.5
isl37	17.10	74	1.23	60.17	vgn403	-32.00	13.00	0.17	76.47
isl36	16.70	67	0.4	167.5	vgn401	-34.00	82.50	0.16	515.63
isl35	16.25	28.5	0.3	95	vgn399	-36.00	44.50	0.20	222.5
isl34	15.90	158.5	1.73	91.62	vgn397	-38.00	45.00	0.28	160.71
isl33	15.60	29.5	0.23	128.26	vgn395	-40.00	137.50	0.31	443.55
isl32	15.15	191	3.54	53.96	vgn393	-42.00	102.50	0.28	366.07
isl31n	15.00	94	0.9	104.44	vgn391	-44.00	28.00	0.26	107.69
isl30n	14.50	105	2.11	49.76	vgn389	-46.00	39.50	0.23	171.74
isl29n	14.00	148.5	0.31	479.03	vgn387	-48.00	31.00	0.19	163.18
isl27n	13.00	94	0.29	324.14	vgn385	-50.00	56.00	0.29	193.10
isl26n	12.50	71	0.5	142	vgn383	-52.00	49.50	0.25	198
isl25n	12.00	94.5	1.23	76.83	vgn381	-54.00	60.50	0.20	302.5
isl23	11.30	98	1.47	66.67	vgn379	-56.00	67.00	0.25	268
isl21	10.30	65	0.29	224.14	vgn377	-58.00	40.50	0.30	135
isl20	9.95	69.5	0.07	992.86	vgn375	-60.00	44.00	0.24	183.33
isl19	9.75	28.5	0.25	114	vgn373	-62.00	59.00	0.29	203.45
isl18	9.55	77.5	0.12	645.84	vgn371	-64.00	61.50	0.29	212.07
isl17	9.40	50	0.2	250	vgn369	-66.00	92.50	0.23	402.17
isl16a	9.05	52.5	0.32	164.06	vgn367	-68.00	22.50	0.23	97.83
isl15a	8.75	58.5	0.24	243.75	vgn365	-70.00	58.50	0.29	201.72
isl15	8.45	44.5	0.33	134.85	vgn363	-72.00	23.00		
isl14b	8.05	14	0.13	107.69	vgn361	-74.00	38.50		
isl14a	7.60	31.5	0.21	150	vgn359	-76.00	55.50		
isl14	7.20	62.5	0.17	367.65	vgn357	-78.00	45.67		
isl13	6.75	101	1.34	75.37	vgn355	-80.00	86.50		
isl12	6.05	123	0.63	195.24	vgn353	-82.00	58.50		
isl11	5.40	75.5	0.74	102.03	vgn351	-84.00	21.50		
isl10a	4.80	118	1.69	69.82	vgn349	-86.00	77.50		
isl10	4.20	56	0.4	140	vgn347	-88.00	84.00		
isl9	3.50	90	1.44	62.5	vgn345	-90.00	74		
isl8	2.80	138.5	2.19	63.24	vgn343	-92.00	123.5		
isl7	2.25	105	0.64	164.063	vgn341	-94.00	72		
isl6	1.80	44.5	0.12	370.83	vgn339	-96.00	69		
vgn436.5n	1.50	11.9	0.14	85	vgn337	-98.00	50.5		
vgn436	1.00	11.5	0.25	46	vgn335	-100.00	62		
isl4	0.80	27.5	0.1	275	vgn333	-102.00	48.5		
isl2	0.00	22.5	0.11	204.55	vgn331	-104.00	61		
vgn435	0.00	14			vgn329	-106.00	106.5		
vgn433	-2.00	15.5	0.42	36.90	vgn327	-108.00	41		
vgn431	-4.00	29.5	0.17	173.53	vgn325	-110.00	39.50		
vgn430	-5.00	48.5	0.47	103.19					

TOC for isl samples from Jarvis and others (2011).
TOC data for vgn samples are new for this study.
All Hg data generated in this study.

TABLE A11

OAE 2 Data: Clot Chevalier

Height (cm)	Hg (ppb)	TOC (wt%)	Hg/TOC	Height (cm)	Hg (ppb)	TOC (wt%)	Hg/TOC
3510	27.5	0.10	275	1740	40.5	1.38	29.35
3480	46	0.12	383.33	1710	31	1.07	28.98
3450	37	0.07	528.57	1680	43	0.60	71.67
3420	35.5	0.13	273.08	1650	34	1.38	24.64
3390	73	0.18	405.56	1620	24.5	0.83	29.52
3360	21.5	0.08	268.75	1590	26	1.07	24.30
3330	29	0.10	290	1560	52.5	1.36	38.60
3300	60	0.07	857.14	1530	39.5	0.78	50.64
3270	36	0.08	450	1500	41	0.10	410
3240	27	0.12	225	1470	46.5	0.22	211.36
3210	41	0.05	820	1440	46.5	0.20	232.5
3180	25.5	0.05	510	1410	30.5	0.34	89.71
3150	26.5	0.10	265	1380	38.5	0.36	106.94
3120	25.5	0.14	182.14	1350	39.5	0.70	56.43
3090	30.5	0.11	277.27	1320	42.5	1.06	40.09
3060	27	0.08	337.5	1290	27	1.03	26.21
3030	31	0.06	516.67	1260	35	1.35	25.93
3000	32	0.14	228.58	1230	35.5	1.67	21.26
2970	30	0.12	250	1200	60.5	1.18	51.27
2940	24.5	0.13	188.46	1170	25.5	0.40	63.75
2910	37	0.73	50.69	1140	23	0.23	100
2880	68	0.11	618.18	1110	32.5	1.10	29.55
2850	28.5	0.12	237.5	1080	25	1.20	20.83
2820	46	0.10	460	1050	27.5	1.07	25.70
2790	44	0.14	314.29	1020	25.5	1.39	18.35
2760	72	0.12	600	990	28	0.29	96.55
2730	70.5	0.20	352.5	960	36	0.42	85.71
2700	56	0.16	350	930	27.5	1.05	26.19
2670	41	0.17	241.18	900	25	1.36	18.38
2640	55.5	0.13	426.92	870	31	1.05	29.52
2610	44.5	0.16	278.13	840	18	0.60	30
2580	36.5	0.10	365	810	21.5	1.03	20.87
2550	73.5	0.13	565.39	780	18	1.36	13.24
2520	66.5	0.28	237.5	750	23	1.50	15.33
2490	27.5	0.19	144.74	720	19.5	1.46	13.36
2460	35	0.27	129.63	690	21.5	1.53	14.05
2430	116	0.40	290	660	18.5	1.15	16.09
2400	68.5	0.22	311.36	630	12.5	0.24	52.08
2370	52	0.23	226.09	600	16.5	0.35	47.14
2340	38	0.35	108.57	570	22.5	0.23	97.83
2310	34	0.47	72.34	540	8	0.11	72.73
2280	19	0.21	90.48	510	38.5	1.07	35.98
2250	21.5	0.24	89.58	480	18	0.30	60
2220	44.5	1.11	40.09	450	9.6	0.20	48
2190	37	0.53	69.81	420	13	0.17	76.47
2160	20	0.22	90.91	390	15	0.22	68.18
2130	31	0.25	124	360	9.5	0.12	79.17
2100	32.5	0.29	112.07	330	6.8	0.09	75.56
2070	29	0.40	72.5	300	27	1.63	16.56
2040	18	0.28	64.29	270	61	0.41	148.78
2010	43.5	0.60	72.5	240	58.5	1.03	56.80
1980	39.5	1.13	34.96	210	6.7	0.11	60.91
1950	19.5	0.10	195	180	8	0.18	44.44
1920	36	0.47	76.60	150	7	0.12	58.33
1890	30	0.94	31.91	120	9.2	0.15	61.33
1860	74.5	1.34	55.60	90	11	0.17	64.71
1830	38.5	1.16	33.19	60	7.5	0.11	68.18
1800	39.5	1.45	27.24	30	6.6	0.06	110
1770	23.5	0.31	75.81	0	9.3	0.28	33.21

TOC data from Gale and others (2018).

TABLE A12

OAE 2 Data: Furlo

Sample	Height (m)	Hg (ppb)	TOC (wt%)	Hg/TOC
BF 48	1.295	88		
BF 47	1.285	62	0.14	442.86
BF 46	1.27	146		
BF 44	1.215	451.5		
BF 43	1.195	135.5	0.16	846.88
BF 42	1.18	253		
BF 41	1.16	212		
BF 40	1.14	260	3.31	78.55
BF 39	1.11	95.5		
BF 36	1.035	276.5	3.37	82.05
BF 34	0.995	652.5	11.09	58.84
BF 33	0.955	570		
BF 32	0.93	479		
BF 30	0.905	264	6.18	42.72
BF 29	0.885	129.5		
BF 28	0.85	36		
BF 26	0.8	220.5	9.77	22.57
BF 25	0.775	84		
BF 24	0.74	106		
BF 23	0.705	890	7.5	118.67
BF 22	0.67	550.5		
BF 21	0.63	203.5		
BF 20	0.56	311	5.1	60.98
BF 19	0.49	317		
BF 18	0.445	80		
BF 17	0.415	255.5		
BF 15	0.35	1215	9.42	128.98
BF 14	0.325	254		
BF 13	0.315	29.5		
BF 12	0.3	14		
BF 11	0.275	182	6.1	29.84
BF 9	0.21	25.5		
BF 7	0.145	171.5	4.04	42.45
BF 6	0.105	298	3.45	86.38
BF 5	0.085	65		
BF 4	0.075	338	4.9	68.98
BF 2	0.035	115.5		
BF 1	0.015	190.5	1.97	96.70
F. Bon -168	-1.68	18.5		
F. Bon -301	-3.01	1885	8.6	219.19
F. Bon - 322	-3.22	468		
F. Bon -392	-3.92	398	8.09	49.20
F. Bon -414	-4.14	171	3.21	53.27
F. Bon -435	-4.35	550		
F. Bon -455	-4.55	786	9.22	85.25
F. Bon -712	-7.12	41	1.19	34.45
F. Bon -799	-7.99	1120	11.25	99.56
F. Bon -824	-8.24	455.5		
F. Bon -850	-8.5	53	0.37	143.24
F. Bon -978	-9.78	5.4		
F. Bon -1082	-10.82	780	3.07	254.07
F. Bon -1173	-11.73	74	2.15	34.42
F. Bon -1199	-11.99	53.5		
F. Bon -1286	-12.86	332.5	4.16	79.93
F. Bon -1464	-14.64	82	0.83	98.80
F. Bon -1564	-15.64	1420	6.26	226.84
F. Bon -1565.5	-15.655	34.5		
F. Bon -1646	-16.46	60.5	0.27	224.07
F. Bon -1803	-18.03	26	0.08	325
F. Bon -1829	-18.29	30.5		

All data generated in this study.

REFERENCES

Abramovich, S., and Keller, G., 2002, High stress late Maastrichtian paleoenvironment: Inference from planktonic foraminifera in Tunisia: Palaeogeography, Palaeoclimatology, Palaeoecology, v. 178, n. 3–4, p. 145–164, https://doi.org/10.1016/S0031-0182(01)00394-7

Allègre, C. J., Birck, J. L., Capmas, F., and Courtillot, V., 1999, Age of the Deccan traps using ^{187}Re–^{187}Os systematics: Earth and Planetary Science Letters, v. 170, n. 3, p. 197–204, https://doi.org/10.1016/S0012-821X(99)00110-7

Alvarez, L. W., 1983, Experimental evidence that an asteroid impact led to extinction of many species 65 million years ago: Proceedings of the National Academy of Sciences of the United States of America, v. 80, n. 2, p. 627–642, https://doi.org/10.1073/pnas.80.2.627

Alvarez, L. W., Alvarez, W., Asaro, F., and Michel, H. V., 1980, Extraterrestrial cause for the Cretaceous-Tertiary extinction: Science, v. 208, n. 4448, p. 1095–1108, https://doi.org/10.1126/science.208.4448.1095

Arens, N. C., and Jahren, A. H., 2000, Carbon isotope excursion in atmospheric CO_2 at the Cretaceous-Tertiary boundary: Evidence from terrestrial sediments: Palaios, v. 15, n. 4, p. 314–322, https://doi.org/10.1669/0883-1351(2000)015<0314:CIEIAC>2.0.CO;2

Arens, N. C., Jahren, A. H., and Kendrick, D. C., 2014, Carbon isotope stratigraphy and correlation of plant megafossil localities in the Hell Creek Formation of eastern Montana, USA, *in* Wilson, G. P., Clemens, W. A., Horner, J. R., and Hartman, J. H., editors, Through the End of the Cretaceous in the Type Locality of the Hell Creek Formation in Montana and Adjacent Areas: Geological Society of America Special Papers, v. 503, p. 149–171, https://doi.org/10.1130/2014.2503(05)

Averitt, P., 1962, Geology and coal resources of the Cedar Mountain quadrangle, Iron County, Utah. U.S.: Geological Survey Professional Paper 389, 72 p.

Bagnato, E., Oliveri, E., Acquavita, A., Covelli, S., Petranich, E., Barra, M., Italiano, F., Parello, F., and Sprovieri, M., 2017, Hydrochemical mercury distribution and air-sea exchange over the submarine hydrothermal vents off-shore Panarea Island (Aeolian arc, Tyrrhenian Sea): Marine Chemistry, v. 194, p. 63–78, https://doi.org/10.1016/j.marchem.2017.04.003

Barclay, R. S., McElwain, J. C., and Sageman, B. B., 2010, Carbon sequestration activated by a volcanic CO_2 pulse during Ocean Anoxic Event 2: Nature Geoscience, v. 3, p. 205–208, https://doi.org/10.1038/NGEO757

Barclay, R. S., Rioux, M., Meyer, L. B., Bowring, S. A., Johnson, K. R., and Miller, I. M., 2015, High precision U–Pb zircon geochronology for Cenomanian Dakota Formation floras in Utah: Cretaceous Research, v. 52, Part A, p. 213–237, https://doi.org/10.1016/j.cretres.2014.08.006

Barnet, J. S., Littler, K., Kroon, D., Leng, M. J., Westerhold, T., Röhl, U., and Zachos, J. C., 2017, A new high-resolution chronology for the late Maastrichtian warming event: Establishing robust temporal links with the onset of Deccan volcanism: Geology, v. 46, n. 2, p. 147–150, https://doi.org/10.1130/G39771.1

Batenburg, S. J., Sprovieri, M., Gale, A. S., Hilgen, F. J., Hüsing, S., Laskar, J., Liebrand, D., Lirer, F., Orue-Etxebarria, X., Pelosi, N., and Smit, J., 2012, Cyclostratigraphy and astronomical tuning of the Late Maastrichtian at Zumaia (Basque country, Northern Spain): Earth and Planetary Science Letters, v. 359–360, p. 264–278, https://doi.org/10.1016/j.epsl.2012.09.054

Batenburg, S. J., Gale, A. S., Sprovieri, M., Hilgen, F. J., Thibault, N., Boussaha, M., and Orue-Etxebarria, X., 2014, An astronomical time scale for the Maastrichtian based on the Zumaia and Sopelana sections (Basque country, northern Spain): Journal of the Geological Society, v. 171, n. 2, p. 165–180, https://doi.org/10.1144/jgs2013-015

Beaudoin, B., M'Ban, E. P., Montanari, A., and Pinault, M., 1996, Lithostratigraphie haute résolution (< 20 ka) dans le Cénomanien du bassin d'Ombrie-Marches (Italie): Comptes rendus de l'Académie des sciences, Série IIa, Sciences de la terre et des planètes, v. 323, p. 689–696.

Beerling, D. J., and Berner, R. A., 2002, Biogeochemical constraints on the Triassic–Jurassic boundary carbon cycle event: Global Biogeochemical Cycles, v. 16, n. 3, 1036, https://doi.org/10.1029/2001GB001637

Behar, F., Beaumont, V., and de B. Penteado, H. L., 2001, Rock-Eval 6 technology: Performances and developments: Oil & Gas Science and Technology, v. 56, n. 2, p. 111–134, https://doi.org/10.2516/ogst:2001013

Benoit, J. M., Gilmour, C. C., Mason, R. P., and Heyes, A., 1999, Sulfide Controls on Mercury Speciation and Bioavailability to Methylating Bacteria in Sediment Pore Waters: Environmental Science & Technology, v. 33, n. 6, p. 951–957, https://doi.org/10.1021/es9808200

Benoit, J. M., Mason, R. P., Gilmour, C. C., and Aiken, G. R., 2001, Constants for mercury binding by dissolved organic matter isolates from the Florida Everglades: Geochimica et Cosmochimica Acta, v. 65, n. 24, p. 4445–4451, https://doi.org/10.1016/S0016-7037(01)00742-6

Birch, H. S., Coxall, H. K., Pearson, P. N., Kroon, D., and Schmidt, D. N., 2016, Partial collapse of the marine carbon pump after the Cretaceous-Paleogene boundary: Geology, v. 44, n. 4, p. 287–290, https://doi.org/10.1130/G37581.1

Blackburn, T. J., Olsen, P. E., Bowring, S. A., McLean, N. M., Kent, D. V., Puffer, J., McHone, G., Rasbury, E. T., and Et-Touhami, M., 2013, Zircon U-Pb geochronology links the end-Triassic extinction with the Central Atlantic Magmatic Province: Science, v. 340, n. 6135, p. 941–945, https://doi.org/10.1126/science.1234204

Blättler, C. L., Jenkyns, H. C., Reynard, L. M., and Henderson, G. M., 2011, Significant increases in global weathering during Oceanic Anoxic Events 1a and 2 indicated by calcium isotopes: Earth and Planetary Science Letters, v. 309, n. 1–2, p. 77–88, https://doi.org/10.1016/j.epsl.2011.06.029

Blum, J. D., Sherman, L. S., and Johnson, M. W., 2014, Mercury isotopes in earth and environmental

sciences: Annual Review of Earth and Planetary Sciences, v. 42, p. 249–269, https://doi.org/10.1146/annurev-earth-050212-124107
Bond, D. P. G., and Wignall, P. B., 2014, Large igneous provinces and mass extinctions: An update, *in* Keller, G., and Kerr, A. C., editors, Volcanism, Impacts, and Mass Extinctions: Causes and Effects: Geological Society of America Special Papers, v. 505, SPE505-02, https://doi.org/10.1130/2014.2505(02)
Bottini, C., Cohen, A. S., Erba, E., Jenkyns, H. C., and Coe, A. L., 2012, Osmium-isotope evidence for volcanism, weathering, and ocean mixing during the early Aptian OAE 1a: Geology, v. 40, n. 7, p. 583–586, https://doi.org/10.1130/G33140.1
Bowman, K. L., Hammerschmidt, C. R., Lamborg, C. H., and Swarr, G., 2015, Mercury in the North Atlantic Ocean: The U.S. GEOTRACES zonal and meridional sections: Deep-Sea Research Part II, v. 116, p. 251–261, https://doi.org/10.1016/j.dsr2.2014.07.004
Bowman, V. C., Francis, J. E., Riding, J. B., Hunter, S. J., and Haywood, A. M., 2012, A latest Cretaceous to earliest Paleogene dinoflagellate cyst zonation from Antarctica, and implications for phytoprovincialism in the high southern latitudes: Review of Palaeobotany and Palynology, v. 171, p. 40–56, https://doi.org/10.1016/j.revpalbo.2011.11.004
Brusatte, S. L., Butler, R. J., Barrett, P. M., Carrano, M. T., Evans, D. C., Lloyd, G. T., Mannion, P. D., Norell, M. A., Peppe, D. J., Upchurch, P., and Williamson, T. E., 2015, The extinction of the dinosaurs: Biological Reviews, v. 90, n. 2, p. 628–642, https://doi.org/10.1111/brv.12128
Bryan, S. E., and Ferrari, L., 2013, Large igneous provinces and silicic large igneous provinces: Progress in our understanding over the last 25 years: Geological Society of America Bulletin, v. 125, n. 7–8, p. 1053–1078, https://doi.org/10.1130/B30820.1
Bryan, S. E., Peate, I. U., Peate, D. W., Self, S., Jerram, D. A., Mawby, M. R., Marsh, J. S., and Miller, J. A., 2010, The largest volcanic eruptions on Earth: Earth-Science Reviews, v. 102, n. 3–4, p. 207–229, https://doi.org/10.1016/j.earscirev.2010.07.001
Buchs, D. M., Kerr, A. C., Brims, J. C., Zapata-Villada, J. P., Correa-Restrepo, T., and Rodríguez, G., 2018, Evidence for subaerial development of the Caribbean oceanic plateau in the Late Cretaceous and palaeo-environmental implications: Earth and Planetary Science Letters, v. 499, p. 62–73, https://doi.org/10.1016/j.epsl.2018.07.020
Burgess, S. D., and Bowring, S. A., 2015, High-precision geochronology confirms voluminous magmatism before, during, and after Earth's most severe extinction: Science Advances, v. 1, n. 7, e1500470, https://doi.org/10.1126/sciadv.1500470
Burgess, S. D., Bowring, S., and Shen, S. Z., 2014, High-precision timeline for Earth's most severe extinction: Proceedings of the National Academy of Sciences of the United States of America, v. 111, n. 9, p. 3316–3321, https://doi.org/10.1073/pnas.1317692111
Burgess, S. D., Bowring, S. A., Fleming, T. H., and Elliot, D. H., 2015, High-precision geochronology links the Ferrar large igneous province with early-Jurassic ocean anoxia and biotic crisis: Earth and Planetary Science Letters, v. 415, p. 90–99, https://doi.org/10.1016/j.epsl.2015.01.037
Burgess, S. D., Muirhead, J. D., and Bowring, S. A., 2017, Initial pulse of Siberian Traps sills as the trigger of the end-Permian mass extinction: Nature Communications, v. 8, https://doi.org/10.1038/s41467-017-00083-9
Chambers, L. M., Pringle, M. S., and Fitton, J. G., 2004, Phreatomagmatic eruptions on the Ontong Java Plateau: an Aptian $^{40}Ar/^{39}Ar$ age for volcaniclastic rocks at ODP Site 1184, *in* Fitton, J. G., Mahoney, J. J., Wallace, P. J., and Saunders, A. D., editors, Origin and Evolution of the Ontong Java Plateau: Geological Society, London, Special Publications, v. 229, p. 325–331, https://doi.org/10.1144/GSL.SP.2004.229.01.18
Channell, J. E. T., Erba, E., and Lini, A., 1993, Magnetostratigraphic calibration of the Late Valanginian carbon isotope event in pelagic limestones from Northern Italy and Switzerland: Earth and Planetary Science Letters, v. 118, p. 145–166, https://doi.org/10.1016/0012-821X(93)90165-6.
Charbonnier, G., and Föllmi, K. B., 2017, Mercury enrichments in lower Aptian sediments support the link between Ontong Java large igneous province activity and oceanic anoxic episode 1a: Geology, v. 45, n. 1, p. 63–66, https://doi.org/10.1130/G38207.1
Charbonnier, G., Boulila, S., Gardin, S., Duchamp-Alphonse, S., Adatte, T., Spangenberg, J. E., Föllmi, K. B., Colin, C., and Galbrun, B., 2013, Astronomical calibration of the Valanginian "Weissert" episode: The Orpierre marl–limestone succession (Vocontian Basin, southeastern France): Cretaceous Research, v. 45, p. 25–42, https://doi.org/10.1016/j.cretres.2013.07.003
Charbonnier, G., Morales, C., Duchamp-Alphonse, S., Westermann, S., Adatte, T., and Föllmi, K. B., 2017, Mercury enrichment indicates volcanic triggering of Valanginian environmental change: Scientific Reports, v. 7, n. 40808, https://doi.org/10.1038/srep40808
Charbonnier, G., Godet, A., Bodin, S., Adatte, T., and Föllmi, K. B., 2018a, Mercury anomalies, volcanic pulses, and drowning episodes along the northern Tethyan margin during the latest Hauterivian-earliest Aptian: Palaeogeography, Palaeoclimatology, Palaeoecology, v. 505, p. 337–350, https://doi.org/10.1016/j.palaeo.2018.06.013
Charbonnier, G., Boulila, S., Spangenberg, J. E., Adatte, T., Föllmi, K. B., and Laskar, J., 2018b, Obliquity pacing of the hydrological cycle during the Oceanic Anoxic Event 2: Earth and Planetary Science Letters, v. 499, p. 266–277, https://doi.org/10.1016/j.epsl.2018.07.029
Chellman, N., McConnell, J. R., Arienzo, M., Pederson, G. T., Aarons, S. M., and Csank, A., 2017, Reassessment of the Upper Fremont Glacier Ice-Core Chronologies by Synchronizing of Ice-Core-Water Isotopes to a Nearby Tree-Ring Chronology: Environmental Science & Technology, v. 51, n. 8, p. 4230–4238, https://doi.org/10.1021/acs.est.6b06574
Chenet, A. L., Quidelleur, X., Fluteau, F., Courtillot, V., and Bajpai, S., 2007, ^{40}K–^{40}Ar dating of the Main Deccan large igneous province: Further evidence of KTB age and short duration: Earth and Planetary Science Letters, v. 263, n. 1–2, p. 1–15, https://doi.org/10.1016/j.epsl.2007.07.011

Chenet, A. L., Fluteau, F., Courtillot, V., Gérard, M., and Subbarao, K. V., 2008, Determination of rapid Deccan eruptions across the Cretaceous-Tertiary boundary using paleomagnetic secular variation: Results from a 1200-m-thick section in the Mahabaleshwar escarpment: Journal of Geophysical Research: Solid Earth, v. 113, B04101, https://doi.org/10.1029/2006JB004635

Chenet, A. L., Courtillot, V., Fluteau, F., Gérard, M., Quidelleur, X., Khadri, S. F. R., Subbarao, K. V., and Thordarson, T., 2009, Determination of rapid Deccan eruptions across the Cretaceous-Tertiary boundary using paleomagnetic secular variation: 2. Constraints from analysis of eight new sections and synthesis for a 3500-m-thick composite section: Journal of Geophysical Research: Solid Earth, v. 114, n. B6, B06103, https://doi.org/10.1029/2008JB005644

Clyde, W. C., Ramezani, J., Johnson, K. R., Bowring, S. A., and Jones, M. M., 2016, Direct high-precision U–Pb geochronology of the end-Cretaceous extinction and calibration of Paleocene astronomical timescales: Earth and Planetary Science Letters, v. 452, p. 272–280, https://doi.org/10.1016/j.epsl.2016.07.041

Coffin, M. F., and Eldholm, O., 1994, Large igneous provinces: Crustal structure, dimensions, and external consequences: Reviews of Geophysics, v. 32, n. 1, p. 1–36, https://doi.org/10.1029/93RG02508

Cohen, A. S., and Coe, A. L., 2002, New geochemical evidence for the onset of volcanism in the Central Atlantic magmatic province and environmental change at the Triassic-Jurassic boundary: Geology, v. 30, n. 3, p. 267–270, https://doi.org/10.1130/0091-7613(2002)030<0267:NGEFTO>2.0.CO;2

_____2007, The impact of the Central Atlantic Magmatic Province on climate and on the Sr- and Os-isotope evolution of seawater: Palaeogeography, Palaeoclimatology, Palaeoecology, v. 244, n. 1–4, p. 374–390, https://doi.org/10.1016/j.palaeo.2006.06.036

Cohen, A. S., Coe, A. L., Bartlett, J. M., and Hawkesworth, C. J., 1999, Precise Re-Os ages of organic-rich mudrocks and the Os isotope composition of Jurassic seawater: Earth and Planetary Science Letters, v. 167, n. 3–4, p. 159–173, https://doi.org/10.1016/S0012-821X(99)00026-6

Courtillot, V., and Renne, P. R., 2003, On the ages of flood basalt events: Comptes Rendus Geoscience, v. 335, n. 1, p. 113–140, https://doi.org/10.1016/S1631-0713(03)00006-3

Courtillot, V., Besse, J., Vandamme, D., Montigny, R., Jaeger, J. J., and Cappetta, H., 1986, Deccan flood basalts at the Cretaceous/Tertiary boundary?: Earth and Planetary Science Letters, v. 80, n. 3–4, p. 361–374, https://doi.org/10.1016/0012-821X(86)90118-4

Crame, J. A., Pirrie, D., Riding, J. B., and Thomson, M. R. A., 1991, Campanian–Maastrichtian (Cretaceous) stratigraphy of the James Ross Island area, Antarctica: Journal of the Geological Society, v. 148, p. 1125–1140, https://doi.org/10.1144/gsjgs.148.6.1125

Crame, J. A., Francis, J. E., Cantrill, D. J., and Pirrie, D., 2004, Maastrichtian stratigraphy of Antarctica: Cretaceous Research, v. 25, n. 3, p. 411–423, https://doi.org/10.1016/j.cretres.2004.02.002

Crumière, J. P., Crumiere-Airaud, C., and Espitalié, J., 1990, Cyclic preservation of amorphous organic-matter in sediments of the Vocontian Basin (southeastern France), around the Cenomanian-Turonian boundary paleoceanographic controls: Bulletin de la Société Géologique de France, v. 6, n. 3, p. 469–478, https://doi.org/10.2113/gssgfbull.VI.3.469

Davies, J. H. F. L., Marzoli, A., Bertrand, H., Youbi, N., Ernesto, M., and Schaltegger, U., 2017, End-Triassic mass extinction started by intrusive CAMP activity: Nature Communications, v. 8, https://doi.org/10.1038/ncomms15596

Dickens, G. R., O'Neil, J. R., Rea, D. K., and Owen, R. M., 1995, Dissociation of oceanic methane hydrate as a cause of the carbon isotope excursion at the end of the Paleocene: Paleoceanography and Paleoclimatology, v. 10, n. 6, p. 965–971, https://doi.org/10.1029/95PA02087

Dickson, A. J., Cohen, A. S., Coe, A. L., Davies, M., Shcherbinina, E. A., and Gavrilov, Y. O., 2015, Evidence for weathering and volcanism during the PETM from Arctic Ocean and Peri-Tethys osmium isotope records: Palaeogeography, Palaeoclimatology, Palaeoecology, v. 438, p. 300–307, https://doi.org/10.1016/j.palaeo.2015.08.019

Dickson, A. J., Jenkyns, H. C., Porcelli, D., van den Boorn, S., and Idiz, E., 2016, Basin-scale controls on the molybdenum-isotope composition of seawater during Oceanic Anoxic Event 2 (Late Cretaceous): Geochimica et Cosmochimica Acta, v. 178, p. 291–306, https://doi.org/10.1016/j.gca.2015.12.036

Dickson, A. J., Saker-Clark, M., Jenkyns, H. C., Bottini, C., Erba, E., Russo, F., Gorbanenko, O., Naafs, B. D. A., Pancost, R. D., Robinson, S. A., van den Boorn, S., and Idiz, E., 2017, A Southern Hemisphere record of global trace-metal drawdown and orbital modulation of organic-matter burial across the Cenomanian–Turonian boundary (Ocean Drilling Program Site 1138, Kerguelen Plateau): Sedimentology, v. 64, n. 1, p. 186–203, https://doi.org/10.1111/sed.12303

Dilek, Y., and Furnes, H., 2011, Ophiolite genesis and global tectonics: Geochemical and tectonic fingerprinting of ancient oceanic lithosphere: Geological Society of America Bulletin, v. 123, n. 3–4, p. 387–411, https://doi.org/10.1130/B30446.1

Dodd, S. C., Mac Niocaill, C., and Muxworthy, A. R., 2015, Long duration (> 4 Ma) and steady-state volcanic activity in the early Cretaceous Paraná–Etendeka Large Igneous Province: New palaeomagnetic data from Namibia: Earth and Planetary Science Letters, v. 414, p. 16–29, https://doi.org/10.1016/j.epsl.2015.01.009

Du Vivier, A. D. C., Selby, D., Sageman, B. B., Jarvis, I., Gröcke, D. R., and Voigt, S., 2014, Marine $^{187}Os/^{188}Os$ isotope stratigraphy reveals the interaction of volcanism and ocean circulation during Oceanic Anoxic Event 2: Earth and Planetary Science Letters, v. 389, p. 23–33, https://doi.org/10.1016/j.epsl.2013.12.024

Du Vivier, A. D. C., Selby, D., Takashima, R., and Nishi, H., 2015, Pacific $^{187}Os/^{188}Os$ isotope chemistry and U–Pb geochronology: Synchroneity of global Os isotope change across OAE 2: Earth and Planetary Science Letters, v. 428, p. 204–216, https://doi.org/10.1016/j.epsl.2015.07.020

Duchamp-Alphonse, S., Gardin, S., Fiet, N., Bartolini, A., Blamart, D., and Pagel, M., 2007, Fertilization of the northwestern Tethys (Vocontian basin, SE France) during the Valanginian carbon isotope perturbation: Evidence from calcareous nannofossils and trace element data: Palaeogeography, Palaeoclimatology, Palaeoecology, v. 243, n. 1–2, p. 132–151, https://doi.org/10.1016/j.palaeo.2006.07.010

Duncan, R. A., and Pyle, D. G., 1988, Rapid eruption of the Deccan flood basalts at the Cretaceous/Tertiary boundary: Nature, v. 333, p. 841–843, https://doi.org/10.1038/333841a0

Elder, W. P., Gustason, E. R., and Sageman, B. B., 1994, Correlation of basinal carbonate cycyles to nearshore parasequences in the Late Cretaceous Greenhorn seaway, Western Interior: US. Geological Society of America Bulletin, v. 106, n. 7, p. 892–902, https://doi.org/10.1130/0016-7606(1994)106<0892:COBCCT>2.3.CO;2

Eldrett, J. S., Minisini, D., and Bergman, S. C., 2014, Decoupling of the carbon cycle during Ocean Anoxic Event 2: Geology, v. 42, n. 7, p. 567–570, https://doi.org/10.1130/G35520.1

Elliot, D. H., Askin, R. A., Kyte, F. T., and Zinsmeister, W. J., 1994, Iridium and dinocysts at the Cretaceous-Tertiary boundary on Seymour Island, Antarctica: Implications for the K-T event: Geology, v. 22, n. 8, p. 675–678, https://doi.org/10.1130/0091-7613(1994)022<0675:IADATC>2.3.CO;2

Emili, A., Koron, N., Covelli, S., Faganeli, J., Acquavita, A., Predonzani, S., and De Vittor, C., 2011, Does anoxia affect mercury cycling at the sediment–water interface in the Gulf of Trieste (northern Adriatic Sea)? Incubation experiments using benthic flux chambers: Applied Geochemistry, v. 26, n. 2, p. 194–204, https://doi.org/10.1016/j.apgeochem.2010.11.019

Erba, E., Duncan, R. A., Bottini, C., Tiraboschi, D., Weissert, H., Jenkyns, H. C., and Malinverno, A., 2015, Environmental consequences of Ontong Java Plateau and Kerguelen Plateau volcanism, *in* Neal, C. R., Sager, W. W., Sano, T., and Erba, E., editors, The Origin, Evolution, and Environmentsl Impact of Oceanic Large Igneous Provinces: Geological Society of America Special Papers, v. 511, SPE511-15, https://doi.org/10.1130/2015.2511(15)

Erbacher, J., Friedrich, O., Wilson, P. A., Birch, H., and Mutterlose, J., 2005, Stable organic carbon isotope stratigraphy across Oceanic Anoxic Event 2 of Demerara Rise, western tropical Atlantic: Geochemistry, Geophysics, Geosystems, v. 6, n. 6, Q06010, https://doi.org/10.1029/2004GC000850

Ernst, R. E. and Youbi, N., 2017, How Large Igneous Provinces affect global climate, sometimes cause mass extinctions, and represent natural markers in the geological record: Palaeogeography, Palaeoclimatology, Palaeoecology, v. 478, p. 30–52, https://doi.org/10.1016/j.palaeo.2017.03.014

Esmeray-Senlet, S., Wright, J. D., Olsson, R. K., Miller, K. G., Browning, J. V., and Quan, T. M., 2015, Evidence for reduced export productivity following the Cretaceous/Paleogene mass extinction: Paleoceanography and Paleoclimatology, v. 30, n. 6, p. 718–738, https://doi.org/10.1002/2014PA002724

Espitalié, J., Madec, M., Tissot, B., Menning, J. J., and Leplat, P., 1977, Source rock characterization methods for petroleum exploration: Houston, Texas, Proceedings of the 1977 Offshore Technology Conference, 3, Document ID OTC-2935-MS, p. 439–443, https://doi.org/10.4043/2935-MS

Falzoni, F., Petrizzo, M. R., Jenkyns, H. C., Gale, A. S., and Tsikos, H., 2016, Planktonic foraminiferal biostratigraphy and assemblage composition across the Cenomanian–Turonian boundary interval at Clot Chevalier (Vocontian Basin, SE France): Cretaceous Research, v. 59, p. 69–97, https://doi.org/10.1016/j.cretres.2015.10.028

Fantasia, A., Föllmi, K. B., Adatte, T., Bernárdez, E., Spangenberg, J. E., and Mattioli, E., 2018, The Toarcian Oceanic Anoxic Event in southwestern Gondwana: An example from the Andean Basin, northern Chile: Journal of the Geological Society, London, https://doi.org/10.1144/jgs2018-008

Fitzgerald, W. F., Lamborg, C. H., and Hammerschmidt, C. R., 2007, Marine biogeochemical cycling of mercury: Chemical Reviews, v. 107, n. 2, p. 641–662, https://doi.org/10.1021/cr050353m

Font, E., Adatte, T., Sial, A. N., de Lacerda, L. D., Keller, G., and Punekar, J., 2016, Mercury anomaly, Deccan volcanism, and the end-Cretaceous mass extinction: Geology, v. 44, n. 2, p. 171–174, https://doi.org/10.1130/G37451.1

Font, E., Adatte, T., Andrade, M., Keller, G., Bitchong, A. M., Carvallo, C., Ferreira, J., Diogo, Z., and Mirão, J., 2018, Deccan volcanism induced high-stress environment during the Cretaceous–Paleogene transition at Zumaia, Spain: Evidence from magnetic, mineralogical and biostratigraphic records: Earth and Planetary Science Letters, v. 484, p. 53–66, https://doi.org/10.1016/j.epsl.2017.11.055

Forster, A., Schouten, S., Moriya, K., Wilson, P. A., and Sinninghe Damsté, J. S., 2007, Tropical warming and intermittent cooling during the Cenomanian/Turonian oceanic anoxic event 2: Sea surface temperature records from the equatorial Atlantic: Palaeoceanography and Paleoclimatology, v. 22, n. 1, PA1219, https://doi.org/10.1029/2006PA001349

Forster, A., Kuypers, M. M., Turgeon, S. C., Brumsack, H. J., Petrizzo, M. R., and Damsté, J. S. S., 2008, The Cenomanian/Turonian oceanic anoxic event in the South Atlantic: New insights from a geochemical study of DSDP Site 530A: Palaeogeography, Palaeoclimatology, Palaeoecology, v. 267, n. 3–4, p. 256–283, https://doi.org/10.1016/j.palaeo.2008.07.006

Frey, F. A., Weis, D., Borisova, A. Y., and Xu, G., 2002, Involvement of Continental Crust in the Formation of the Cretaceous Kerguelen Plateau: New Perspectives from ODP Leg 120 Sites: Journal of Petrology, v. 43, n. 7, p. 1207–1239, https://doi.org/10.1093/petrology/43.7.1207

Galbrun, B., and Gardin, S., 2004, New chronostratigraphy of the Cretaceous–Paleogene boundary interval at Bidart (France): Earth and Planetary Science Letters, v. 224, n. 1–2, p. 19–32, https://doi.org/10.1016/j.epsl.2004.04.043

Gale, A. S., and Christensen, W. K., 1996, Occurrence of the belemnite *Actinocamax plenus* in the Cenomanian of SE France and its significance: Bulletin of the Geological Society of Denmark, v. 43, p. 68–77.

Gale, A.S., Jenkyns, H.C., Kennedy, W. J., and Corfield, R. M., 1993, Chemostratigraphy versus biostratigraphy: Data from around the Cenomanian–Turonian boundary: Journal of the Geological Society, London, v. 150, p. 29–32, https://doi.org/10.1144/gsjgs.150.1.0029

Gale, A. S., Jenkyns, H. C., Tsikos, H., van Breugel, Y., Sinninghe Damsté, J. S., Bottini, C., Erba, E., Russo, F., Falzoni, F., Petrizzo, M. R., Dickson, A. J., and Wray, D. S., 2018, High-resolution bio- and chemostratigraphy of an expanded record of Oceanic Anoxic Event 2 (Late Cenomanian–Early Turonian) at Clot

Chevalier, near Barrême, SE France (Vocontian Basin): Newsletters on Stratigraphy, https://doi.org/10.1127/nos/2018/0445
Gambacorta, G., Jenkyns, H. C., Russo, F., Tsikos, H., Wilson, P. A., Faucher, G., and Erba, E., 2015, Carbon-and oxygen-isotope records of mid-Cretaceous Tethyan pelagic sequences from the Umbria–Marche and Belluno Basins (Italy): Newsletters on Stratigraphy, v. 48, n. 3, p. 299–323, https://doi.org/10.1127/nos/2015/0066
Ganino, C., and Arndt, N. T., 2009, Climate changes caused by degassing of sediments during the emplacement of large igneous provinces: Geology, v. 37, n. 4, p. 323–326, https://doi.org/10.1130/G25325A.1
Gardin, S., Galbrun, B., Thibault, N., Coccioni, R., and Silva, I. P., 2012, Bio-magnetochronology for the upper Campanian–Maastrichtian from the Gubbio area, Italy: New results from the Contessa Highway and Bottaccione sections: Newsletters on Stratigraphy, v. 45, n. 1, p. 75–103, https://doi.org/10.1127/0078-0421/2012/0014
Georgiev, S. V., Stein, H. J., Hannah, J. L., Henderson, C. M., and Algeo, T. J., 2015, Enhanced recycling of organic matter and Os-isotopic evidence for multiple magmatic or meteoritic inputs to the Late Permian Panthalassic Ocean, Opal Creek, Canada: Geochimica et Cosmochimica Acta, v. 150, p. 192–210, https://doi.org/10.1016/j.gca.2014.11.019
Gibson, S. A., Dale, C. W., Geist, D. J., Day, J. A., Brügmann, G., and Harpp, K. S., 2016, The influence of melt flux and crustal processing on Re–Os isotope systematics of ocean island basalts: Constraints from Galápagos: Earth and Planetary Science Letters, v. 449, p. 345–359, https://doi.org/10.1016/j.epsl.2016.05.021
Gill, G. A., and Fitzgerald, W. F., 1988, Vertical mercury distributions in the oceans: Geochimica et Cosmochimica Acta, v. 52, n. 6, p. 1719–1728, https://doi.org/10.1016/0016-7037(88)90240-2
Glaze, L. S., Self, S., Schmidt, A., and Hunter, S. J., 2017, Assessing eruption column height in ancient flood basalt eruptions: Earth and Planetary Science Letters, v. 457, p. 263–270, https://doi.org/10.1016/j.epsl.2014.07.043
Gong, Q., Wang, X., Zhao, L., Grasby, S. E., Chen, Z. Q., Zhang, L., Li, Y., Cao, L., and Li, Z., 2017, Mercury spikes suggest volcanic driver of the Ordovician-Silurian mass extinction: Scientific Reports, v. 7, article number 5304, https://doi.org/10.1038/s41598-017-05524-5
Grasby, S. E., Sanei, H., Benoit, B., and Chen, Z., 2013, Mercury deposition through the Permo–Triassic Biotic Crisis: Chemical Geology, v. 351, p. 209–216, https://doi.org/10.1016/j.chemgeo.2013.05.022
Grasby, S. E., Beauchamp, B., Bond, D. P. G., Wignall, P. B., and Sanei, H., 2016, Mercury anomalies associated with three extinction events (Capitanian Crisis, Latest Permian Extinction and the Smithian/Spathian Extinction) in NW Pangea: Geological Magazine, v. 153, Special Issue 2 (Mass Extinctions), p. 285–297, https://doi.org/10.1017/S0016756815000436
Grasby, S. E., Wenjie, S., Runsheng, Y., Gleason, J. D., Blum, J. D., Lepak, R. F., Hurley, J. P., and Beauchamp, B., 2017, Isotopic signatures of mercury contamination in latest Permian oceans: Geology, v. 45, n. 1, p. 55–58, https://doi.org/10.1130/G38487.1
Grosheny, D., Beaudoin, B., Morel, L., and Desmares, D., 2006, High-resolution biostratigraphy and chemostratigraphy of the Cenomanian/Turonian boundary event in the Vocontian Basin, southeast France: Cretaceous Research, v. 27, n. 5, p. 629–640, https://doi.org/10.1016/j.cretres.2006.03.005
Gutjahr, M., Ridgwell, A., Sexton, P. F., Anagnostou, E., Pearson, P. N., Pälike, H., Norris, R. D., Thomas, E., and Foster, G. L., 2017, Very large release of mostly volcanic carbon during the Palaeocene–Eocene Thermal Maximum: Nature, v. 548, p. 573–577, https://doi.org/10.1038/nature23646
Hall, J. L. O., Newton, R. J., Witts, J. D., Francis, J. E., Hunter, S. J., Jamieson, R. A., Harper, E. M., Crame, J. A., and Haywood, A. M., 2018, High benthic methane flux in low sulfate oceans: Evidence from carbon isotopes in Late Cretaceous Antarctic bivalves: Earth and Planetary Science Letters, v. 497, p. 113–122, https://doi.org/10.1016/j.epsl.2018.06.014
Hardas, P., and Mutterlose, J., 2006, Calcareous nannofossil biostratigraphy of the Cenomanian/Turonian boundary interval of ODP Leg 207 at the Demerara Rise: Revue de Micropaléontologie, v. 49, n. 3, p. 165–179, https://doi.org/10.1016/j.revmic.2006.04.005
Hesselbo, S. P., Gröcke, D. R., Jenkyns, H. C., Bjerrum, C. J., Farrimond, P., Morgans-Bell, H. S., and Green, O. R., 2000, Massive dissociation of gas hydrates during a Jurassic Oceanic Anoxic Event: Nature, v. 406, p. 392–395, https://doi.org/10.1038/35019044
Hetzel, A., Böttcher, M. E., Wortmann, U. G., and Brumsack, H.-J., 2009, Paleo-redox conditions during OAE 2 reflected in Demerara Rise sediment geochemistry (ODP Leg 207): Palaeogeography, Palaeoclimatology, Palaeoecology, v. 273, n. 3–4, p. 302–328, https://doi.org/10.1016/j.palaeo.2008.11.005
Hildebrand, A. R., Penfield, G. T., Kring, D. A., Pilkington, M., Camargo, A., Jacobsen, S. B., and Boynton, W. V., 1991, Chicxulub crater: A possible Cretaceous/Tertiary boundary impact crater on the Yucatán Peninsula, Mexico: Geology, v. 19, n. 9, p. 867–871, https://doi.org/10.1130/0091-7613(1991)019<0867:CCAPCT>2.3.CO;2
Holmden, C., Jacobson, A. D., Sageman, B. B., and Hurtgen, M. T., 2016, Response of the Cr isotope proxy to Cretaceous Ocean Anoxic Event 2 in a pelagic carbonate succession from the Western Interior Seaway: Geochimica et Cosmochimica Acta, v. 186, p. 277–295, https://doi.org/10.1016/j.gca.2016.04.039
Horan, M. F., Walker, R. J., Fedorenko, V. A., and Czamanske, G. K., 1995, Osmium and neodymium isotopic constraints on the temporal and spatial evolution of Siberian flood basalt sources: Geochimica et Cosmochimica Acta, v. 59, n. 4, p. 5159–5168, https://doi.org/10.1016/0016-7037(96)89674-8
Jarvis, I., Lignum, J. S., Gröcke, D. R., Jenkyns, H. C., and Pearce, M. A., 2011, Black shale deposition, atmospheric CO_2 drawdown, and cooling during the Cenomanian–Turonian Oceanic Anoxic Event: Paleoceanography and Paleoclimatology, v. 26, n. 3, PA3201, https://doi.org/10.1029/2010PA002081
Jay, A. E., Mac Niocaill, C., Widdowson, M., Self, S., and Turner, W., 2009, New palaeomagnetic data from the Mahabaleshwar Plateau, Deccan Flood Basalt Province, India: Implications for the volcanostratigraphic

architecture of continental flood basalt provinces: Journal of the Geological Society, v. 166, n. 1, p. 13–24, https://doi.org/10.1144/0016-76492007-150

Jefferies, R. P. S., 1963, The stratigraphy of the *Actinocamax plenus* Subzone (Turonian) in the Anglo-Paris Basin: Proceedings of the Geologists' Association, v. 74, n. 1, p. 1–33, https://doi.org/10.1016/S0016-7878(63)80011-5

Jenkyns, H. C., 1988, The early Toarcian (Jurassic) anoxic event: Stratigraphic, sedimentary, and geochemical evidence: American Journal of Science, v. 288, n. 2, p. 101–151, https://doi.org/10.2475/ajs.288.2.101

_____2010, Geochemistry of Oceanic Anoxic Events: Geochemistry, Geophysics, Geosystems, v. 11, n. 3, Q03004, https://doi.org/10.1029/2009GC002788

Jenkyns, H. C., Gale, A. S., and Corfield, R. M., 1994, Carbon-and oxygen-isotope stratigraphy of the English Chalk and Italian Scaglia and its palaeoclimatic significance: Geological Magazine, v, 131, n. 1, p. 1–34, https://doi.org/10.1017/S0016756800010451

Jenkyns, H. C., Matthews, A., Tsikos, H., and Erel, Y., 2007, Nitrate reduction, sulfate reduction, and sedimentary iron isotope evolution during the Cenomanian–Turonian oceanic anoxic event: Paleoceanography and Paleoclimatology, v. 22, n. 3, PA3208, https://doi.org/10.1029/2006PA001355

Jenkyns, H. C., Dickson, A. J., Ruhl, M., and van den Boorn, S. H. J., 2017, Basalt-seawater interaction, the Plenus Cold Event, enhanced weathering and geochemical change: Deconstructing Oceanic Anoxic Event 2 (Cenomanian–Turonian, Late Cretaceous): Sedimentology, v. 64, n. 1, p. 16–43, https://doi.org/10.1111/sed.12305

Jin, H., and Liebezeit, G., 2013, Distribution of total mercury in coastal sediments from Jade Bay and its catchment, Lower Saxony, Germany: Journal of Soils and Sediments, v. 13, n. 2, p. 441–449, https://doi.org/10.1007/s11368-012-0626-6

Jones, C. E., and Jenkyns, H. C., 2001, Seawater strontium isotopes, oceanic anoxic events, and seafloor hydrothermal activity in the Jurassic and Cretaceous: American Journal of Science, v. 301, n. 2, p. 112–149, https://doi.org/10.2475/ajs.301.2.112

Jones, D. S., Martini, A. M., Fike, D. A., and Kaiho, K., 2017, A volcanic trigger for the Late Ordovician mass extinction? Mercury data from south China and Laurentia: Geology, v. 45, n. 7, p. 631–634, https://doi.org/10.1130/G38940.1

Keller, G., Mateo, P., Punekar, J., Khozyem, H., Gertsch, B., Spangenberg, J., Bitchong, A. M., and Adatte, T., 2018, Environmental changes during the Cretaceous-Paleogene mass extinction and Paleocene-Eocene thermal maximum: Implications for the Anthropocene: Gondwana Research, v. 56, p. 69–89, https://doi.org/10.1016/j.gr.2017.12.002

Kingsbury, C. G., Kamo, S. L., Ernst, R. E., Söderland, U., and Cousens, B. L., 2018, U-Pb geochronology of the plumbing system associated with the Late Cretaceous Strand Fiord Formation, Axel Heiberg Island, Canada: Part of the 130-90 Ma High Arctic large igneous province: Journal of Geodynamics, v. 118, p. 106–117, https://doi.org/10.1016/j.jog.2017.11.001

Kolonic, S., Wagner, T., Forster, A., Sinninghe Damsté, J. S., Walsworth-Bell, B., Erba, E., Turgeon, S., Brumsack, H. J., Chellai, E. H., Tsikos, H., Kuhnt, W., and Kuypers, M. M. M., 2005, Black shale deposition on the northwest African Shelf during the Cenomanian/Turonian oceanic anoxic event: Climate coupling and global organic carbon burial: Paleoceanography and Paleoclimatology, v. 20, n. 1, https://doi.org/10.1029/2003PA000950

Kongchum, M., Hudnall, W. H., and Delaune, R. D., 2011, Relationship between sediment clay minerals and total mercury: Journal of Environmental Science and Health, Part A, v. 46, n. 5, p. 534–539, https://doi.org/10.1080/10934529.2011.551745

Krupp, R., 1988, Physicochemical aspects of mercury metallogenesis: Chemical Geology, v. 69, n. 3–4, p. 345–356, https://doi.org/10.1016/0009-2541(88)90045-9

Kuhnt, W., Nederbragt, A., and Leine, L., 1997, Cyclicity of Cenomanian-Turonian organic-carbon-rich sediments in the Tarfaya Atlantic Coastal Basin (Morocco): Cretaceous Research, v. 18, n. 4, p. 587–601, https://doi.org/10.1006/cres.1997.0076

Kuhnt, W., Holbourn, A. E., Beil, S., Aquit, M., Krawczyk, T., Flögel, S., Chellai, E. H., and Jabour, H., 2017, Unraveling the onset of Cretaceous Oceanic Anoxic Event 2 in an extended sediment archive from the Tarfaya-Laayoune Basin, Morocco: Paleoceanography and Paleoclimatology, v. 32, n. 8, p. 923–946, https://doi.org/10.1002/2017PA003146

Kuroda, J., Ogawa, N. O., Tanimizu, M., Coffin, M. F., Tokuyama, H., Kitazato, H., and Ohkouchi, N., 2007, Contemporaneous massive subaerial volcanism and late Cretaceous Oceanic Anoxic Event 2: Earth and Planetary Science Letters, v. 256, n. 1–2, p. 211–223, https://doi.org/10.1016/j.epsl.2007.01.027

Kuroda, J., Hori, R. S., Suzuki, K., Gröcke, D. R., and Ohkouchi, N., 2010, Marine osmium isotope record across the Triassic-Jurassic boundary from a Pacific pelagic site: Geology, v. 38, n. 12, p. 1095–1098, https://doi.org/10.1130/G31223.1

Kuroda, J., Tanimizu, M., Hori, R. S., Suzuki, K., Ogawa, N. O., Tejada, M. L., Coffin, M. F., Coccioni, R., Erba, E., and Ohkouchi, N., 2011, Lead isotopic record of Barremian–Aptian marine sediments: Implications for large igneous provinces and the Aptian climatic crisis: Earth and Planetary Science Letters, v. 307, n. 1–2, p. 126–134, https://doi.org/10.1016/j.epsl.2011.04.021

Lamborg, C. H., Von Damm, K. L., Fitzgerald, W. F., Hammerschmidt, C. R., and Zierenberg, R., 2006, Mercury and monomethylmercury in fluids from Sea Cliff submarine hydrothermal field, Gorda Ridge: Geophysical Research Letters, v. 33, n. 17, L17606, https://doi.org/10.1029/2006GL026321

Lanci, L., Muttoni, G., and Erba, E., 2010, Astronomical tuning of the Cenomanian Scaglia Bianca Formation at Furlo, Italy: Earth and Planetary Science Letters, v. 292, n. 1–2, p. 231–237, https://doi.org/10.1016/j.epsl.2010.01.041

Larsen, L. M., Fitton, J. G., and Pedersen, A. K., 2003, Paleogene volcanic ash layers in the Danish Basin:

Compositions and source areas in the North Atlantic Igneous Province: Lithos, v. 71, n. 1, p. 47–80, https://doi.org/10.1016/j.lithos.2003.07.001

Laurin, J., and Sageman, B. B., 2001, Tectono-sedimentary evolution of the western margin of the Colorado Plateau during the latest Cenomanian and Early Turonian *in* Erskine, M. C., Faulds, J. E., Bartley, J. M., and Rowley, P. D., editors, The Geologic Transition, High Plateaus to Great Basin: A symposium and field guide: The Mackin Volume, American Association of Petroleum Geologists, p. 57–74.

_____2007, Cenomanian–Turonian coastal record in SW Utah, USA: Orbital-scale transgressive–regressive events during Oceanic Anoxic Event II: Journal of Sedimentary Research, v. 77, n. 9, p. 731–756, https://doi.org/10.2110/jsr.2007.076

LeCain, R., Clyde, W. C., Wilson, G. P., and Riedel, J., 2014, Magnetostratigraphy of the Hell Creek and lower Fort Union Formations in northeastern Montana: Geological Society of America Special Papers, v. 503, p. 137–147, https://doi.org/10.1130/2014.2503(04)

Li, L., and Keller, G., 1998a, Diversification and extinction in Campanian-Maastrichtian planktic foraminifera of Northwestern Tunisia: Eclogae Geologicae Helvetiae, v. 91, n. 1, p. 75–102.

_____1998b, Abrupt deep-sea warming at the end of the Cretaceous: Geology, v. 26, n. 11, p. 995–998, https://doi.org/10.1130/0091-7613(1998)026<0995:ADSWAT>2.3.CO;2

Liu, S. A., Wu, H., Shen, S. Z., Jiang, G., Zhang, S., Lv, Y., Zhang, H., and Li, S., 2017, Zinc isotope evidence for intensive magmatism immediately before the end-Permian mass extinction: Geology, v. 45, n. 4, p. 343–346, https://doi.org/10.1130/G38644.1

Liu, X., Xu, L., Chen, Q., Sun, L., Wang, Y., Yan, H., Liu, Y., Luo, Y., and Huang, J., 2012, Historical change of mercury pollution in remote Yongle archipelago, South China Sea: Chemosphere, v. 87, n. 5, p. 549–556, https://doi.org/10.1016/j.chemosphere.2011.12.065

Macellari, C. E., 1988, Stratigraphy, sedimentology, and paleoecology of Upper Cretaceous/Paleocene shelf-deltaic sediments of Seymour Island, *in* Feldmann, R. M., and Woodburne, M. O., editors, Geology and Paleontology of Seymour Island Antarctic Peninsula: Geological Society of America Memoirs, v. 169, p. 25–54, https://doi.org/10.1130/MEM169-p25

MacLeod, K. G., Martin, E. E., and Blair, S. W., 2008, Nd isotopic excursion across Cretaceous oceanic anoxic event 2 (Cenomanian-Turonian) in the tropical North Atlantic: Geology, v. 36, n. 10, p. 811–814, https://doi.org/10.1130/G24999A.1

Martin, E. E., MacLeod, K. G., Berrocoso, A. J., and Bourbon, E., 2012, Water mass circulation on Demerara Rise during the Late Cretaceous based on Nd isotopes: Earth and Planetary Science Letters, v. 327–328, p. 111–120, https://doi.org/10.1016/j.epsl.2012.01.037

Marzoli, A., Bertrand, H., Knight, K. B., Cirilli, S., Buratti, N., Vérati, C., Nomade, S., Renne, P. R., Youbi, N., Martini, R., Allenbach, K., Neuwerth, R., Rapaille, C., Zaninetti, L., and Bellieni, G., 2004, Synchrony of the Central Atlantic magmatic province and the Triassic-Jurassic boundary climatic and biotic crisis: Geology, v. 32, n. 11, p. 973–976, https://doi.org/10.1130/G20652.1

Mason, R. P., Laporte, J.-M., and Andres, S., 2000, Factors controlling the Bioaccumulation of Mercury, Methylmercury, Arsenic, Selenium, and Cadmium by Freshwater Invertebrates and Fish: Archives of Environmental Contamination and Toxicology, v. 38, n. 3, p. 283–297, https://doi.org/10.1007/s002449910038

McClintock, M., and White, J. D., 2006, Large phreatomagmatic vent complex at Coombs Hills, Antarctica: Wet, explosive initiation of flood basalt volcanism in the Ferrar-Karoo LIP: Bulletin of Volcanology, 68, n. 3, p. 215–239, https://doi.org/10.1007/s00445-005-0001-1

McElwain, J. C., Wade-Murphy, J., and Hesselbo, S. P., 2005, Changes in carbon dioxide during an oceanic anoxic event linked to intrusion into Gondwana coals: Nature, v. 435, p. 479–482, https://doi.org/10.1038/nature03618

Meyers, P. A., Yum, J. G., and Wise, S. W., 2009, Origins and maturity of organic matter in mid-Cretaceous black shales from ODP Site 1138 on the Kerguelen Plateau: Marine and Petroleum Geology, v. 26, n. 6, p. 909–915, https://doi.org/10.1016/j.marpetgeo.2008.09.003

Meyers, S. R., Sageman, B. B., and Arthur, M. A., 2012a, Obliquity forcing of organic matter accumulation during Oceanic Anoxic Event 2: Paleoceanography and Paleoclimatology, v. 27, n. 3, https://doi.org/10.1029/2012PA002286

Meyers, S. R., Siewert, S. E., Singer, B. S., Sageman, B. B., Condon, D. J., Obradovich, J. D., Jicha, B. R., and Sawyer, D. A., 2012b, Intercalibration of radioisotopic and astrochronologic time scales for the Cenomanian-Turonian boundary interval, Western Interior Basin, USA: Geology, 40, n. 1, p. 7–10, https://doi.org/10.1130/G32261.1

Miller, K. G., Sugarman, P. J., Browning, J. V., Olsson, R. K., Pekar, S. F., Reilly, T. J., Cramer, B. S., Aubry, M. P., Lawrence, R. P., Curran, J., Stewart, M., Metzger, J. M., Uptegrove, J., Bukry, D., Burckle, L. H., Wright, J. D., Feigenson, M. D., Brenner, G. J., and Dalton, R. F., 1998, Bass River Site, *in* Miller, K. G., Sugarman, P. J., Browning, J. V., and others, editors, Proceedings of the Ocean Drilling Program, Initial Reports, 174AX: College Station, Texas (Ocean Drilling Program), p. 5–43, https://doi.org/10.2973/odp.proc.ir.174ax.101.1998

Mohr, B. A., Wähnert, V., and Lazarus, D., 2002, Mid-Cretaceous paleobotany and palynology of the central Kerguelen Plateau, Southern Indian Ocean (ODP leg 183, site 1138): Proceedings of the Ocean Drilling Program, Scientific Results, v. 183, p. 1–39, https://doi.org/10.2973/odp.proc.sr.183.008.2002

Molina, E., Alegret, L., Arenillas, I., Arz, J. A., Gallala, N., Grajales-Nishimura, J. M., Murillo-Munetón, G., and Zaghbib-Turki, D., 2009, The Global Boundary Stratotype Section and Point for the base of the Danian Stage (Paleocene, Paleogene," Tertiary", Cenozoic): Auxiliary sections and correlation: Episodes, v. 32, n. 2, p. 84–95.

Moore, T. C., Jr., Rabinowitz, P. D., Boersma, A., Borella, P. E., Chave, A. D., Duee, G., Futterer, D. K., Jiang, M. G., Kleinert, K., Lever, A., Manivit, H., O'Connell, S., Richardson, S. H., and Shackleton, N. J., 1983, The Walvis Ridge transect, Deep Sea Drilling Project Leg 74: The geologic evolution of an oceanic

plateau in the south Atlantic Ocean: Geological Society of America Bulletin, v. 94, n. 7, p. 907–925, https://doi.org/10.1130/0016-7606(1983)94<907:TWRTDS>2.0.CO;2
Mort, H. P., Adatte, T., Föllmi, K. B., Keller, G., Steinmann, P., Matera, V., Berner, Z., and Stüben, D., 2007, Phosphorus and the roles of productivity and nutrient recycling during oceanic anoxic event 2: Geology, v. 35, n. 6, p. 483–486, https://doi.org/10.1130/G23475A.1
Mort, H. P., Adatte, T., Keller, G., Bartels, D., Föllmi, K. B., Steinmann, P., Berner, Z., and Chellai, E. H., 2008, Organic carbon deposition and phosphorus accumulation during Oceanic Anoxic Event 2 in Tarfaya, Morocco: Cretaceous Research, v. 29, n. 5–6, p. 1008–1023, https://doi.org/10.1016/j.cretres.2008.05.026
Munthe, J., Wängberg, I., and Shang, L., 2009, The origin and fate of mercury species in the natural environment: Euro Chlor Science Dossier 14.
Neal, C. R., Mahoney, J. J., Kroenke, L. W., Duncan, R. A., and Petterson, M. G., 1997, The Ontong–Java Plateau, *in* Mahoney, J. J., and Coffin, M. F., editors, Large igneous provinces: Continental, oceanic and planetary flood volcanism: Geophysical Monograph Series, v. 100, p. 183–216, https://doi.org/10.1029/GM100p0183
Nerlich, R., Clark, S. R., and Bunge, H. P., 2014, Reconstructing the link between the Galapagos hotspot and the Caribbean Plateau: GeoResJ, v. 1–2, p. 1–7, https://doi.org/10.1016/j.grj.2014.02.001
Obrist, D., Johnson, D. W., and Edmonds, R. L., 2012, Effects of vegetation type on mercury concentrations and pools in two adjacent coniferous and deciduous forests: Journal of Plant Nutrition and Soil Science, v. 175, n. 1, p. 68–77, https://doi.org/10.1002/jpln.201000415
Ogg, J. G., Ogg, G., and Gradstein, F. M., 2016, A Concise Geologic Time Scale: 2016: Amsterdam, Elsevier, 240 p.
Olsen, P. E., Kinney, S. T., Hemming, S., Jarett, S. J., Rasbury, E. T., and Philpotts, A. R., 2017, CAMP Ashes and the ETE: 27th Goldschmidt Conference, abstract 2991.
Olsson, R. K., Miller, K. G., Browning, J. V., Wright, J. D., and Cramer, B. S., 2002, Sequence stratigraphy and sea-level change across the Cretaceous-Tertiary boundary on the New Jersey passive margin, *in* Koeberly, C., and MacLeod, K. G., editors, Catastrophic events and mass extinctins: Impacts and Beyond: Geological Society of America, Special Papers, v. 356, p. 97–108, https://doi.org/10.1130/0-8137-2356-6.97
Orth, C. J., Attrep, M., Jr., Quintana, L. R., Elder, W. P., Kauffman, Diner, R., and Villamil, T., 1993, Elemental abundance anomalies in the late Cenomanian extinction interval: A search for the source(s): Earth and Planetary Science Letters, v. 117, n. 1–2, p. 189–204, https://doi.org/10.1016/0012-821X(93)90126-T
Outridge, P. M., Sanei, H., Stern, G. A., Hamilton, P. B., and Goodarzi, F., 2007, Evidence for control of mercury accumulation rates in Canadian High Arctic lake in sediments by variations of aquatic primary productivity: Environmental Science & Technology, v. 41, n. 15, p. 5259–5265, https://doi.org/10.1021/es070408x
Owens, J. D., Lyons, T. W., Hardisty, D. S., Lowery, C. M., Lu, Z., Lee, B., and Jenkyns, H. C., 2017, Patterns of local and global redox variability during the Cenomanian–Turonian Boundary Event (Oceanic Anoxic Event 2) recorded in carbonates and shales from central Italy: Sedimentology, v. 64, n. 1, p. 168–185, https://doi.org/10.1111/sed.12352
Pálfy, J., and Zajzon, N., 2012, Environmental changes across the Triassic–Jurassic boundary and coeval volcanism inferred from elemental geochemistry and mineralogy in the Kendlbachgraben section (Northern Calcareous Alps, Austria): Earth and Planetary Science Letters, v. 335–336, p. 121–134, https://doi.org/10.1016/j.epsl.2012.01.039
Palmer, M. R., and Edmund, J. M., 1989, The strontium isotope budget of the modern ocean: Earth and Planetary Science Letters, v. 92, n. 1, p. 11–26, https://doi.org/10.1016/0012-821X(89)90017-4
Paul, C. R. C., Lamolda, M. A., Mitchell, S. F., Vaziri, M. R., Gorostidi, A., and Marshall, J. D., 1999, The Cenomanian-Turonian boundary at Eastbourne (Sussex, UK): A proposed European reference section: Palaeogeography, Palaeoclimatology, Palaeoecology, v. 150, n. 1–2, p. 83–121, https://doi.org/10.1016/S0031-0182(99)00009-7
Pearce, M. A., Jarvis, I., and Tocher, B. A., 2009, The Cenomanian–Turonian boundary event, OAE2 and palaeoenvironmental change in epicontinental seas: New insights from the dinocyst and geochemical records: Palaeogeography, Palaeoclimatology, Palaeoecology, v. 280, n. 1–2, p. 207–234, https://doi.org/10.1016/j.palaeo.2009.06.012
Percival, L. M. E., Witt, M. L. I., Mather, T. A., Hermoso, M., Jenkyns, H. C., Hesselbo, S. P., Al-Suwaidi, A. H., Storm, M. S., Xu, W., and Ruhl, M., 2015, Globally enhanced mercury deposition during the end-Pliensbachian extinction and Toarcian OAE: A link to the Karoo–Ferrar Large Igneous Province: Earth and Planetary Science Letters, v. 428, p. 267–280, https://doi.org/10.1016/j.epsl.2015.06.064
Percival, L. M. E., Cohen, A. S., Davies, M. K., Dickson, A. J., Hesselbo, S. P., Jenkyns, H. C., Leng, M. J., Mather, T. A., Storm, M. S., and Xu, W., 2016, Osmium isotope evidence for two pulses of increased continental weathering linked to Early Jurassic volcanism and climate change: Geology, v. 44, n. 9, p. 759–762, https://doi.org/10.1130/G37997.1
Percival, L. M. E., Ruhl, M., Hesselbo, S. P., Jenkyns, H. C., Mather, T. M., and Whiteside, J. H., 2017, Mercury evidence for pulsed volcanism during the end-Triassic mass extinction: Proceedings of the National Academy of Sciences of the United States of America, v. 114, n. 30, p. 7929–7934, https://doi.org/10.1073/pnas.1705378114
Petersen, S. V., Dutton, A., and Lohmann, K. C., 2016, End-Cretaceous extinction in Antarctica linked to both Deccan volcanism and meteorite impact via climate change: Nature Communications, v. 7, https://doi.org/10.1038/ncomms12079
Peterson, F., 1969, Cretaceous sedimentation and tectonism in the southeastern Kaiparowits region, Utah: U.S. Geological Survey Open File Report 69-202, 259 p.

Peucker-Ehrenbrink, B., and Jahn, B. M., 2001, Rhenium-osmium isotope systematics and platinum group element concentrations: Loess and the upper continental crust: Geochemistry, Geophysics, Geosystems, v. 2, n. 10, https://doi.org/10.1029/2001GC000172
Peucker-Ehrenbrink, B., and Ravizza, G., 2000, The marine osmium isotope record: Terra Nova, v. 12, n. 5, p. 205–219, https://doi.org/10.1046/j.1365-3121.2000.00295.x
Pinto, V. M., Hartmann, L. A., Santos, J. O. S., McNaughton, N. J., and Wildner, W., 2011, Zircon U–Pb geochronology from the Paraná bimodal volcanic province support a brief eruptive cycle at ~ 135 Ma: Chemical Geology, v. 281, n. 1–2, p. 93–102, https://doi.org/10.1016/j.chemgeo.2010.11.031
Pogge von Strandmann, P. A. E., Jenkyns, H. C., and Woodfine, R. G., 2013, Lithium isotope evidence for enhanced weathering during Ocean Anoxic Event 2: Nature Geoscience, v. 6, p. 668–672, https://doi.org/10.1038/ngeo1875
Polteau, S., Hendriks, B. W. H., Planke, S., Ganerød, M., Corfu, F., Faleide, J. I., Midtkandal, I., Svensen, H. S.. and Myklebust, R., 2016, The Early Cretaceous Barents Sea Sill Complex: Distribution, $^{40}Ar/^{39}Ar$ geochronology, and implications for carbon gas formation: Palaeogeography, Palaeoclimatology, Palaeoecology, v. 441, Part 1, p. 83–95, https://doi.org/10.1016/j.palaeo.2015.07.007
Poulton, S. W., Henkel, S., März, C., Urquhart, H., Flögel, S., Kasten, S., Damsté, J. S. S., and Wagner, T., 2015, A continental-weathering control on orbitally driven redox-nutrient cycling during Cretaceous Oceanic Anoxic Event 2: Geology, v. 43, n. 11, p. 963–966, https://doi.org/10.1130/G36837.1
Pujalte, V., Baceta, J. I., Dinarès-Turell, J., Orue-etxebarria, X., Parés, J. M., and Payros, A., 1995, Biostratigraphic and magnetostratigraphic intercalibration of latest Cretaceous and Paleocene depositional sequences from the deep-water Basque basin, western Pyrenees, Spain: Earth and Planetary Science Letters, v. 136, n. 1–2, p. 17–30, https://doi.org/10.1016/0012-821X(95)00157-9
Pujol, F., Berner, Z., and Stüben, D., 2006, Palaeoenvironmental changes at the Frasnian/Famennian boundary in key European sections: Chemostratigraphic constraints: Palaeogeography, Palaeoclimatology, Palaeoecology, v. 240, n. 1–2, p. 120–145, https://doi.org/10.1016/j.palaeo.2006.03.055
Pyle, D. M., and Mather, T. A., 2003, The importance of volcanic emissions for the global atmospheric mercury cycle: Atmospheric Environment, v. 37, n. 36, p. 5115–5124, https://doi.org/10.1016/j.atmosenv.2003.07.011
Racki, G., Racka, M., Matyja, H., and Devleeschouwer, X., 2002, The Frasnian/Famennian boundary interval in the South Polish–Moravian shelf basins: Integrated event-stratigraphical approach: Palaeogeography, Palaeoclimatology, Palaeoecology, v. 181, n. 1–3, p. 251–297, https://doi.org/10.1016/S0031-0182(01)00481-3
Racki, G., Rakociński, M., Marynowski, L., and Wignall, P. B., 2018, Mercury enrichments and the Frasnian-Famennian biotic crisis: A volcanic trigger proved?: Geology, v. 46, n. 6, p. 543–546, https://doi.org/10.1130/G40233.1
Rakociński, M., Zatoń, M., Marynowski, L., Gedl, P., and Lehmann, J., 2018, Redox conditions, productivity, and volcanic input during deposition of uppermost Jurassic and Lower Cretaceous organic-rich siltstones in Spitsbergen, Norway: Cretaceous Research, v. 89, p. 126–147, https://doi.org/10.1016/j.cretres.2018.02.014
Ravichandran, M., 2004, Interactions between mercury and dissolved organic matter – a review: Chemosphere, v. 55, n. 3, p. 319–331, https://doi.org/10.1016/j.chemosphere.2003.11.011
Ravizza, G., and Peucker-Ehrenbrink, B., 2003, Chemostratigraphic evidence of Deccan volcanism from the marine osmium isotope record: Science, v. 302, n. 5649, p. 1392–1395, https://doi.org/10.1126/science.1089209
Renne, P. R., Sprain, C. J., Richards, M. A., Self, S., Vanderkluysen, L., and Pande, K., 2015, State shift in Deccan volcanism at the Cretaceous-Paleogene boundary, possibly induced by impact: Science, v. 350, n. 6256, p. 76–78, https://doi.org/10.1126/science.aac7549
Robertson, A. H. F., 2002, Overview of the genesis and emplacement of Mesozoic ophiolites in the Eastern Mediterranean Tethyan region: Lithos, v. 65, n. 1–2, p. 1–67, https://doi.org/10.1016/S0024-4937(02)00160-3
Robinson, N., Ravizza, G., Coccioni, R., Peucker-Ehrenbrink, B., and Norris, R., 2009, A high-resolution marine $^{187}Os/^{188}Os$ record for the late Maastrichtian: Distinguishing the chemical fingerprints of Deccan volcanism and the KP impact event: Earth and Planetary Science Letters, v. 281, n. 3–4, p. 159–168, https://doi.org/10.1016/j.epsl.2009.02.019
Ross, P. S., Peate, I. U., McClintock, M. K., Xu, Y. G., Skilling, I. P., White, J. D. L., and Houghton, B. F., 2005, Mafic volcaniclastic deposits in flood basalt provinces: A review: Journal of Volcanology and Geothermal Research, v. 145, n. 3–4, p. 281–314, https://doi.org/10.1016/j.jvolgeores.2005.02.003
Ruiz, W. L. G., and Tomiyasu, T., 2015, Distribution of mercury in sediments from Kagoshima Bay, Japan, and its relationship with physical and chemical factors: Environmental Earth Sciences, v. 74, n. 2, p. 1175–1188, https://doi.org/10.1007/s12665-015-4104-5
Sabatino, N., Ferraro, S., Coccioni, R., Bonsignore, M., Del Core, M., Tancredi, V., and Sprovieri, M., 2018, Mercury anomalies in upper Aptian-lower Albian sediments from the Tethys realm: Palaeogeography, Palaeoclimatology, Palaeoecology, v. 495, p. 163–170, https://doi.org/10.1016/j.palaeo.2018.01.008
Sanei, H., Grasby, S., and Beauchamp, B., 2012, Latest Permian mercury anomalies: Geology, v. 40, n. 1, p. 63–66, https://doi.org/10.1130/G32596.1
Saunders, A. D., 2016, Two LIPs and two Earth-system crises: The impact of the North Atlantic Igneous Province and the Siberian Traps on the Earth-surface carbon cycle: Geological Magazine, v. 153, n. 2, p. 201–222, https://doi.org/10.1017/S0016756815000175
Scaife, J. D., Ruhl, M., Dickson, A. J., Mather, T. A., Jenkyns, H. C., Percival, L. M. E., Hesselbo, S. P., Cartwright, J., Eldrett, J. S., Bergman, S. C., and Minisini, D., 2017, Sedimentary Mercury Enrichments as a Marker for Submarine Large Igneous Province Volcanism? Evidence from the Mid-Cenomanian

Event and Oceanic Anoxic Event 2 (Late Cretaceous): Geochemistry, Geophysics, Geosystems, v. 18, n. 12, p. 4253–4275, https://doi.org/10.1002/2017GC007153
Schlanger, S. O., and Jenkyns, H. C., 1976, Cretaceous Oceanic Anoxic Events: Causes and Consequences: Geologie en Mijnbouw, v. 55, n. 3, p. 179–184.
Schoene, B., Samperton, K. M., Eddy, M. P., Keller, G., Adatte, T., Bowring, S. A., Khadri, S. F. R., and Gertsch, B., 2015, U-Pb geochronology of the Deccan Traps and relation to the end-Cretaceous mass extinction: Science, v. 347, n 6218, p. 182–184, https://doi.org/10.1126/science.aaa0118
Schoepfer, S. D., Henderson, C. M., Garrison, G. H., Foriel, J., Ward, P. D., Selby, D., Hower, J. C., Algeo, T. J., and Shen, Y., 2013, Termination of a continent-margin upwelling system at the Permian–Triassic boundary (Opal Creek, Alberta, Canada): Global and Planetary Change, v. 105, p. 21–35, https://doi.org/10.1016/j.gloplacha.2012.07.005
Schroeder, W. H., and Munthe J., 1998, Atmospheric mercury - An overview: Atmospheric Environment, v. 32, n. 5, p. 809–822, https://doi.org/10.1016/S1352-2310(97)00293-8
Schuster, P. F., Krabeenhoft, D. P., Naftz, D. L., Cecil, L. D., Olson, M. L., Dewild, J. F., Susong, D. D., Green, J. R., and Abbott, M. L., 2002, Atmospheric mercury deposition during the last 270 years: A glacial ice core record of natural and anthropogenic sources: Environmental Science & Technology, v. 36, n. 11, p. 2303–2310, https://doi.org/10.1021/es0157503
Self, S., Schmidt, A., and Mather, T. A., 2014, Emplacement characteristics, time scales, and volcanic gas release rates of continental flood basalt eruptions on Earth, *in* Keller, G., and Kerr, A. C., editors, Volcanism, Impacts, and Mass Extinctions: Causes and Effects: Geological Society of America Special Papers, v. 505, https://doi.org/10.1130/2014.2505(16)
Selin, N. E., 2009, Global Biogeochemical Cycling of Mercury: A Review: Annual Review of Environment and Resources, v. 34, p. 43–63, https://doi.org/10.1146/annurev.environ.051308.084314
Sell, B., Ovtcharova, M., Guex, J., Bartolini, A., Jourdan, F., Spangenberg, J. E., Vicente, J. C., and Schaltegger, U., 2014, Evaluating the temporal link between the Karoo LIP and climatic–biologic events of the Toarcian Stage with high-precision U–Pb geochronology: Earth and Planetary Science Letters, v. 408, p. 48–56, https://doi.org/10.1016/j.epsl.2014.10.008
Seton, M., Müller, R. D., Zahirovic, S., Gaina, C., Torsvik, T., Shephard, G., Talsma, A., Gurnis, M., Turner, M., Maus, S., and Chandler, M., 2012, Global continental and ocean basin reconstructions since 200 Ma: Earth-Science Reviews, v. 113, n. 3–4, p. 212–270, https://doi.org/10.1016/j.earscirev.2012.03.002
Sial, A. N., Lacerda, L. D., Ferreira, V. P., Frei, R., Marquillas, R. A., Barbosa, J. A., Gaucher, C., Windmöller, C. C., and Pereira, N. S., 2013, Mercury as a proxy for volcanic activity during extreme environmental turnover: The Cretaceous–Paleogene transition: Palaeogeography, Palaeoclimatology, Palaeoecology, v. 387, p. 153–164, https://doi.org/10.1016/j.palaeo.2013.07.019
Sial, A. N., Chen, J., Lacerda, L. D., Peralta, S., Gaucher, C., Frei, R., Cirilli, S., Ferreira, V. P., Marquillas, R. A., Barbosa, J. A., Pereira, N. S., and Belmino, I. K. C., 2014, High-resolution Hg chemostratigraphy: A contribution to the distinction of chemical fingerprints of the Deccan volcanism and Cretaceous–Paleogene Boundary impact event: Palaeogeography, Palaeoclimatology, Palaeoecology, v. 414, p. 98–115, https://doi.org/10.1016/j.palaeo.2014.08.013
Sial, A. N., Chen, J., Lacerda, L. D., Frei, R., Tewari, V. C., Pandit, M. K., Gaucher, C., Ferreira, V. P., Cirilli, S., Peralta, S., Korte, C., Barbosa, J. A., and Pereira, N. S., 2016, Mercury enrichment and Hg isotopes in Cretaceous–Paleogene boundary successions: Links to volcanism and palaeoenvironmental impacts: Cretaceous Research, v. 66, p. 60–81, https://doi.org/10.1016/j.cretres.2016.05.006
Slemr, F., Schuster, G., and Seiler, W., 1985, Distribution, speciation, and budget of atmospheric mercury: Journal of Atmospheric Chemistry, v. 3, n. 4, p. 407–434, https://doi.org/10.1007/BF00053870
Smit, J., 1999, The global stratigraphy of the Cretaceous-Tertiary boundary impact ejecta: Annual Review of Earth and Planetary Sciences, v. 27, p. 75–113, https://doi.org/10.1146/annurev.earth.27.1.75
Smit, J., and Van der Kaars, S., 1984, Terminal Cretaceous extinctions in the Hell Creek area, Montana: Compatible with catastrophic extinction: Science, v. 223, n. 4641, p. 1177–1180, https://doi.org/10.1126/science.223.4641.1177
Snow, L. J., Duncan, R. A., and Bralower, T. J., 2005, Trace element abundances in the Rock Canyon Anticline, Pueblo, Colorado, marine sedimentary section and their relationship to Caribbean plateau construction and oxygen anoxic event 2: Paleoceanography and Paleoclimatology, v. 20, n. 3, PA3005, https://doi.org/10.1029/2004PA001093
Sprain, C. J., Renne, P. R., Wilson, G. P., and Clemens, W. A., 2015, High-resolution chronostratigraphy of the terrestrial Cretaceous-Paleogene transition and recovery interval in the Hell Creek region, Montana: Geological Society of America Bulletin, v. 127, n. 2–3, p. 393–409, https://doi.org/10.1130/B31076.1
Sprain, C. J., Renne, P. R., Clemens, W. A., and Wilson, G. P., 2018, Calibration of chron C29r: New high-precision geochronologic and paleomagnetic constraints from the Hell Creek region, Montana: Geological Society of America Bulletin, v. 130, n. 9–10, p. 1615–1644, https://doi.org/10.1130/B31890.1
Storey, M., Mahoney, J. J., Saunders, A. D., Duncan, R. A., Kelley, S. P., and Coffin, M. F., 1995, Timing of hot spot-Related volcanism and the breakup of Madagascar and India: Science, v. 267, n. 5199, p. 852–855, https://doi.org/10.1126/science.267.5199.852
Svensen, H., Planke, S., Malthe-Sørenssen, A., Jamtveit, B., Myklebust, R., Eidem, T. R., and Rey, S.S., 2004, Release of methane from a volcanic basin as a mechanism for initial Eocene global warming: Nature, v. 429, p. 542–545, https://doi.org/10.1038/nature02566
Svensen, H., Planke, S., Chevalier, L., Malthe-Sørenssen, A., Corfu, F., and Jamtveit, B., 2007, Hydrothermal venting of greenhouse gases triggering Early Jurassic global warming: Earth and Planetary Science Letters, v. 256, n. 3–4, p. 554–566, https://doi.org/10.1016/j.epsl.2007.02.013
Svensen, H., Planke, S., Polozov, A. G., Schmidbauer, N., Corfu, F., Podladchikov, Y. Y. and Jamtveit, B., 2009,

Siberian gas venting and the end-Permian environmental crisis: Earth and Planetary Science Letters, v. 277, p. 490–500, https://doi.org/10.1016/j.epsl.2008.11.015
Svensen, H., Corfu, F., Polteau, S., Hammer, Ø., and Planke, S., 2012, Rapid magma emplacement in the Karoo large igneous province: Earth and Planetary Science Letters, v. 325–326, p. 1–9, https://doi.org/10.1016/j.epsl.2012.01.015
Sweere, T. C., Dickson, A. J., Jenkyns, H. C., Porcelli, D., Elrick, M., van den Boorn, S. H., and Henderson, G. M., 2018, Isotopic evidence for changes in the zinc cycle during Oceanic Anoxic Event 2 (Late Cretaceous): Geology, v. 46, n. 5, p. 463–466, https://doi.org/10.1130/G40226.1
Swisher, C. C., III, Dingus, L., and Butler, R. F., 1993, $^{40}Ar/^{39}Ar$ dating and magnetostratigraphic correlation of the terrestrial Cretaceous-Paleogene boundary and Puercan Mammal Age, Hell Creek–Tullock formations, eastern Montana: Canadian Journal of Earth Sciences, v. 30, n. 9, p. 1981–1996, https://doi.org/10.1139/e93-174
Tegner, C., Storey, M., Holm, P. M., Thorarinsson, S. B., Zhao, X., Lo, C. H., and Knudsen, M. F., 2011, Magmatism and Eurekan deformation in the High Arctic Large Igneous Province: ^{40}Ar-^{39}Ar age of Kap Washington Group volcanics, North Greenland: Earth and Planetary Science Letters, v. 303, n. 3–4, p. 203–214, https://doi.org/10.1016/j.epsl.2010.12.047
Tejada, M. L. G., Suzuki, K., Kuroda, J., Coccioni, R., Mahoney, J. J., Ohkouchi, N., Sakamoto, T., and Tatsumi, Y., 2009, Ontong Java Plateau eruption as a trigger for the early Aptian oceanic anoxic event: Geology, v. 37, n. 9, p. 855–858, https://doi.org/10.1130/G25763A.1
Thibault, N., Husson, D., Harlou, R., Gardin, S., Galbrun, B., Huret, E., and Minoletti, F., 2012, Astronomical calibration of upper Campanian–Maastrichtian carbon isotope events and calcareous plankton biostratigraphy in the Indian Ocean (ODP Hole 762C): Implication for the age of the Campanian–Maastrichtian boundary: Palaeogeography, Palaeoclimatology, Palaeoecology, v. 337–338, p. 52–71, https://doi.org/10.1016/j.palaeo.2012.03.027
Thibodeau, A. M., and Bergquist, B. A., 2017, Do mercury isotopes record the signature of massive volcanism in marine sedimentary records?: Geology, v. 45, n. 1, p. 95–96, https://doi.org/10.1130/focus012017.1
Thibodeau, A. M., Ritterbush, K., Yager, J. A., West, J., Ibarra, Y., Bottjer, D. J., Berelson, W. M., Bergquist, B. A., and Corsetti, F. A., 2016, Mercury anomalies and the timing of biotic recovery following the end-Triassic mass extinction: Nature Communications, v. 7, https://doi.org/10.1038/ncomms11147
Thiede, D. S., and Vasconcelos, P. M., 2010, Paraná flood basalts: Rapid extrusion hypothesis confirmed by new $^{40}Ar/^{39}Ar$ results: Geology, v. 38, n. 8, p. 747–750, https://doi.org/10.1130/G30919.1
Thompson, P. M. E., Kempton, P. D., White, R. V., Kerr, A. C., Tarney, J., Saunders, A. D., Fitton, J. G., and McBirney, A., 2004, Hf–Nd isotope constraints on the origin of the Cretaceous Caribbean plateau and its relationship to the Galápagos plume: Earth and Planetary Science Letters, v. 217, n. 1–2, p. 59–75, https://doi.org/10.1016/S0012-821X(03)00542-9
Thordarson, T., 2004, Accretionary-lapilli-bearing pyroclastic rocks at ODP Leg 192 Site 1184: A record of subaerial phreatomagmatic eruptions on the Ontong Java Plateau, *in* Fitton, J. G., Mahoney, J. J., Wallace, P. J., and Saunders, A. D., editors, Origin and Evolution of the Ontong Java Plateau: Geological Society of London, Special Publications, v. 229, p. 275–306, https://doi.org/10.1144/GSL.SP.2004.229.01.16
Tobin, T. S., Ward, P. D., Steig, E. J., Olivero, E. B., Hilburn, I. A., Mitchell, R. N., Diamond, M. R., Raub, T. D., and Kirschvink, J. L., 2012, Extinction patterns, $\delta^{18}O$ trends, and magnetostratigraphy from a southern high-latitude Cretaceous–Paleogene section: Links with Deccan volcanism: Palaeogeography, Palaeoclimatology, Palaeoecology, v. 350–352, p. 180–188, https://doi.org/10.1016/j.palaeo.2012.06.029
Tsikos, H., Jenkyns, H. C., Walsworth-Bell, B., Petrizzo, M. R., Forster, A., Kolonic, S., Erba, E., Premoli-Silva, I. P., Baas, M., Wagner, T., and Sinninghe Damsté, J. S., 2004, Carbon-isotope stratigraphy recorded by the Cenomanian–Turonian Oceanic Anoxic Event: Correlation and implications based on three key localities: Journal of the Geological Society, London, v. 161, p. 711–719, https://doi.org/10.1144/0016-764903-077
Turgeon, S., and Brumsack, H. J., 2006, Anoxic vs dysoxic events reflected in sediment geochemistry during the Cenomanian–Turonian Boundary Event (Cretaceous) in the Umbria–Marche Basin of central Italy: Chemical Geology, v. 234, n. 3–4, p. 321–339, https://doi.org/10.1016/j.chemgeo.2006.05.008
Turgeon, S. C., and Creaser, R. A., 2008, Cretaceous oceanic anoxic event 2 triggered by a massive magmatic episode: Nature, v. 454, p. 323–326, https://doi.org/10.1038/nature07076
Voigt, S., Gale, A. S., and Flögel, S., 2004, Midlatitude shelf seas in the Cenomanian-Turonian greenhouse world: Temperature evolution and North Atlantic circulation: Paleoceanography and Paleoclimatology, v. 19, n. 4, PA4020, https://doi.org/10.1029/2004PA001015
Voigt, S., Gale, A.S. and Voigt, T., 2006, Sea-level change, carbon cycling and palaeoclimate during the Late Cenomanian of northwest Europe; an integrated palaeoenvironmental analysis: Cretaceous Research, v. 27, n. 6, p. 836–858, https://doi.org/10.1016/j.cretres.2006.04.005
Wang, X., Cawood, P. A., Zhao, H., Zhao, L., Grasby, S. E., Chen, Z. Q., Wignall, P. B., Lv, Z., and Han, C., 2018, Mercury anomalies across the end Permian mass extinction in South China from shallow and deep water depositional environments: Earth and Planetary Science Letters, v. 496, p. 159–167, https://doi.org/10.1016/j.epsl.2018.05.044
Wellman, P., and McElhinny, M. W., 1970, K–Ar age of the Deccan traps, India: Nature, v. 227, p. 595–596, https://doi.org/10.1038/227595a0
Westermann, S., Vance, D., Cameron, V., Archer, C., and Robinson, S. A., 2014, Heterogeneous oxygenation states in the Atlantic and Tethys oceans during Oceanic Anoxic Event 2: Earth and Planetary Science Letters, v. 404, p. 178–189, https://doi.org/10.1016/j.epsl.2014.07.018
Wieczorek, R., Fantle, M. S., Kump, L. R., and Ravizza, G., 2013, Geochemical evidence for volcanic activity prior to and enhanced terrestrial weathering during the Paleocene Eocene Thermal Maximum: Geochimica et Cosmochimica Acta, v. 119, p. 391–410, https://doi.org/10.1016/j.gca.2013.06.005

Witts, J. D., Bowman, V. C., Wignall, P. B., Crame, J. A., Francis, J. E., and Newton, R. J., 2015, Evolution and extinction of Maastrichtian (Late Cretaceous) cephalopods from the López de Bertodano Formation, Seymour Island, Antarctica: Palaeogeography, Palaeoclimatology, Palaeoecology, v. 418, p. 193–212, https://doi.org/10.1016/j.palaeo.2014.11.002

Witts, J. D., Whittle, R. J., Wignall, P. B., Crame, J. A., Francis, J. E., Newton, R. J., and Bowman, V. C., 2016, Macrofossil evidence for a rapid and severe Cretaceous-Paleogene mass extinction in Antarctica: Nature Communications, v. 7, https://doi.org/10.1038/ncomms11738

Woelders, L., Vellekoop, J., Kroon, D., Smit, J., Casadío, S., Prámparo, M. B., Dinarès-Turell, J., Peterse, F., Sluijs, A., Lenaerts, J. T. M., and Speijer, R. P., 2017, Latest Cretaceous climatic and environmental change in the South Atlantic region. Paleoceanography and Paleoclimatology, v. 32, n. 5, p. 466–483, https://doi.org/10.1002/2016PA003007

Xu, W., Mac Niocaill, C., Ruhl, M., Jenkyns, H. C., Riding, J. B., and Hesselbo, S. P., 2018, Magnetostratigraphy of the Toarcian Stage (Lower Jurassic) of the Llanbedr (Mochras Farm) Borehole, Wales: Basis for a global standard and implications for volcanic forcing of palaeoenvironmental change: Journal of the Geological Society, v. 174, n. 4, p. 594–604, https://doi.org/10.1144/jgs2017-120

Zheng, X.-Y., Jenkyns, H. C., Gale, A. S., Ward, D. J., and Henderson, G. M., 2013, Changing ocean circulation and hydrothermal inputs during Ocean Anoxic Event 2 (Cenomanian–Turonian): Evidence from Nd-isotopes in the European shelf sea: Earth and Planetary Science Letters, v. 375, p. 338–348, https://doi.org/10.1016/j.epsl.2013.05.053